DOE F 241.3
(2-01) p.1 of 2

UNITED STATES DEPARTMENT OF ENERGY (DOE)
Announcement of Scientific and Technical Information (STI)
(For Use By Financial Assistance Recipients and Non-M&O/M&I Contractors)

OMB CONTROL NO. 1910-1400

PART I: STI PRODUCT DESCRIPTION
(To be completed by Recipient/Contractor)

A. STI Product Identifiers

1. REPORT/PRODUCT NUMBER(s)
None

2. DOE AWARD/CONTRACT NUMBER(s)
DE-FC36-97ID13554

3. OTHER IDENTIFYING NUMBER(s)
None

B. Recipient/Contractor

Colorado School of Mines, Department of Metallurgical and Materials Engineering, Golden, CO 80401

C. STI Product Title

Improved Criteria for Acceptable Yield Point Elongation in Surface Critical Steels

D. Author(s)

David Matlock
John Speer

E-mail Address(es):
jspeer@mines.edu
dmatlock@mines.edu

E. STI Product Issue Date/Date of Publication

05 (MM) 30 (DD) 2007 (YYYY)

F. STI Product Type (*Select only one*)

☒ 1. TECHNICAL REPORT
☒ *Final* ☐ *Other (specify)* _____

☐ 2. CONFERENCE PAPER/PROCEEDINGS

Conference Information (title, location, dates)

☐ 3. JOURNAL ARTICLE
a. TYPE: ☐ *Announcement Citation Only* ☐ *Preprint* ☐ *Postprint*
b. JOURNAL NAME
c. VOLUME _____ *d. ISSUE* _____
e. SERIAL IDENTIFIER (e.g. ISSN or CODEN)

☐ 4. OTHER, SPECIFY

G. STI Product Reporting Period

12 (MM) 08 (DD) 2004 (YYYY) Thru 05 (MM) 30 (DD) 2007 (YYYY)

H. Sponsoring DOE Program Office

Office of Industrial Technologies (OIT)(EE20)

I. Subject Categories *(list primary one first)*

32 Energy Conservation, Consumption and Utilization
Keywords: Sheet Steel, YPE, High Strength Steels

J. Description/Abstract

Yield point elongation (YPE) is considered undesirable in surface-critical applications where steel is formed since "strain lines" or Luders bands are created during forming. This project will examine in detail the formation of Luders bands in industrially relevant strain states including the influence of substrate properties and coatings on Luders appearance. Mechanical testing and surface profilometry were the primary methods of investigation.

K. Intellectual Property/Distribution Limitations

(must select at least one; if uncertain contact your Contracting Officer (CO))

☒ 1. UNLIMITED ANNOUNCEMENT *(available to U.S. and non-U.S. public; the Government assumes no liability for disclosure of such data)*

☐ 2. COPYRIGHTED MATERIAL: *Are there any restrictions based on copyright?* ☐ *Yes* ☒ *No.*
If yes, list the restrictions as contained in your award document

☐ 3. PATENTABLE MATERIAL: THERE IS PATENTABLE MATERIAL IN THE DOCUMENT.
INENTION DISCLOSURE SUBMITTED TO DOE:
DOE Docket Number: S-
(Sections are marked as restricted distribution pursuant to 35 USC 205)

☐ 4. PROTECTED DATA: ☐ CRADA ☐ *Other, specify*
Release date (required) no more than 5 years from date listed in Part I.E. above ___ (MM) ___ (DD) ____ (YYYY)

☐ 5. SMALL BUSINESS INNOVATION RESEARCH (SBIR) DATA
Release date (required) no more than 4 years from date listed in Part I.E. above ___ (MM) ___ (DD) ____ (YYYY)

☐ 6. SMALL BUSINESS TECHNOLOGY TRANSFER RESEARCH (STTR) DATA
Release date (required) no more than 4 years from date listed in Part I.E. above ___ (MM) ___ (DD) ____ (YYYY)

☐ 7. OFFICE OF NUCLEAR ENERGY APPLICED TECHNOLOGY

L. Recipient/Contract Point of Contact *Contact for additional information (contact or organization name To be included in published citations and who would Receive any external questions about the content of the STI Product or the research contained herein)*

Dr. John Speer
Name and/or Position
jspeer@mines.edu (303) 273-3897
E-mail *Phone*
Advanced Steel Processing and Products Research Center, Department of Metallugical and Material Engineering, Colorado School of Mines, Golden, CO

UNITED STATES DEPARTMENT OF ENERGY (DOE)
Announcement of Scientific and Technical Information (STI)
(For Use By Financial Assistance Recipients and Non-M&O/M&I Contractors)

OMB CONTROL NO.
1910-1400

PART II: STI PRODUCT MEDIA/FORMAT and LOCATION/TRANSMISSION

(To be completed by Recipient/Contractor)

A. Media/Format Information:

1. MEDIUM OF STI PRODUCT IS:
   ☒ Electronic Document ☐ Computer Medium
   ☐ Audiovisual Material ☐ Paper ☐ No Full-text
2. SIZE OF STI PRODUCT 155 Pages , 14,300 KB
3. SPECIFY FILE FORMAT OF ELECTRONIC DOCUMENT BEING TRANSMITTED, INDICATE:
   ☐ SGML ☐ HTML ☐ XML ☒ PDF Normal
   ☐ PDF Image ☐ TIFFG4
   ☐ WP-indicate Version (*5.0 or greater)* _____
   Platform/operation system _____
   ☐ MS-indicate Version (*5.0 or greater)* _____
   Platform/operation system _____
   ☐ Postscript _____
4. IF COMPUTER MEDIUM OR AUDIOVISUAL MATERIAL:
   a. Quantity/type (*specify)* _____
   b. Machine compatibility (*specify)* _____
   c. Other information about product format a user needs to know:
   _____

B. Transmission Information:

1. STI PRODUCT IS BEING TRANSMITTED:
   ☒ a. Electronically via E-Link
   b. Via mail or shipment to address indicated in award document (*Paper product, CD-ROM, diskettes, video cassettes, etc.)*
   _____
2. INFORMATION PRODUCT FILE NAME
   ☒ *(of transmitted electronic format)*
   TRP9944NonPropFinal.

PART III: STI PRODUCT REVIEW/RELEASE INFORMATION

(To be completed by DOE)

A. STI Product Reporting Requirements Review.

☐ 1. THIS DELIVERABLE COMPLETES ALL REQUIRED DELIVERABLES FOR THIS AWARD
☐ 2. THIS DELIVERABLE FULFILLS A TECHNICAL INFORMATION REPORTING REQUIREMENT, BUT SHOULD NOT BE DISSEMINATED BEYOND DOE.

B. Award Office Is the Source of STI Product Availability

☐ THE STI PRODUCT IS NOT AVAILABLE IN AN ELECTRONIC MEDIUM. THE AWARDING OFFICE WILL SERVE AS THE INTERIM SOURCE OF AVAILABILITY.

C. DOE Releasing Official

☐ 1. I VERIFY THAT ALL NECESSARY REVIEWS HAVE BEEN COMPLETED AS DESCRIBED IN DOE G 241.1-1A, PART II, SECTION 3.0 AND THAT THE STI PRODUCT SHOULD BE RELEASED IN ACCORDANCE WITH THE INTELLECTUAL PROPERTY/DISTRIBUTION LIMITATION ABOVE.

Release by (*name)* _____

Date ___ ___ _____
MM DD YYYY

E-Mail _____

Phone _____

Report Documentation Page

Title and Subtitle: AISI/DOE Technology Roadmap Program
Improved Criteria for Acceptable Yield Point Elongation
In Surface Critical Steels
TRP 9944

Author(s): David Matlock, Co-Principal Investigator
John Speer, Co-Principal Investigator

Performing Organization Advanced Steel Processing and Products Research Center
Department of Metallurgical and Materials Engineering
Colorado School of Mines
Golden, CO 80401

Abstract:

Yield point elongation (YPE) is considered undesirable for surface-critical applications where the steel is formed, since “strain lines” or Lüders bands are created during forming. Thus, steel manufacturers usually aim for zero YPE in these applications, tailoring their alloy and process design strategies and operating practices accordingly. In practice, a small amount of YPE (e.g. a few tenths of 1%) is usually considered acceptable, although there are no clear or uniform acceptance criteria, and decisions are usually made on a local basis by manufacturers, substantially influenced by commercial issues, and without clear technical guidance. This project will examine in detail the formation of Lüders bands in industrially relevant strain states, to examine the influence of starting (substrate property) conditions, and to better understand the influence of galvanized/galvannealed coatings on Lüders appearance. Mechanical testing and surface profilometry will be the primary methods employed.

DOCUMENT AVAILABILITY

Reports are available free via the U.S. Department of Energy (DOE) Information Bridge:

Website: http://www.osti.gov/bridge

Reports are available to DOE employees, DOE contractors, Energy Technology Data Exchange (ETDE) representatives, and Informational Nuclear Information System (INIS) representatives from the following source:

Office of Scientific and Technical Information
P.O. Box 62
Oak Ridge, TN 37831
Tel: (865) 576-8401
Fax: (865) 576-5728
E-mail: reports@osti.gov
Website: http://www.osti.gov/contract.html

Acknowledgement: "This report is based upon work supported by the U.S. Department of Energy under Cooperative Agreement No. DE-FC36-97ID13554."

Final Report

Improved Criteria for Acceptable Yield Point Elongation In Surface Critical Steels

by

Dr. John G. Speer
Dr. David K. Matlock
Mr. Bryce Lakamp
Dr. Rongjie Song

Advanced Steel Processing and Products Research Center
Dept. of Metallurgical and Materials Engineering
Colorado School of Mines
Golden, Colorado 80401

Work performed under Cooperative Agreement No. DE-FC36-97ID13554

Prepared for
U.S. Department of Energy

Prepared by
American Iron and Steel Institute
Foster Plaza Building 10
680 Anderson Drive
Pittsburgh, PA 15220-2700

May 30, 2007

EXECUTIVE SUMMARY

It is necessary for exposed steel sheet panels to be free of noticeable surface imperfections such as Lüders bands. Lüders bands are formed during non-uniform yielding of the sheet. The extent of non-uniform yielding is measured from the stress-strain behavior by the yield point elongation (YPE) and is of concern for low carbon sheet steels in surface sensitive applications. Discontinuous or non-uniform yielding has been studied extensively using stress-strain data in tension for many years, but the detailed geometrical characteristics of the Lüders band surface imperfections have received much less attention. Modern three-dimensional surface profilometry instrumentation has become capable of quantitatively characterizing the surface geometry. The work conducted here was thus intended to characterize the topographical features of Lüders bands that are created during forming of low-carbon sheet steels, and their *development* with strain. YPE is both a quality and production-yield issue in surface critical applications, and is encountered sporadically by sheet steel producers, particularly in grades such as coated BH210 where precise control of interstitial solute levels is critical. One project sponsor has reported that, while yield losses are insignificant, conservative countermeasures have been taken to prevent such losses, which add cost to the products. Another sponsor reported that 5% of production coils tested indicate YPE levels above 1%, although rejection of most of these coils is avoided by retesting further away from the welds between coil ends, and the rejected coils are captured in other imperfection classifications.

The project plan developed in conjunction with the sponsoring steel company representatives involved characterization of Lüders band topography in four steels, including three commercially temper rolled bake-hardening automotive 0.030 in (0.76mm) BH210 sheet steels with different coatings: electrogalvanized (EG), hot-dip galvanized (GI), and galvannealed (GA), and a hot-dip galvanized low-carbon (LC) aluminum-killed steel having approximately double the thickness (0.060 in or 1.52 mm). Laboratory processing (involving controlled aging at elevated temperature for the BH210 steels and temper rolling plus aging for the LC steel) provided controlled variations in the

YPE of each material, at levels of 0.25%, 0.5%, 0.75% and 1%, as determined in the transverse direction. (An additional EG material with a much greater YPE was also used for selected studies where magnified effects were desired.) Forming simulations involved uniaxial tension, and selected biaxial strain states including plane strain and balanced biaxial stretching (using in-plane Marciniak techniques). Deformations in both longitudinal and transverse directions were included. An *in-situ* straining apparatus was designed and constructed to allow both straining and surface characterization under load, i.e. without removing the test specimen from the profilometer stage. Aging procedures were developed for each material to obtain the desired YPE levels; some differences in the aging responses of the as-received materials were noted. For example, controllable YPE levels were developed at 150°C in the BH210 GI and EG materials, and at 100°C in the BH210 GA and low-carbon (LC) GI materials (due to their much faster aging kinetics at 150°C). Transverse specimens given identical aging treatments as the longitudinal specimens generally exhibited a (slightly) greater extent of YPE. Lüders bands were found to exhibit corresponding features on both sides of a steel sheet, and a brittle polymer coating (StressCoat^{TM}) was used on one side of the sheet to help identify the presence of discontinuous yielding, and locate specific bands for surface topography analysis.

Lüders band geometries were characterized primarily in terms of depth and width relative to the overall surface, and were determined through analyses of three-dimensional optical profilometry results. The geometries were assessed using two different procedures. In the first procedure, the development of individual Lüders bands was monitored with increasing strain levels. The maximum depth was found to occur at low strains (below 0.5% strain), with higher strains leading to less pronounced features as the overall "background" roughness increased with deformation. In the second case, multiple bands were characterized as they appeared with increased strain in each specimen, and thus each individual band should exhibit a depth close to its corresponding maximum. For both cases, in a given material, the maximum depth increased with increasing YPE (as controlled by aging), while the associated width was relatively unaffected by YPE level. The Lüders band widths were on the order of a few millimeters, while the maximum depths ranged up to a few microns.

It was found that the band geometries (depth and width) formed at a given YPE level, were not substantially changed relative to the inherent variability in the measurements as a function of rolling orientation (longitudinal vs. transverse). Similarly, the band geometries were not found to be sensitive to sample width (i.e. strain path) for conditions near plane strain or where drawing strain states were encountered. Again, Lüders band depth in general did increase with increasing YPE (as would be expected), although the apparent width of individual Lüders band features was not substantially influenced by the YPE level in the sheet.

In balanced biaxial strain states characteristic of equi-biaxial stretch-forming modes, Lüders bands were not apparent after straining in any of the experimental materials having YPE levels up to 1%. This behavior has not been reported previously, and is speculated to result from the specimen constraint inherent in balanced biaxial deformation, which is believed to suppress strain localization necessary for discontinuous deformation.

The Lüders band topography measurements were compared among the four materials: BH210 with EG, GI, or GA coatings, and a LC GI steel having double the thickness of the other steels. The presence of the zinc coatings, each with a characteristic roughness greater than for the highly polished samples examined previously, somewhat obscured the Lüders band profiles when obtaining topography measurements, because the sheet roughness amplitude was comparable to the Lüders band topography. The EG material exhibited the greatest scatter in Lüders band depths and the largest overall depth values. The EG material was also the most difficult material in which to obtain high quality 3-D topography data using the low magnification objective lens employed for area scans in the present work, due to its lower reflectivity presumably associated with higher micro-roughness characteristics. The Lüders band depths in the GA material appeared to be slightly lower than in the other materials, for a given YPE level. It was expected that an increase in sheet thickness should increase the dimensions (at least the depth) of a Lüders band, and this expectation was the reason that the thicker GI steel was included in the study. However, it was found unexpectedly that most of the Lüders bands in the thicker material were of comparable dimensions to those found in the thinner steels. Regions of intersection between two propagating Lüders bands were found to be

associated with greater depths than were applicable to individual bands. It should be recognized that that the Lüders band measurements were applicable to the exposed surface of the coating, and the behavior of the underlying substrate surface or an identical uncoated substrate may have been somewhat different.

In comparing the results of different steels, it should be noted that the sample materials were produced by different manufacturers using different alloying and processing approaches, and that single (rather than multiple) coils were examined. Thus, it is not yet possible to conclude that observed differences are characteristic of the full class of materials represented by the different steels. Nonetheless, a slightly reduced Lüders band depth in the galvannealed coating in comparison to the two pure zinc coatings is interesting, and may be related to the higher hardness of the GA coating as well as a somewhat different temper rolling response, although further work would be needed to examine these aspects.

The results reported here are unique in that Lüders bands were measured on coated surfaces, the band topographies were monitored *in-situ* during deformation, and low YPE levels of interest to industry (up to 1%) were the focus, rather than much higher YPE levels more typically examined in fundamental studies of discontinuous deformation. The observation of multiple bands is different than most previous studies where it is more typically reported that an individual band propagates over a large portion of the specimen length. This difference is not understood, but perhaps may be associated with the lower YPEs applicable to the present materials, and/or the effect of temper rolling. (All of the test materials were temper rolled, which is not usually the case in fundamental studies of discontinuous yielding.) The work has demonstrated the utility of three-dimensional surface profiling for characterizing Lüders band topographic features. Nonetheless, tension testing remains a somewhat more sensitive technique for monitoring overall differences in yielding behavior of different steels.

The project was initially proposed to provide data to develop criteria that might form the basis for industry consideration of specifications for YPE in exposed automotive or other applications, but project participants indicated that the data would be useful to individual companies for their own internal practices, and that industry-wide consideration of the results would be more appropriate at a later time. Nonetheless, it

should be noted that the Lüders band depths (a few microns) in the materials evaluated here are generally less than the depths of many surface imperfections on sheet steels whose depths were characterized in previous research and found to be either completely invisible or barely visible after subsequent painting with a typical multilayer automotive paint system. While acceptable YPE levels are currently established on a company and part specific basis, the ability to supply materials with YPE levels up to 1% would provide steel manufacturers with additional flexibility, with potential benefits in yield, increased levels of bake-hardening, reduced levels of temper rolling reduction (and thus improved formability), lower cost, etc. Substantial discussion and follow-up research would be needed for industry to adopt a change in perspective on allowable YPE levels for sheet steels. However, it is mutually beneficial for users and producers of surface critical steels to consider this issue on an ongoing basis, as additional data become available and painting practice modifications/developments are understood.

ACKNOWLEDGEMENTS

The AISI/DOE Technology Roadmap Program along with project sponsor companies Dofasco, Severstal North America, Stelco, U.S. Steel, and USS-POSCO are gratefully acknowledged for financial support, experimental materials, and project input. Peter Badgley, Robert Cutler, Dennis Haezebrouck, Masamichi Ichikawa, Ronnie Pierce, Ron Radzilowski and Michael Thorpe are specifically acknowledged for their contributions to the work. The Advanced Steel Processing and Products Research Center, an Industry/University Cooperative Research Center at Colorado School of Mines is acknowledged for administrative support. Dr. Richard Krahenbuhl and Dr. Misac Nabighian from the Department of Geophysics at CSM are acknowledged for assistance with analysis of topography data sets.

TABLE OF CONTENTS

LIST OF FIGURES

LIST OF FIGURES

LIST OF FIGURES

LIST OF FIGURES

LIST OF TABLES

1.0 GENERAL INTRODUCTION

Exposed panels are surface-critical components in the manufacturing industry. To improve corrosion resistance, exposed panels are generally coated with zinc through a galvanizing process. Surface defects such as dents, scratches, bulges and Lüders bands are undesirable. Lüders bands can appear during the forming of the panels in response to non-uniform yielding. Non-uniform yielding is measured by yield point elongation (YPE), a component of the stress-strain response of the material. Very small amounts of YPE (0.4 %) have been noted to be industrially acceptable,[1] although there are no uniform acceptance criteria. Many investigations of Lüders bands and discontinuous yielding were conducted in the past; a renewed interest in Lüders bands has come about because of new developments in surface analysis technology and newer classes of materials.

In this work, a focused investigation to examine the formation of Lüders bands in industrially relevant conditions is presented. These conditions include using common bake-hardenable sheet steels, with variations in strain-state, and different galvanized and galvannealed coatings. Each factor is examined to better understand their influence on Lüders band appearance. Mechanical testing and surface profilometry are the primary methods employed to analyze Lüders band appearance. Specialized equipment and methods developed to analyze Lüders bands in-situ and under load are also discussed.

Lüders band formation on zinc coated sheet steels was considered. The topographies of the bands were recorded with a three-dimensional optical profilometer. From these topographies, Lüders band characteristic dimensions were determined and comparisons of these characteristics are made between each industrially relevant condition.

This investigation is intended to support steel industry efforts to reduce yield losses, thereby reducing cost, energy usage, and environmental impact. Yield losses occur when product is rejected “in-house” or by the customer during manufacturing, and opportunity costs arise through conservative steel product designs and production practices that steel manufacturers may employ to avoid YPE.

The following sections present a review of background literature concerning Lüders band formation, experimental methods and procedures conducted to determine Lüders band characteristics, results of the Lüders band characteristics, and discussion of the results.

2.0 BACKGROUND

The surface quality of exposed steel is important to the modern steel industry. The formation of Lüders bands was a surface imperfection of historic concern, and still remains one today. Lüders band formation was noted in mild steel over 150 years ago by Piobert[2] and later by Lüders,[3] in 1842 and 1860 respectively. Over the years these features have been referred to as stretcher strains, Hartmann lines, the Piobert effect, flow lines, and strain figures.[4,5] These surface imperfections are most commonly referred to as Lüders bands when formed in uniaxial tension, and stretcher strains when the strain path is more complex. No matter what their name, they result from non-uniform yielding during a forming process. Much research has been conducted to better understand this yielding phenomenon and the macroscopic, microscopic and microstructural aspects of Lüders band formation (for example see Hall[6]). The process of understanding was aided with improvement of technology, experimental procedure and equipment. Currently, improvements in surface metrology are thought to provide new opportunities for topographical analyses of Lüders bands generated in coated automotive sheet steels.

In the following sections, factors that affect non-uniform yielding and its analysis are discussed. These sections include discussion about strain paths, yield point elongation, static strain aging, temper rolling of sheet steel, dislocation dynamics, Lüders bands, optical methods used to identify Lüders bands, and current optical metrology capabilities.

2.1 Sheet Steel Strain Paths

The complex geometry of exposed auto body panels can induce a wide range of strain in the sheet. Strains in sheet are described by two principal surface strains: the major strain and the minor strain, ε_1 and ε_2 respectively. Figure 2.1 indicates the characteristics of these strains relative to uniaxial loading. The major strain is always positive while the minor strain can be positive or negative. In many cases, the ratio of ε_2 to ε_1 is used to describe the strain path. There is a continuum of strain ratios in complex

forming operations with several named relationships: uniaxial, plane strain, and balanced biaxial as indicated by Figure 2.2. The strain-states on the left side of the figure are considered to represent "drawing" of the sheet, while those strain-states on the right side are considered to represent "stretching" of the sheet.

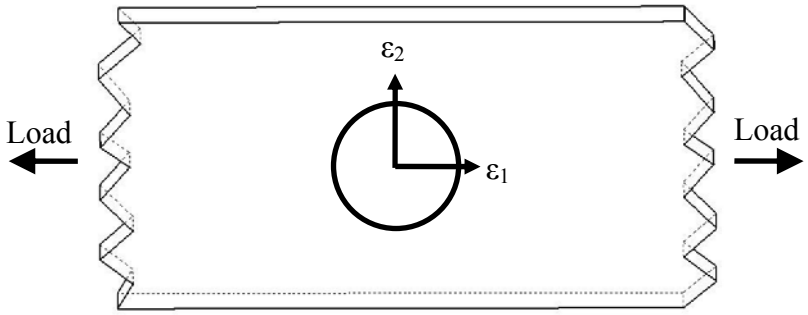

Figure 2.1 Orientations of the major strain and the minor strain in sheet metal forming in a uniaxial tensile test.

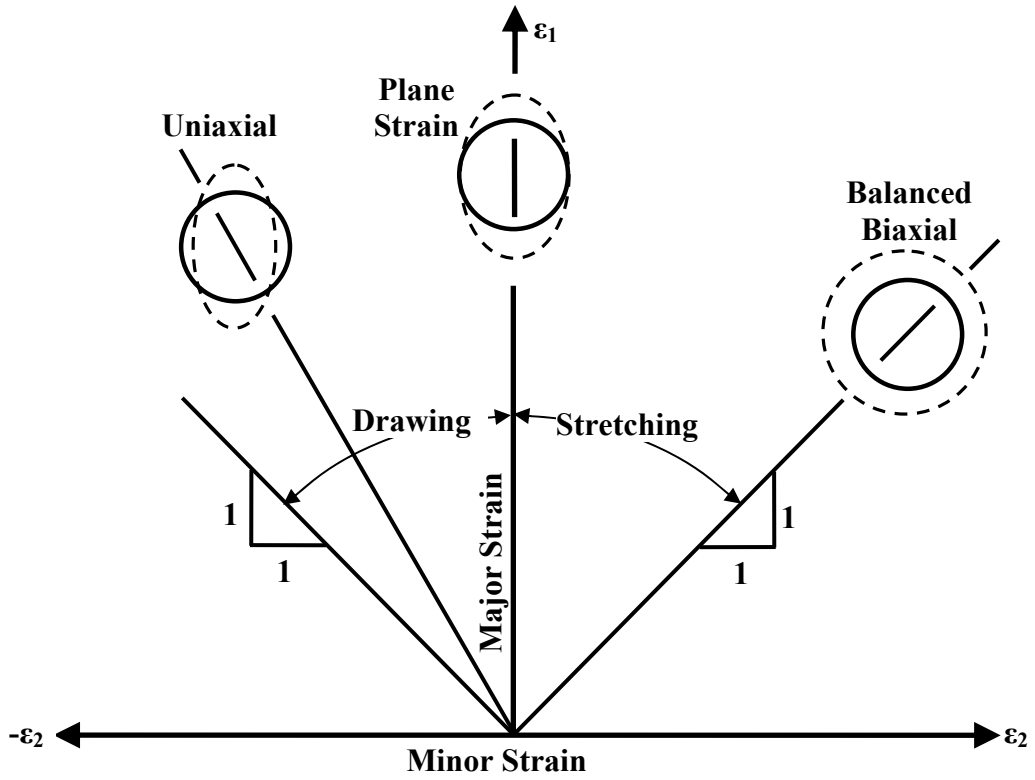

Figure 2.2 Common strain paths for sheet metal forming. Dashed ellipses represent as-formed shape of original solid circles. Illustration reproduced from similar representation by Marciniak.[7]

2.1.1 Uniaxial Tension

Uniaxial tension occurs when a sample is loaded in only one direction. In a homogenous isotropic material the ratio between ε_2 and ε_1 is -0.5. Engineering materials can deviate from this value because of geometry and inhomogeneities within the material. Uniaxial tension is commonly used to determine mechanical properties of materials. The behavior of the material during deformation is noted by strain (relative change in length) and a corresponding stress (load per unit area of the sample) plotted as a continuous curve. The deformation behavior of the metal is broken between an elastic region of recoverable deformation, and a plastic region of non-recoverable deformation. Of primary concern in this investigation is the transition between these two regions, the yield point.

2.1.2 Plane Strain

The plane strain condition exists when ε_2 is zero. When loaded in one direction, this condition occurs when the dimension of the sample in the ε_2 direction is sufficiently large to resist deformation.

2.1.3 Balanced Biaxial Tension

Biaxial tension occurs when a sample is loaded in tension in more than one direction. During industrial forming of automotive panels, biaxial strain paths are more common than uniaxial strain. Biaxial tensile strain and stretch forming occur when the ratio between ε_2 and ε_1 is greater than zero. These strains can vary, but when they are equal, a balanced biaxial strain is achieved. In a laboratory setting, different "strain ratios" can be created by varying the dimensions of uniaxially loaded test samples or by using specialized equipment to impose load or strain in more than one direction.

2.2 Yield Point Elongation

It is common for many mild and low carbon steels to exhibit non-uniform yielding. Figure 2.3 shows a schematic of a stress-strain curve of mild steel at yielding. An important feature of the curve is the transition from the elastic region to plastic deformation via a decrease in stress (load drop). At this point, a local maximum is found, the upper yield stress (UYS). On the sample surface, the load drop is associated with the nucleation of localized plastic flow. The material continues to increase in length through formation and subsequent broadening of bands of local plastic deformation, without increasing the applied load and thus the calculated applied engineering stress. This applied engineering stress value is the lower yield stress (LYS). Once deformation (broadened bands) has spread over the sample gage length, the stress in the sample rises rapidly due to homogenous deformation and strain hardening.

Yield point elongation (YPE) is the difference in strains between the strain at UYS and the strain at the end of LYS region. YPE is commonly expressed as an absolute strain percent. In low-YPE materials, the transition from the LYS to homogenous deformation can be difficult to determine, so the following definition from ASTM E8-04 (section 3.1.4) and Figure 2.4 are used:

> …in a uniaxial test, [YPE is] the strain (expressed in percent) separating the stress-strain curve's first point of zero-slope from the point of transition from discontinuous yielding to uniform strain hardening. If the transition occurs over a range of strain, the YPE end point is, the intersection between (a) a horizontal line drawn tangent to the curve at the last zero-slope and (b) a line drawn tangent to the strain hardening portion of the stress-strain curve at the point of inflection. If there is no point at or near the onset of yielding at which the slope reaches zero, the material has 0% YPE.[8]

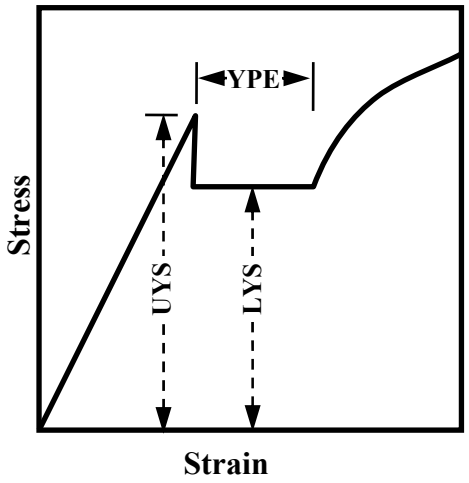

Figure 2.3 Schematic representation of stress-strain behaviors of mild steel at yielding defining elongation upper and lower yield strengths.

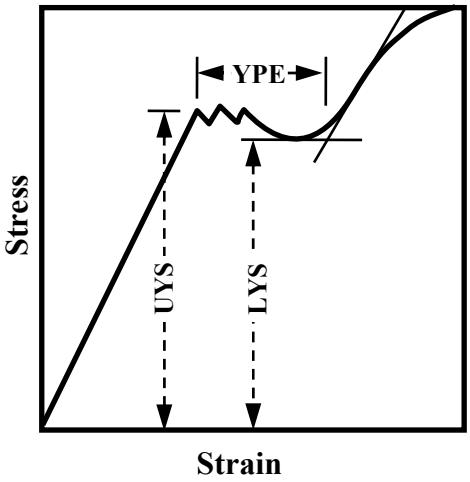

Figure 2.4 Stress-strain diagram showing yield point elongation upper and lower yield strengths, reproduced from ASTM E8-04.[8]

2.3 Static Strain Aging

The yield drop and YPE in mild steel are closely associated with static strain aging, which can occur during material storage. In 1948, Cottrell and Bilby proposed that during aging, interstitial atoms diffuse to dislocation cores to relieve strain energy in the crystalline lattice.[9] Interstitial migration is enhanced by favorable conditions of higher

temperatures and longer times. The interstitial atoms form an atmosphere around the dislocations, and increase the energy needed to move the dislocation through the lattice. When this occurs dislocations are considered pinned.[9] The rate of atmosphere formation was proposed to be proportional to aging time to the 2/3 power at constant temperature.[9]

Cottrell's and Bilby's original theory concentrated on long-range diffusion of interstitial atoms, but short-range diffusion of interstitials, called Snoek ordering, is now thought to precede atmosphere formation. Snoek ordering is the short-range diffusion of interstitial solute atoms to favored octahedral sites under stress.[10] Snoek ordering may also impede dislocation motion.[11,12] The final step of dislocation pinning involves precipitation of carbides and nitrides on dislocations.

Any atom which is interstitial in α-Fe can contribute to low-temperature dislocation pinning, reportedly including H,[13] B,[6] N, and C. The diffusion coefficient and size of these interstitial elements control their effectiveness to pin dislocations.[14] H and B are only reported to be effective at very low temperatures where atom mobility is low.[15] At and just above room temperature, N and C are very effective at pinning dislocations.[16]

Static strain aging is an interest and concern for the steel production industry. Aging increases the UYS of a material and it also causes non-homogenous yielding. These two factors are principal in bake-hardenable sheet steel products. Bake-hardenable material is desired to yield continuously when forming. After forming, exterior paint is applied and heated at 170 °C for 20 min, until the paint is cured. Simultaneously, the material undergoes static strain aging, increasing the yield stress and dent resistance of the panel.[17] The N content of steel can be controlled by stabilizers such as Ti and Al. In this process, solute C is the primary element used for bake-hardenablility.[17,18]

2.4 Dislocation Dynamics

In a material which has undergone static strain aging, a decrease in stress after yielding is often noted. Cottrell and Bilby proposed that this decrease is caused by pinned dislocations breaking away from their atmospheres, and that the stress needed to propagate free dislocations is lower than the stress needed to free them. The theory continues that once a dislocation is mobile, local stresses help promote neighboring

dislocations to break free. A cascading effect of mobile dislocations leads to the decrease in flow stress.[9]

An alternative theory of load drop was proposed by Hahn in 1962.[19] He theorized that the yield drop was due to a rapid generation of dislocations and a relatively low stress dependence of dislocation velocity. Other experimental work demonstrated that dislocations are generated from grain boundaries.[20,21,22] This supports Hahn's theory, because dislocation unpinning would initially generate dislocations in the bulk of the grain. Hahn's theory does not exclude dislocation unpinning, however. Wilson found that after the first stage of atmosphere formation, dislocations can be unpinned, but after precipitation formation, new mobile dislocations must be generated.[23] Other investigations suggest that unpinning is difficult even when associated with solute atmospheres.[24,25]

2.5 Lüders Bands

The load drop in a uniaxial test corresponds to a formation of locally yielded regions in the sample. This local yielding is associated with a Lüders band, which can have a variety of appearances. Under stress, Lüders bands form and propagate across the length of the sample. As they propagate, the material goes through a distinct strain profile.

2.5.1 Lüders Appearance

Lüders bands are most frequently described as a "surface" phenomenon. There are many metallurgical and experimental factors which affect their appearance, such as grain size, strain rate, free interstitial concentration and sample geometry.

Simple Lüders band appearances (Figure 2.5a) are formed in uniaxial tension at low strain rates, with small grain diameters, small cross-sections (width and thickness), and large gage lengths.[26] Lüders bands can cause "kinks" to develop in tensile samples. Low bending constraints such as small width and thickness, and longer lengths, allow the samples to comply with these kinks without generating stress concentrations. Fujita and

Miyazaki found that samples with greater than 10 grain diameters in thickness had a well defined band structure.[27] It is possible to nucleate and propagate a single Lüders band across the full gage length.[26] If a single band is propagated, it can have a very sharp, planar interface distinguishing yielded and unyielded material (Figure 2.5a).

Lüders appearance can be complex. Large sample dimensions and biaxial forces can create local stress concentrations leading to simultaneous nucleation of multiple bands. Multiple bands can form patterns with varying complexity. The patterns may be crosshatched arrays with bands formed at regular intervals and oriented in specific directions. More complex networks of bands can also develop that are not uniformly spaced and are not at the same orientations (Figure 2.5b). These networks are usually classified as stretcher strains.

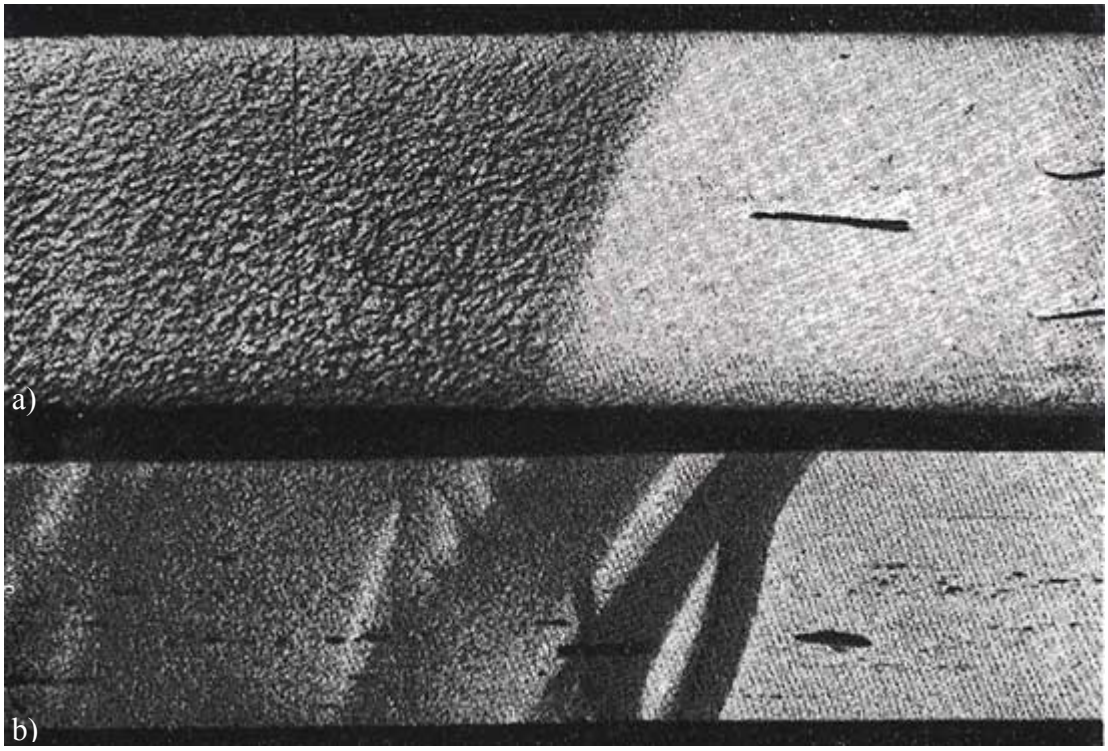

Figure 2.5 Lüders bands in uniaxial tensile samples: a) single Lüders band propagating across sample; b) complex network of Lüders bands propagating across sample.[30] (Note: background interference contrast is an artifact in the reproduced images.)

Samples with polyhedral cross sections have been used to determine the internal plane on which Lüders bands appear. Angle measurements of Lüders bands relative to the sample edges (α and β in Figure 2.6) are used to determine the internal plane normal (or "band front"), and its angle to the tensile axis (θ in Figure 2.6). The polyhedral cross sections include rectangular,[28,29] square,[28] octagonal,[28] hexagonal,[28] rhombohedral,[29] and pentagonal[30]. Results have reported the angle to be 45° [29], 45° to 55° [28] and 48° ± 1.5° [30]. Deviations from the angle are assumed to be due to moments generated from kinks and grip effects.[28,30] Explorations into complex stress states have shown that Lüders bands form along the plane of maximum shear,[31] which further supports the 45° angle, the plane of maximum shear in uniaxial tension (in an isotropic material).

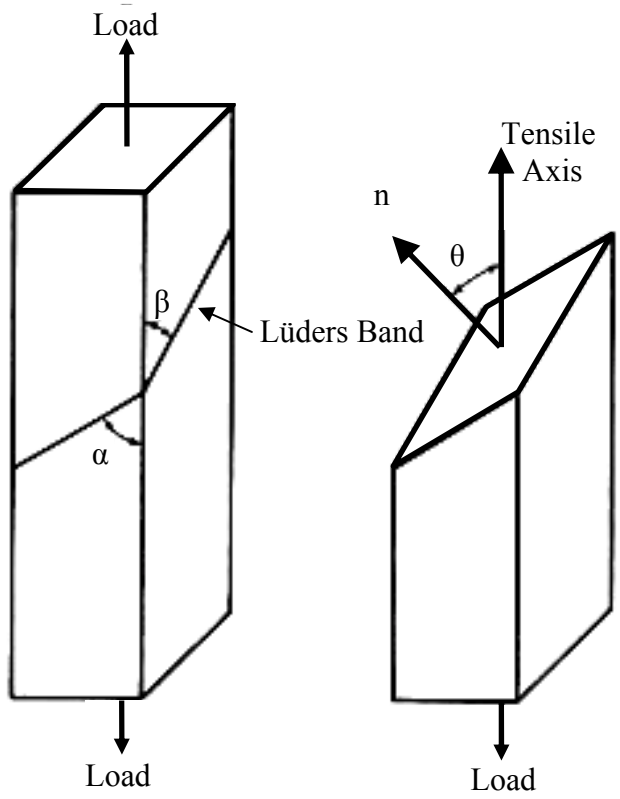

Figure 2.6 Schematic illustration of Lüders band which forms on different faces of samples with polyhedral cross section. Using the angles of band orientation to the sample edges (α and β), the orientation of a plane normal (n) containing the Lüders bands can be calculated.[28]

2.5.2 Lüders Band Initiation

Lüders bands are nucleated at stress concentrations. Stress concentrations can be caused by macroscopic geometry changes[5] or internal incompatibilities of elastic modulus (grain misalignment, inclusions, etc.)[22,28]. It is hypothesized by Friedel that local deformation starts at the stress concentration and expands out across the sample (Figure 2.7).[32] The local deformation increases stress in neighboring grains, causing them to yield.[19]

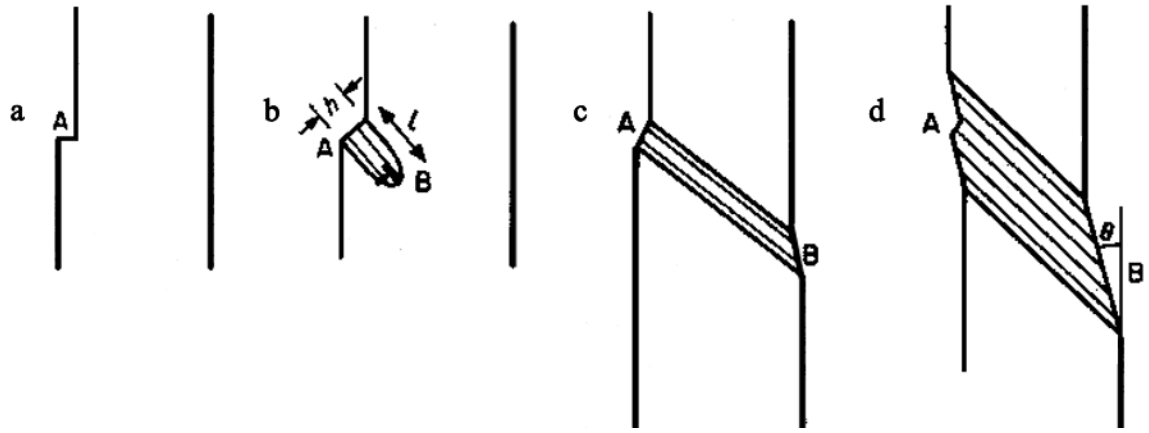

Figure 2.7 Process of Lüders band nucleation; a) ledge (A) causing stress concentration and nucleation, b) dislocation pileup at B raising local stress, c) band traverses to opposite side of sample, d) Lüders band begins to broaden.[32]

2.5.3 Lüders Propagation

Propagation of a Lüders band occurs when a nucleated Lüders band deforms nearby material. The moving deformation region is known as the band front. The deformation can traverse the entire gage length in a uniaxial test (if there is a single Lüders band), or propagate until it intersects another Lüders band. Most systematic studies of Lüders band propagation were conducted with a single band in the sample.

With a single band, a noticeable kink develops at the band front, illustrated in Figure 2.7d, and Figure 2.8. The angle of kinking (θ in Figure 2.7d) has been found to be on the order of 1°[26] and decreases with an increase in grain size.[33,34] This kink generates bending stresses in the sample, which help to stabilize the propagation of the band front.[28,30,35]

Theories have developed describing the non-uniform deformation of the Lüders band as a large scale shearing phenomenon, affecting the whole cross section nearly simultaneously. The orientation of the front and geometrically induced kink is close to the plane of maximum shear.[26,28,30] Explorations into complex stress states have shown that Lüders bands form along the plane of maximum shear.[31] Further support for a macroscopic shear mechanism is the observations that after the passage of a Lüders band, a tensile sample with circular cross section becomes elliptical in cross section.[5] A pure shear mechanism does not completely explain an observed reduction in cross sectional area,[26] so a second step is also theorized, whereby the sample elongates (reducing in cross sectional area) after shearing i.e. tensile strain. The mechanism of elongation is considered to be a decelerating flow under constant stress and has been called a creep phenomenon.[28,30,36]

Literature shows that the propagation of a Lüders band is believed to be a multi-component process. Each of these mechanistic components was investigated by different authors. Hahn makes a conjecture that as a Lüders band is formed, "dislocations generated within the band are injected a small distance into the surrounding matrix".[19] This region can be considered the band front. Experimental observations by Worthington and Smith and by Carrington and McLean have shown that slip lines develop prior to macroscopic yielding[20] and form at the band front.[21] The slip lines indicate generation of mobile dislocations forming at grain boundaries, preceding the Lüders band. An increase in mobile dislocations can initially reduce the grain's resistance to flow, seen as work-softening.[37] Work softening localizes deformation at a high strain rate.[38] The amount of strain in this local deformation was calculated by Hart[39] and Hahn[19] and experimentally determined by Prewo *et al.*[38] and Iricibar *et al.*[40] to be a value which is the Lüders strain. Beyond this strain value, the material in this region begins to work harden.[21] With work-hardening, the flow strength in the deforming region increases to the yield strength of the

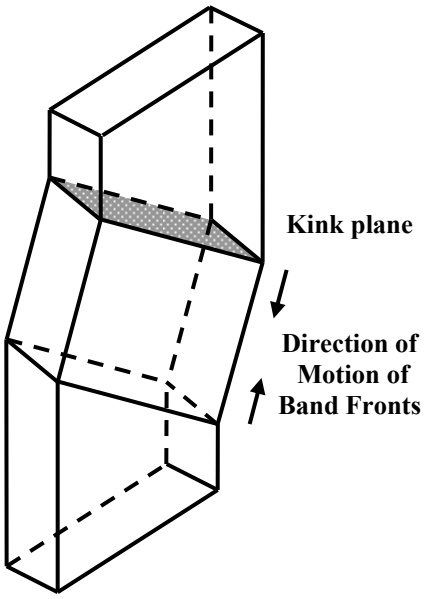

Figure 2.8 Kink formation in a propagating Lüders band fronts. Illustration reproduced from Sylwestrowicz and Hall.[5]

neighboring undeformed region.[41] Eventually, the neighboring grains are induced to flow and the process continues. Each yielded region grows larger as the band propagates.

Numerical models of Lüders band propagation use continuum descriptions for simplicity.[19,39] Alternatively, mechanistic theories of Lüders band propagation propose that propagation occurs through the incremental annexation of discrete volumes of nearby material.[21,27,42] In general this annexation distance is on the order of a grain. Iricibar *et al.* also theorized that the band front moves by "annexation". Their results indicated that the band front moved via a series of ledges (approximately a grain diameter wide) from one side of the sample to the other (Figure 2.9). This theory is able to explain the formation of a kink without appealing to the pure shear mechanism (previously mentioned).[40,43] The ledge mechanism was further explored with finite element models. The models predicted that the ledge mechanism required lower stresses to propagate (therefore a more stable front) compared to a straight elastic-plastic interface which resembles the shear mechanism of propagation.[44]

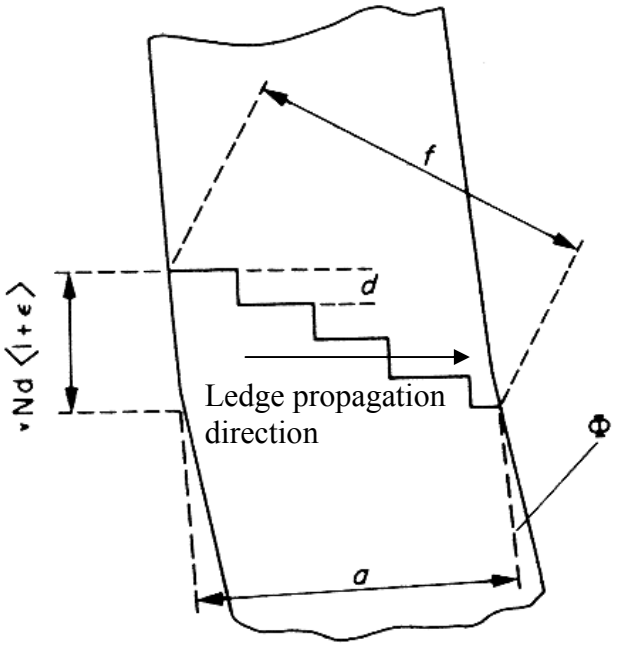

Figure 2.9 Kink developed from ledge propagation model, each ledge is d wide (approximately a grain diameter) and total kink misorientation angle is θ (schematic).[43]

The velocity of a band front is proportional to the macroscopic strain rate,[39] internal stresses, mobile dislocation velocity,[45] and inversely proportional to the number of bands present in the sample.[46] Higher stresses are needed to induce higher velocities.[35] It has been noted by Conrad and Stone that these stresses are the local "effective" stress at a band front, and not the stress applied to the sample.[47] Prewo *et al.* summarize the relationship between front velocity and mobile dislocations as, "[the front velocity]…is directly proportional to the product of the mobile dislocation density and average dislocation velocity, and inversely proportional to the strain gradient."[38]

If a uniaxial test is paused part way through the propagation of a Lüders band and load is maintained, the band is found to propagate during stress relaxation. This propagation distance can be on the order of 50 grain diameters in length.[48] Prewo *et al.* suggest that during stress relaxation, when the local "effective" stress at the band front decreases to the propagation stress of the band, the band stops propagating.[38]

2.5.4 Lüders Strain and Profile

It is commonly held that material which undergoes non-uniform yielding by Lüders band deformation is strained by an amount equal to the YPE of the material.[19,39] This strain amount is called the Lüders strain. The functional relationship of instantaneous plastic strain relative to the position of a Lüders front was determined using extensometers (Figure 2.10).[40,48] The profile within a Lüders band starts at the band front and is shown relative to the distance behind the front. The strain imposed by the Lüders front increases rapidly until it is brought to a uniform strain equal to the Lüders strain.[38,49] The Lüders strain can be affected by the front velocity and will increase with a faster moving front,[5,45,48] consistent with a higher observed YPE at high strain rates.[50]

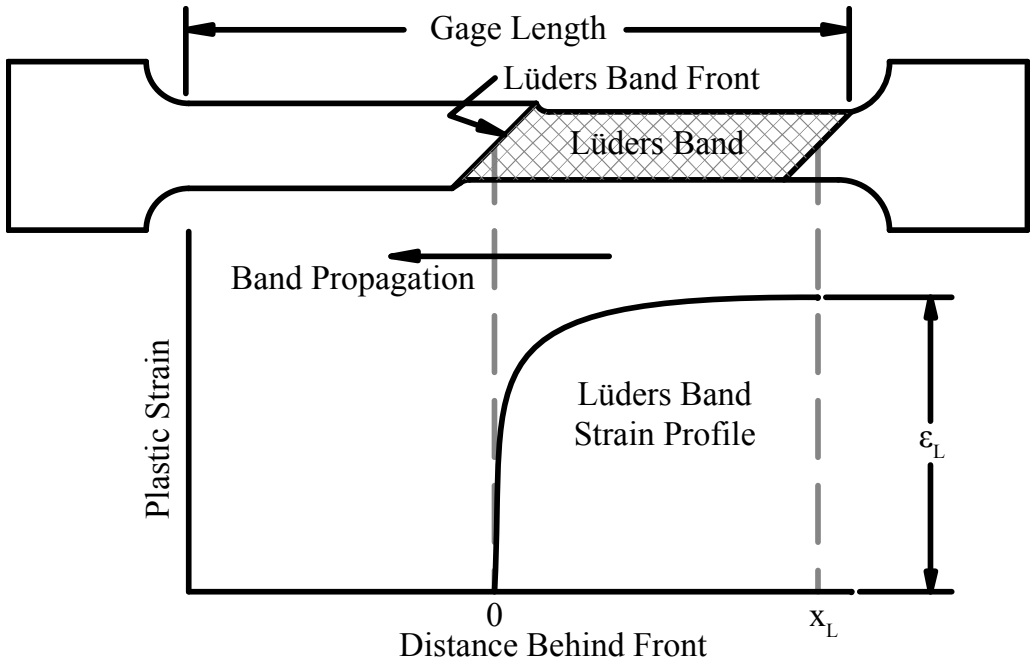

Figure 2.10 Schematic representation of a specimen and associated strain distribution along the tensile axis for a single propagating Lüders band front (with Lüders strain, ε_L and distance behind the front, x_L.[19,49]

2.6 Visual Characterization of Lüders Bands

Many optical methods have been used in order to study Lüders bands, specifically their formation and propagation. These fall into two classes, stationary and dynamic.

Stationary methods generally require removal of specimen from the load frame during a test in order to determine useful information about the surface or microstructure. They also generally require a referencing method such as scratches,[26,38] grids,[38] or microhardness indents.[51] These markings help to identify points of interest relative to a point on a surface.[52] Dynamic methods generally identify bands in-situ, while the sample is still attached to the tensile test frame. Verel and Sleeswyk[48] reviewed common dynamic methods and found them to include: application of StressCoat™,[35,42] application of electroplated coating, using the optical "Töpler Schlieren" method, and affixing transducers.[40,48] Each dynamic method will be explained in turn.

Polishing the sample prior to testing is one of the most common methods of observing Lüders bands dynamically.[28,29,48,52,53] Because Lüders bands are a localized deformation, variations in the reflectivity of the surface indicate the presence of Lüders bands and band fronts.[5] In a different method, Verel and Sleeswyk projected a grid onto the polished surface of a tensile sample.[48] As the material deformed and roughened, the reflection of the grid pattern was not reflected back to the observing camera. By tracking the disappearance of the grid, Verel and Sleeswyk were able to track the progression of a Lüders front.

Hall recorded band movement via the "Töpler Schlieren" illumination method.[26] A light was projected onto a wire sample which cast a partial shadow onto moving photographic film (a rotating drum camera). Variations in the edge (drawing marks, scratches, flecks of rust etc.) generated a "spotted optical image". As the drum camera rotated, these spots were represented as lines of light and dark patterns on the film. By tracking the progress of these lines, the movement of the band front was tracked.[54]

Brittle coatings such as electroplating or StressCoat™ identify Lüders bands by cracking when the substrate undergoes non-uniform deformation. Of interest to the present investigation is the use of StressCoat™ to identify non-uniform yielding. StressCoat™ is a brittle lacquer coating applied via atomized spray to the sample. When dry, the coating is brittle, semi-transparent and amber in color. Deformation of the sample near the yield strain causes the coating to crack. Using oblique lighting, the cracks in the coating appear as discolorations, changing color from amber to a lighter yellow.

StressCoat™ on non-uniformly yielding samples cracks at the locations of non-uniform yield, clearly indicating the points of Lüders band formation.

Iricibar, Mazza and Cabo[43,55] used a direct interferometry technique to analyze surface variations on a polished surface due to Lüders band deformation. Interferometry uses the interference (constructive and destructive) properties of coherent light. Bright and dark bands (fringes) are formed, indicating changes in surface height relative to the angle of the camera. On a polished surface, interference fringes are equally spaced apart. If the surface deforms, such as during the passing of a Lüders band, the fringe pattern changes the image, and movement can be analyzed to indicate the change in surface height.

2.7 Surface Topography Analysis

Recent developments in surface metrology technology should allow for new methods to be applied in the optical analysis of Lüders bands. A Lüders band's surface topography perhaps can be recorded directly, and subsequently analyzed. On a macroscopic scale, materials have a general form and shape, the overall geometry. As the scale of observation is magnified to microscopic dimensions, the variations in the heights of the surface become apparent. The variations can be separated into different components based on length scales. Descriptive parameters can be used on in order to numerically describe the surface topography, and different components. These parameters help to characterize the surface.

2.7.1 Surface Topography Components

Variations in surface heights can be broken into components based on length scales. Schaffer explains surface texture, stating:

> "Consider a theoretically smooth flat surface. If this [surface] has a ... small hollow in the middle, it is still smooth but curved. Two or more equidistant such hollows produce a wavy surface. As the spacing between such waves decreases, the resulting surface would be considered flat but rough. In fact, surfaces having the same height of irregularities are

> regarded as curved, wavy, or rough, according to the spacing of these irregularities.… Surface texture includes closely spaced random roughness irregularities and more widely spaced repetitive waviness irregularities."[56]

Curvature, also known as form, is a function of very widely spaced "irregularities" (features). In Figure 2.11, a two-dimensional representation of a surface was broken down into three profile components with appropriate spatial wavelength cutoffs for roughness, waviness, and form.[57] Individual Lüders bands have been observed to be on the order of 1 mm in width after formation.[52] Based on this spatial length, Lüders bands could be classified in the waviness profile.

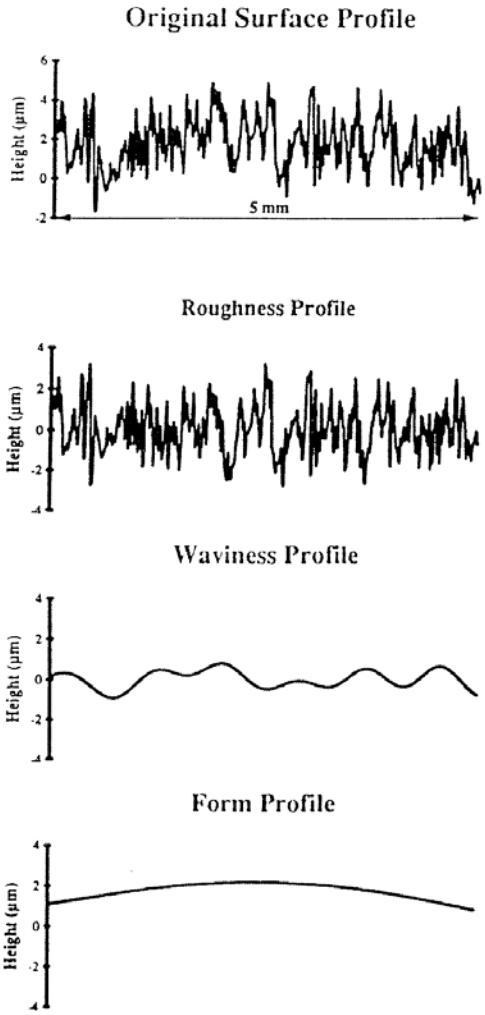

Figure 2.11 The decomposition of a profile into roughness, waviness, and form. The addition of the three components yields the original surface.[57]

2.7.2 Surface Measurement with Optical Interferometry

The measurement of surface topography is conducted with a surface profilometer. Measuring topography, such as a Lüders band, allows for quantitative analysis of the characteristic geometry of the surface. For the current investigation, surface profiles were recorded with a three-dimensional optical interferometric profilometer. An interferometric profilometer measures surface heights over a scanned area, generating a three-dimensional surface profile. Figure 2.12 illustrates the various components of a vertical scanning interferometer. Interferometric measurements use the constructive/destructive property of parallel light to locate the surface height of each point on a surface. Lippold and Podlesny state, "Light reflected from a reference mirror combines with light reflected from a sample to produce interference fringes, where the best-contrast fringe occurs at best focus…."[58] This method has a very high vertical resolution, less than the wavelength of light. Optical measurement methods are limited when a reflective surface is angled very steeply or when the surface is non-reflective. In these cases, the light impinging on the sample does not return to the camera for analysis. This physical characteristic acts as a low pass filter, removing some high angle features.

2.7.3 Numerical Analysis of Surface Profiles

Two- and three-dimensional parameters are based on mathematical manipulations of height values obtained from a surface. These manipulations are done with the intention of being able to compare surfaces without retaining the original data. These surface parameters, most notably the surface roughness, correlate with performance attributes.[59]

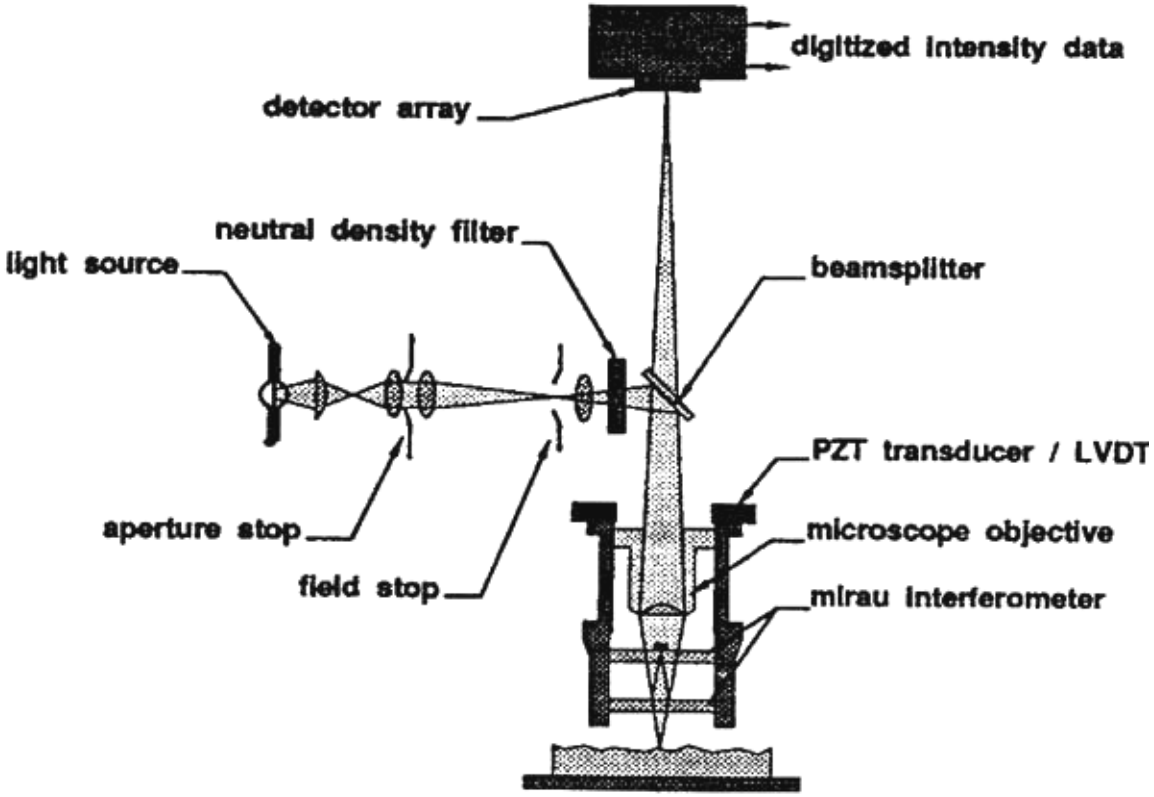

Figure 2.12 Schematic illustration of an interferometric profilometer.[58]

Analysis of surface parameters can be tuned to emphasize desired length scales of the surface. This is analogous to high and low pass filters for electrical signal processing. In a two-dimensional analysis, an average line, or fitted polynomial is used to remove general tilting or low frequency waveforms (curvature) from the sample surface (Figure 2.13). The average line can either be a linear least-squares line, or a polynomial function. The difference between the values of the fitted polynomial and a base (horizontal) line are then subtracted from the surface profile data. The resulting profile is centered about a flat reference plane. On a three-dimensional surface, a least-squares plane is calculated and then removed from the data in an analogous way. Other reference surfaces can be removed from three-dimensional data including cylindrical and spherical surfaces (Figure 2.14).

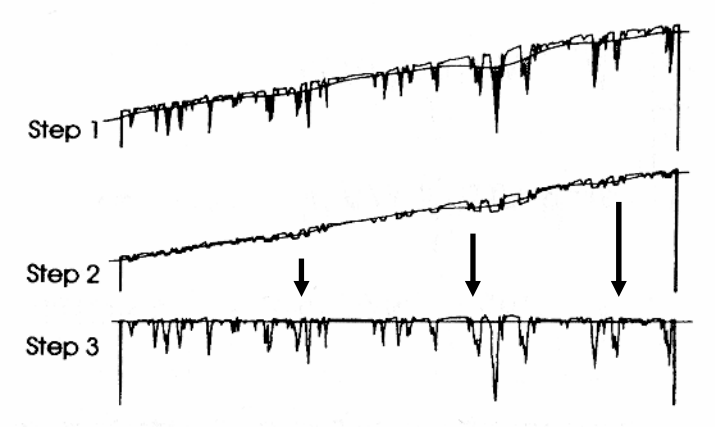

Figure 2.13 Steps to remove surface tilt in two-dimensions. Step 1: define least-squares or polynomial reference line; Step 2: subtract values corresponding to the reference; Step 3: plot remaining data.[60]

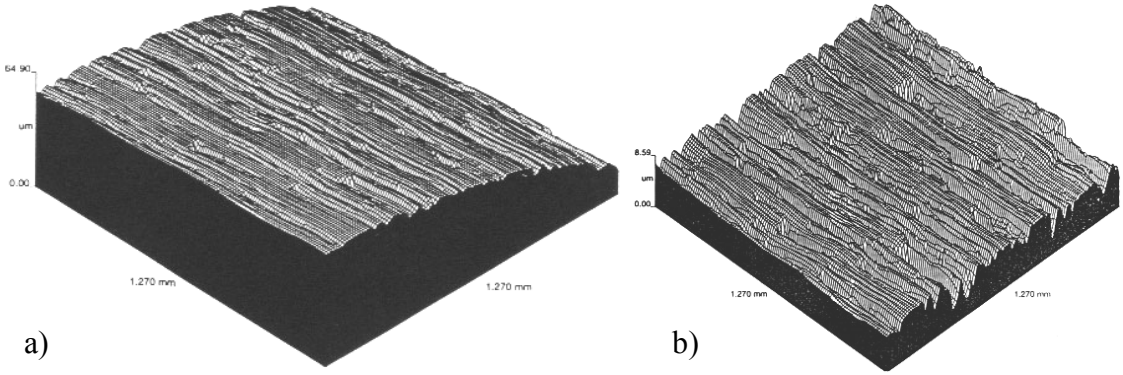

a) b)

Figure 2.14 Three-dimensional topography of gear tooth a) original; b) with curvature terms removed. [61]

2.7.4 Prior Investigation of Lüders Band Surface Topography

Humble[52] used three-dimensional optical profilometry to study the evolution of Lüders bands in on uncoated and polished bake-hardenable sheet steel. The samples were artificially aged to exhibit multiple levels of YPE. He found that bands develop and propagate in three stages, nucleation, propagation into the sample thickness, and propagation laterally across the surface. The most "severe" topography of a Lüders band was considered to be a condition of maximum Lüders band depth, and consequently the condition most readily visible to the naked eye. He found that the most "severe"

topography was observed at early strains, at the transition between the Lüders band growing into the sample and growing across the sample. After larger strains than the nucleation strain, residual topography of the Lüders band remained. The depth of the Lüders band also increased linearly with increasing YPE.

2.8 Temper Rolling of Material Containing YPE

Temper rolling, through a reduction up to about 1-2 %, has been found to be an effective means of removing YPE from sheet steel. This reduction creates a material with a stress gradient through the thickness of the material, with stress components parallel to the longitudinal axis; compressive stress states are at the surface and tensile stresses are more central. It is held that residual stresses help to mask YPE when the material is deformed.[62,63] The amount of residual stored elastic surface compressive strain of a material with 1.5 % reduction was -0.01 % strain, as determined by X-ray diffraction.[64]

There is some debate over the mechanism for the masking of YPE by temper rolling, but all theories agree that residual stresses/strains are responsible. Residual stresses and corrosponding strains have been discussed in literature as macrostrains and microstrains.[63] Macrostrains have been shown to develop in the rolling direction, directly influenced by the residual stress gradient.[63] Microstrains are intergranular strains and tend to develop in the transverse direction.[63]

In an early theory, Hundy[63] believed that the yielding in tension of temper-rolled sheet takes place progressivly at increasing applied stresses. Material fibers, oriented longitudinally, first yield in the residual tension layers and deformation progressively transfers into the residual compression layers. A band cannot form through the thickness of the material because of this progressive yielding.[63] Other experiemental data has determined that macroscopic residual stresses are not responsible, or are a minor effect for masking YPE.[14,53] The microscopic residual stresses are found to contribute more to masking.

Temper rolling at a reduction of less than 3% does not deform 100% of the volume of the material.[65] It has been documented that small bands of yielded (~180 μm wide) and unyielded (~500 μm wide) material are found after rolling, oriented

perpendicular to the rolling direction.[53] Uniaxial tension in the longitudinal direction apparently yields the previously unyielded regions first, and distributes strain among many closely spaced regions.[53] At higher deformations, the sample surface can roughen and form periodic surface imprefections because of the non-uniform yielding, as noted by Chatfield and Beiser.[66] The magnitudes of imperfections are a function of the amount of temper rolling reduction.

The return of YPE in temper-rolled samples is different for longitudinal and transverse samples. YPE returns in the transverse direction before the longitudinal direction when the rolling reduction is less than 2-3 %. For larger reductions, the reverse is true.[14,53] This point of transition coincides with the material being deformed throughout the thickness during temper rolling.

2.9 Lüders Band Formation in Cup Drawing

Butler and Wilson have explored Lüders band appearance during the deep drawing of a cup. They have noted what they consider biaxial loading, Lüders bands tend not to be well defined, even after prolonged aging of the steel prior to forming. Compared to appearance in biaxial tension, in uniaxial tension Lüders bands become more sharply defined with increased aging.[26] For the cup drawing process, an increase in strain rate makes the bands more visible, and they appear more evident perpendicular to rolling direction (Figure 2.15).[53] These observations were the only specific comments found in the literature concerning Lüders band appearance in strain states other than uniaxial tension.

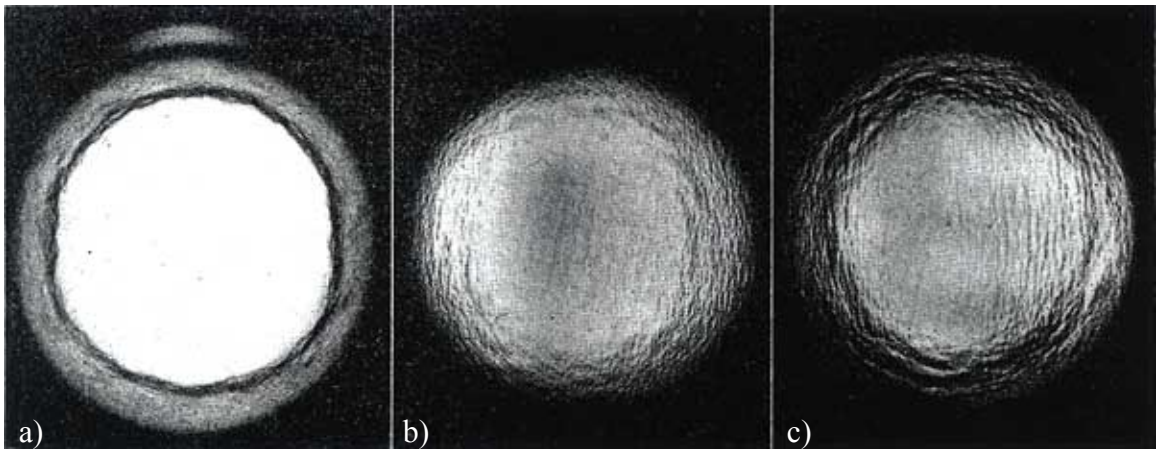

Figure 2.15 Lüders band development in cup drawing operation. Bottom of cup shown. The temper rolling direction is horizontal with respect to figure. a) approximately circular band front produced, annealed condition; b) non-homogenous yielding pattern seen in bottom and edge of cup, temper rolled 1.2 %, aged at room temperature for 6 months, punch speed 2 ft/min c) non-homogenous yielding pattern increased and formed perpendicular to rolling direction, temper rolled 1.2 %, aged at room temperature for 6 months, punch speed 65 ft/min.

3.0 RESEARCH OBJECTIVES

The research performed for this investigation was designed to provide an improved understanding of surface changes experienced during non-uniform yielding. Surface changes were to be analyzed on zinc coated, low carbon sheet steel with controlled amounts of YPE. The surface changes of concern were the evolution of Lüders topography and the condition of the most severe Lüders topography. Three-dimensional optical profilometry was used to capture Lüders band topography and related characteristics. The materials selected were galvanized/galvannealed bake-hardenable sheet steels because of their current industrial relevance as exposed surface critical material.

The relationships between the topography of Lüders bands and several industrially relevant conditions were chosen for evaluation. These conditions included systematic variations in YPE, several zinc coating types, varying strain paths, sample orientation to rolling direction, and material thickness. Additionally, the investigation was to provide methods and equipment to evaluate Lüders band formations in-situ in an optical profilometer.

4.0 EXPERIMENTAL PROCEDURES

A procedure was created to facilitate the generation of data in order to achieve the research objectives. Materials were selected to provide a variety of zinc coatings. Samples for different strain paths were machined from these materials. YPE levels were varied in the machined samples. Samples were subsequently deformed using appropriate methods to generate Lüders bands. The topographies of these Lüders bands were measured, and characteristic geometries were determined. The following sections detail the components of the above steps of the procedure.

4.1 Material

Three commercially produced 210 MPa bake-hardenable sheet steels and one low carbon sheet steel were selected for this investigation. These materials were chosen because of their use in different surface critical applications. Each material would exhibit YPE if the manufacturers did not take preventive steps.

Each material was provided by different commercial manufacturers. The three bake-hardenable steels were provided with different zinc coatings. These coatings included electrogalvanized (BH210 EG), galvannealed (BH210 GA), and spangle free hot-dipped galvanized (BH210 GI). These bake-hardenable materials were nominally 0.76 mm (0.030 in) thick and temper-rolled prior to shipping. The low carbon sheet was provided with a spangled hot-dipped galvanized coating (LC GI). It had a nominal thickness of 1.52 mm (0.060 in), and was not temper-rolled prior to shipping. In addition to the four selected materials in the project design, a fifth material was also used for the purpose of developing deformation techniques in biaxial strain. The extra material developed high levels of YPE and produced Lüders bands that were easier to identify than Lüders bands developed in the four test materials at the 1.0 % target YPE level.

The heat chemistries of each material, as provided by the suppliers, are given in Table 4.1. Other material properties are included in Table 4.2. The yield stress was obtained from transverse samples and is quoted at a 0.2% offset for all materials. The

quoted value for LC GI was the lower yield strength. Grain sizes of substrates were determined using a single circle intercept method. Light optical micrographs of as-received materials show ferritic microstructures (Figure 4.1). The application weights of the zinc coatings were approximately 60 g/m^2 per side, resulting in an approximate nominal thickness of 8.3 μm. Apparent thicknesses measurements of a single side were determined using light optical micrography and are presented in Table 4.2.

Table 4.1 Heat chemistries of experimental materials in weight per cent (balance is Fe).*

Material	C	Mn	Si	Ti	P	S	N	Al	Nb
BH210 EG	0.008	0.25	0.0025	0.0013	0.05	0.0069	0.0042	0.0419	0.0011
BH210 GA	0.003	0.37	0.01	-	0.07	0.009	0.003	0.055	0.009
BH210 GI	0.002	0.36	-	0.013	0.047	0.007	0.0022	0.035	0.008
LC GI	0.031	0.18	0.008	0.002	0.007	0.005	0.0045	0.054	-
High-YPE EG	0.057	-	0.03	<0.01	0.033	0.015	-	0.12	<0.01

Material	Cu	Ni	Cr	Mo	V	Sn	B	As	Ca
BH210 EG	0.031	0.01	0.0189	0.0057	0.0009	0.0009	-	-	0.0005
BH210 GA	0.016	0.011	0.035	0.01	0.002	0.002	-	-	-
BH210 GI	-	-	-	-	-	-	-	-	-
LC GI	0.03	0.01	0.03	0.01	-	0.01	0.0001	0.003	-
High-YPE EG		0.05	0.04	0.01	<0.01	-	<0.01	-	-

* Values indicated with "-" were not reported by the manufacturer

Table 4.2 As-received material properties of experimental materials

Material	Yield Stress (MPa)	UTS (Mpa)	Uniform Elong. (%)	Total Elong. (%)	Grain Size (μm)	Uncertainty in Grain Size (μm)	Apparent Coating Thickness (μm)
BH210 EG	223	311	22.4	40.3	18.4	3.6	27
BH210 GA	245	359	19.4	32.5	9.8	1.2	18
BH210 GI	255	358	22.2	49.2	9.1	1.6	20
LC GI	318	360	21.6	36.5	7.9	1.2	15

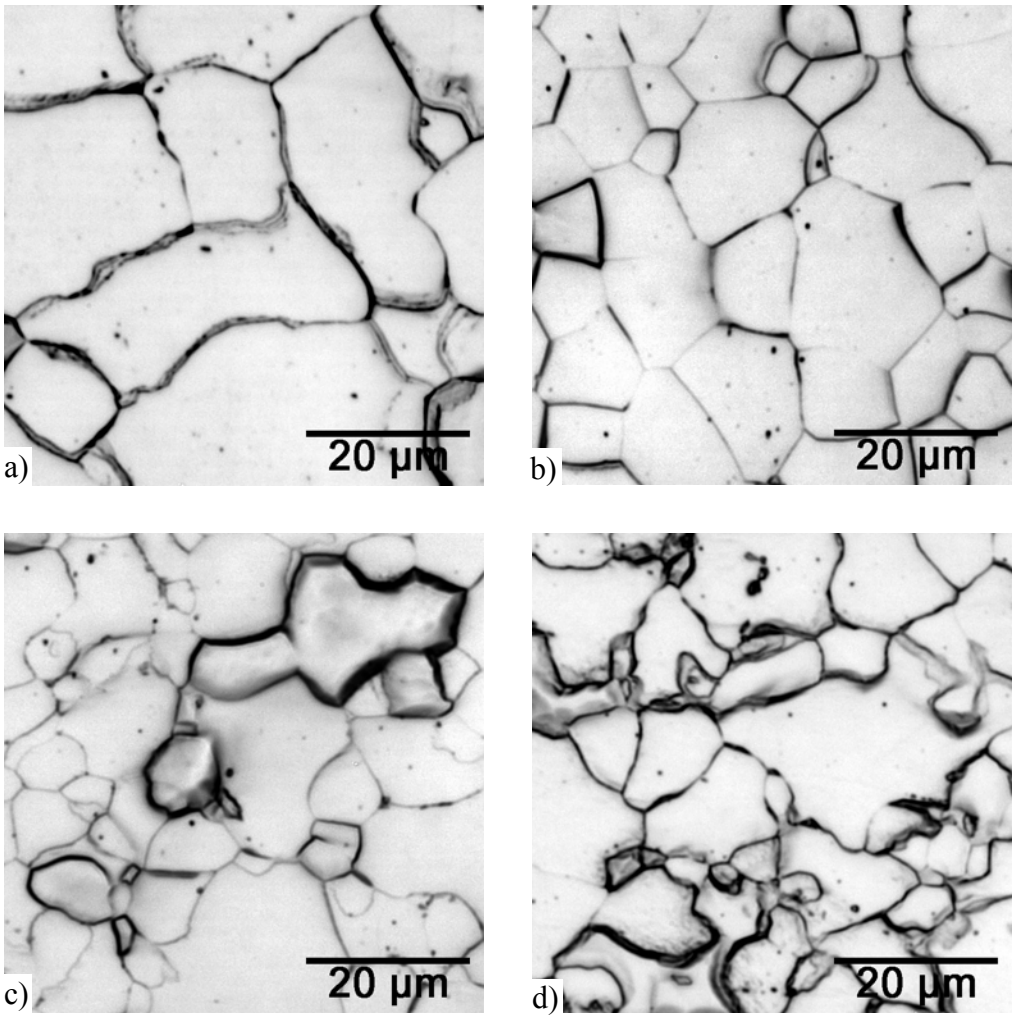

Figure 4.1 Light optical micrographs of test material substrates (2% nital etch, rolling direction horizontal); a) BH210 EG, b) BH210 GA, c) BH210 GI, d) LC GI.

All materials were stored in a freezer, at -20 °C, to suppress aging when they were not being machined, heat-treated, or tested.

4.2 Sample Preparation

Test samples were machined and prepared for the various test conditions necessary to explore Lüders band topography changes. Several preliminary and investigative steps were taken to characterize the materials prior to final analysis.

Mechanical properties and yielding behaviors were determined using uniaxial tensile tests. Temper rolling was performed on the LC GI samples to remove initial YPE. Strain paths and strain amounts were determined with biaxial samples. Rate of YPE return with artificial aging was determined for each material. Artificial aging was conducted in order introduce controlled amounts of YPE into the samples. The aged materials were coated with StressCoat™ before generating Lüders bands to indicate the locations of non-uniform yielding.

4.2.1 Uniaxial Tensile Samples

Uniaxial tensile samples were machined according to the ASTM E-8 standard.[67] The standard provides dimensions for machining (shown in Figure 4.2 and

Table 4.3) and methods for interpreting data. For this investigation, samples were machined in both the longitudinal and transverse directions. The as-received uniaxial stress-strain yielding response of the materials is shown in Figure 4.3 and Figure 4.4.

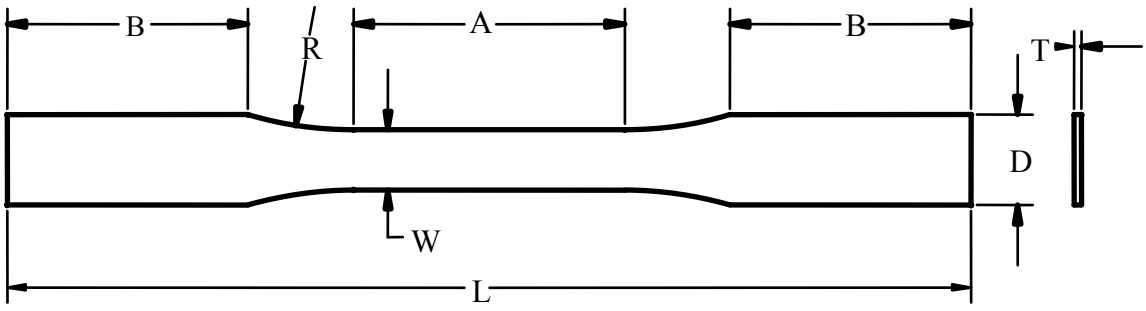

Figure 4.2 Machined sample geometry, reproduced from ASTM standard E8.[67]

Table 4.3 Dimensions associated with Figure 4.2

Symbol	Description	Dimension
A	Length of Reduced Section	57.2 mm (2.250 in)
B	Length of Grip Section	50.8 mm (2.0 in)
D	Width of Grip Sections	19.1 mm (0.750 in)
L	Overall Length	203.2 mm (8.0 in)
R	Radius of Fillet	12.7 mm (0.50 in)
T	Thickness	Thickness of Material
W	Width of Reduced Section	12.7 ± 2.54 mm (0.500 ± .010 in)

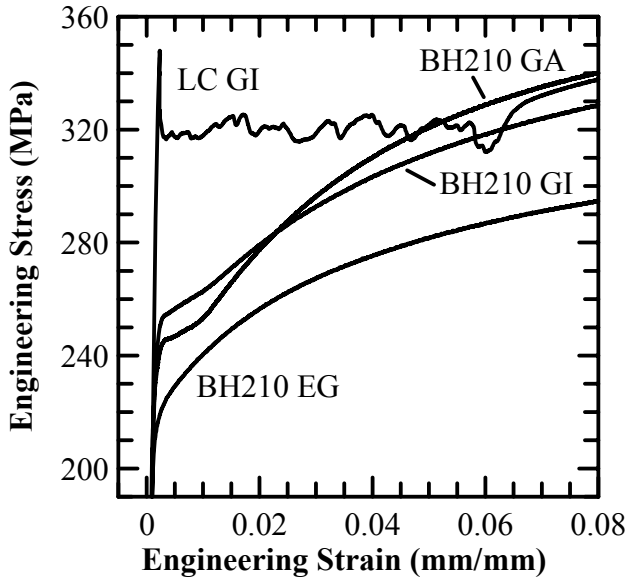

Figure 4.3 Partial engineering stress-strain curves emphasizing yielding for test materials (transverse direction) in the as-received condition: BH210 EG, BH210 GA, BH210 GI, LC GI.

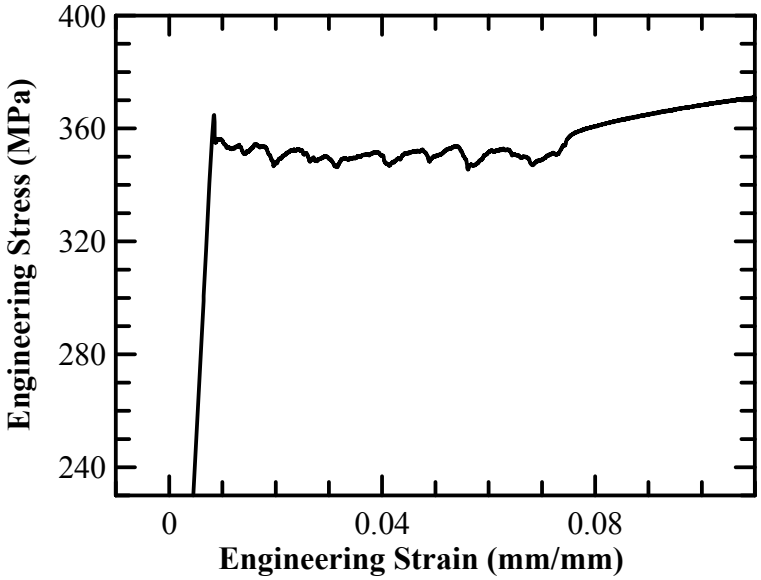

Figure 4.4 Partial engineering stress-strain curve emphasizing yielding for high-YPE EG material, 7.3 % YPE, aged at 150 °C for 43.5 h.

4.2.2 Biaxial Tension Samples

Biaxial tensile strain was imposed via stretch forming. Samples from the three BH210 materials were sheared into rectangular shapes. The samples were 203.2 mm (8 in) long with varying widths. The variations in widths provided a means to vary the strain ratio in the sample. Five widths were tested, 76.2 mm (3 in), 101.6 mm (4 in), 134.8 mm (5.31 in), 135.3 mm (5.33 in), and 203.2 mm (8 in). The 76.2 mm and 101.6 mm samples were sheared with both longitudinal and transverse directions for use in producing strain ratios which could be considered drawing. The 134.8 mm and 135.3 mm samples were sheared only in the transverse direction for use in producing strain ratios near plane strain. The 203.2 mm wide samples were used to produce balanced biaxial strains.

4.2.3 Temper Rolling

The LC GI material was not temper-rolled prior to shipping. Initial uniaxial tensile tests indicated the material had a YPE of 6.0 % as shown in Figure 4.3. Temper

rolling was used to remove this YPE from machined tensile samples. Temper rolling was performed on a Fenn two-high laboratory rolling mill. Reductions were performed on test pieces until the LC GI exhibited continuous yielding (Figure 4.5). All remaining material was rolled with a single pass through the same roll gap. An average total reduction of 1.9 % (measured by thickness) was imposed on the specimens and sufficiently removed YPE. The width of the mill was insufficient to roll full size tensile samples (203.2 mm long) in the transverse direction. Consequently, the transverse samples of this steel were also temper-rolled in the longitudinal direction. Due to this circumstance, the transverse LC GI may have some mixed orientation character. The degree to which it had a mixed orientation character was not evaluated.

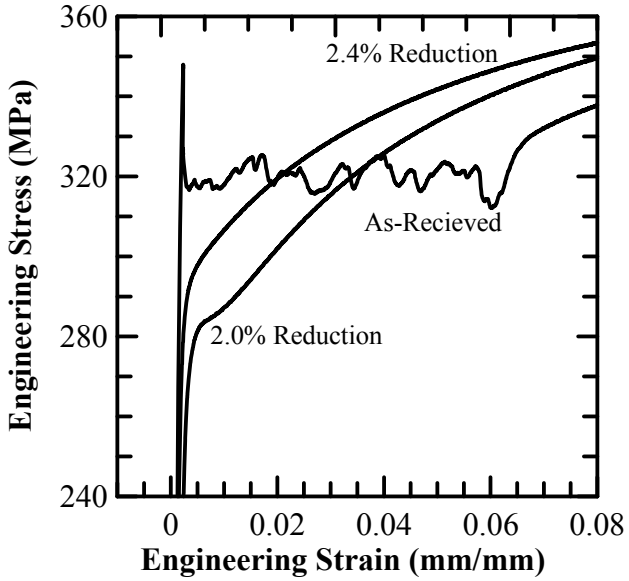

Figure 4.5 Stress-strain behavior of LC GI after systematic applications of temper rolling. A final reduction of 1.9 % (on average) removed all YPE.

4.2.4 Reintroduction of YPE

In order to study the effects of YPE on non-uniform yielding of the test materials, controlled amounts of YPE were introduced into the materials. YPE was introduced through artificial aging at elevated temperatures. The YPE values of interest were 0.25 %, 0.50 %, 0.75 % and 1.00 %. Each material had a different processing history and

substrate chemistry. Consequently, each responded differently to aging temperatures and times. An analysis of aging kinetics at a constant temperature and varying time was conducted for each material. These results allowed for controlled amounts of YPE to be introduced into the material for non-uniform yielding evaluation.

BH210 EG and BH210 GI samples were aged at 150 ºC. BH210 GA and LC GI samples were aged at 100 °C due to their much faster aging response at 150 °C. All samples for the aging study were uniaxial samples machined transverse to the rolling direction.

Artificial aging was performed using oil baths set to the temperatures of 100 °C and 150 °C. The aging study was carried out by first removing a sample from the freezer and allowing it to warm to room temperature. It was placed in the bath for a desired amount of time. At the end of the aging time, the sample was removed and rapidly cooled to room temperature with water.

After aging, the samples were tested in uniaxial tension to determine the amount of YPE corresponding to the aging time. Each material exhibited similar aging behaviors; an increase in aging time led to a more pronounced yield drop, a gradual increase in upper yield stress, lower yield stress, and increase in YPE, consistent with other observations.[14,68] An example is shown by stress-strain curves of BH210 GI in Figure 4.6. The criterion from ASTM standard E-8, section 3.1.4 was used to quantify YPE.

The variation in YPE with aging time for all materials is shown in Figure 4.7. A linear relationship between YPE and aging time was suitable to characterize YPE for the conditions examined. The resulting least-squares fits for each material are plotted in Figure 4.7. The equations of these fits are:

BH210 EG:	$YPE = 0.022t - 0.00339$	[4.1]
BH210 GA:	$YPE = 0.115t - 0.0531$	[4.2]
BH210 GI:	$YPE = 0.082t + 0.217$	[4.3]
LC GI:	$YPE = 0.019t + 0.339$	[4.4]

where YPE is in per cent and age time (t) is in hours.

All BH210 materials were able to achieve the four desired levels of YPE for testing. LC GI was only able to achieve the largest three levels of YPE. In the LC GI material, the as-temper-rolled stress-strain curve was fully continuous, and continuous yielding was also indicated by StressCoat™. Aging this material to a point where a load drop was evident, resulted in a YPE greater than 0.25%. Shorter aging times resulted in an inflection in the stress-strain curve without a distinct YPE.

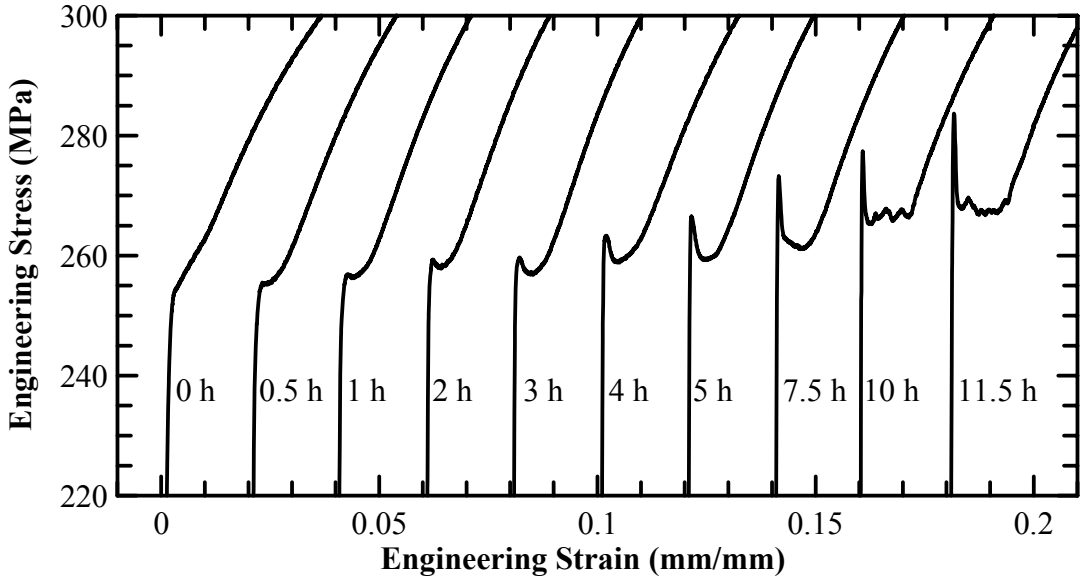

Figure 4.6 Partial stress-strain curves of materials BH210 GI, after artificial aging at 150 °C for the time indicated. Note: curves are displaced for clarity, all samples are transverse orientation.

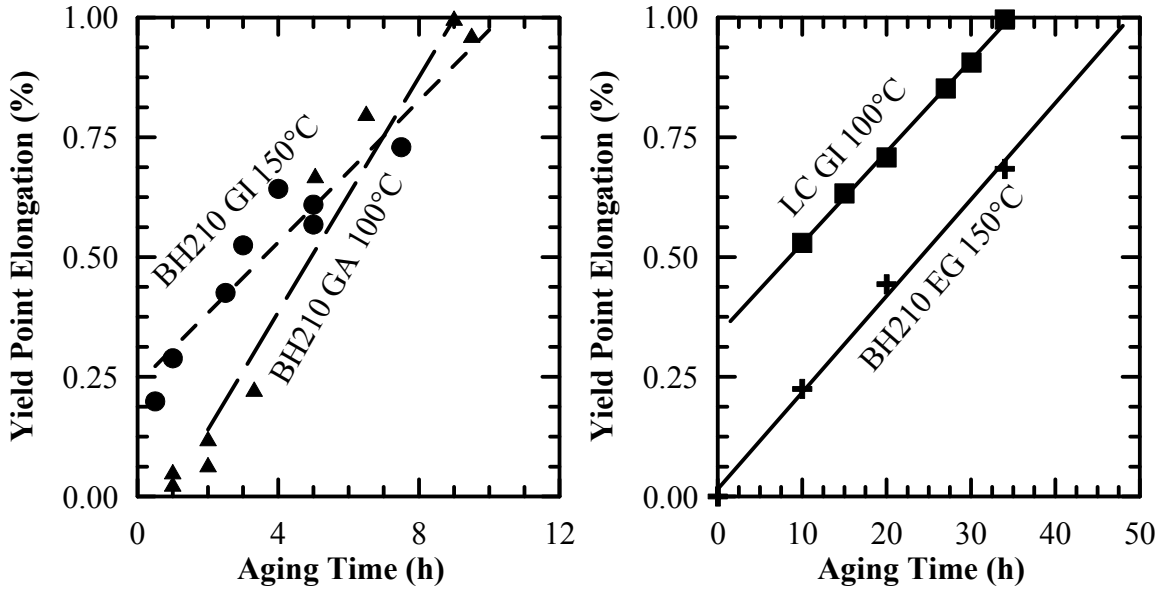

Figure 4.7 YPE as a function of aging time at indicated aging temperature for all materials. Two plots are used, with different x-axes for clarity.

4.2.5 Application of StressCoat™

StressCoat™ was applied to test samples in order to indicate the location of non-uniform yielding. Because of its brittle nature, the coating cannot plastically reach the same strains as the underlying material, and instead cracks. The cracking is evident with oblique lighting at low strains, ~0.15 % strain. The light impinges on the internal cracks and returns to the observer. Qualitatively, an increase in crack density indicates increases in strain. When the patterns of increased crack density appear as local linear features, it is interpreted that the underlying material is undergoing non-uniform deformation. Uniform deformation is marked with StressCoat™ by a constant crack density across the sample.

Prior to StressCoat™ application, all samples were cleaned with a degreasing agent (Formula 409®) and acetone, and wiped thoroughly with a paper towel. A compressed air sprayer, similar to an aerosol can, was used to apply the StressCoat™ at room temperature. The coating was applied in two to four even coats on one side of the material. Thirty seconds elapsed between each application to allow for some drying to take place. Complete drying of the StressCoat™ took up to two hours at room

temperature. As soon as they were dry they were tested. Samples were coated and tested individually to reduce aging at room temperature.

Techniques in StressCoat™ application were developed to limit several factors which decreased the optical quality of the coating; these factors included the amount of entrapped air bubbles in the coating and the thickness of the final coating layer. Entrapped bubbles reflected oblique lighting, obscuring cracks during testing. Thicker coatings did not provide a high contrast between the cracked and uncracked regions of the coating. Samples with StressCoat™ applied were not returned to the freezer. The thermal contraction/expansion experienced by the test samples after returning them to the freezer, "pre-cracked" the StressCoat™ obscuring new cracks initiated by non-uniform yielding.

Some uniaxial tensile specimens were masked so that StressCoat™ was only applied to one half of the gage area, indicated in Figure 4.8. Topography measurements were performed on the exposed half of the material, allowing the Lüders band to be identified by the StressCoat™ behavior, while avoiding any effects of s StressCoat™ on the topography measurements.

Figure 4.8 Uniaxial tensile specimen with half of gage area coated with StressCoat™; a) schematic, b) photograph.

Biaxial tensile specimens were masked and a central 127 mm by 127 mm square was coated with StressCoat™. This region fully covered the area being stretch formed. Topography measurements were performed on the reverse side. Deformation behaves the same on both sides, as shown by a sample of high-YPE EG (7.3 % YPE). Topography and photographed sample with StressCoat™ on the surface are shown in Figure 4.9. The

major strain in the sample was 0.3 %. The procedure to form the biaxial samples is described further in Section 4.4.

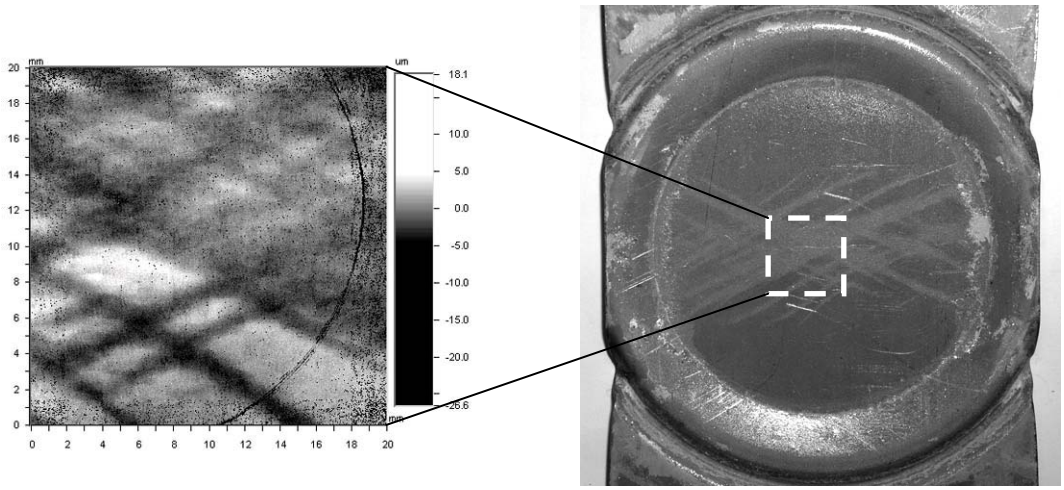

Figure 4.9 Topography of high-YPE EG (7.3% % YPE) from reverse of sample (uncoated side). The topography image is a mirror image of the region outlined in the photograph (coated side) of a 122.5 mm wide sample.

4.3 Uniaxial Tension Testing

Samples tested by uniaxial tension were used to develop and assess Lüders band topography for various levels in YPE, coating differences, and orientation effects. Individual bands were able to be imaged before the sample reached a strain equal to the Lüders strain.

Uniaxial tension analysis consisted of a planned thirty-two test conditions. These conditions comprised four materials (BH210 EG, BH210 GA, BH210 GI, and LC GI), four YPE levels (0.25 %, 0.50 %, 0.75 %, and 1.00 %), and two orientations (longitudinal and transverse). The longitudinal and transverse conditions of LC GI at 0.25 % were not tested because this YPE level was not obtained in the aging studies.

Straining of the test samples was performed on two separate screw driven frames; the first was a commercial frame, the second was designed and manufactured to facilitate topographic measurements in-situ.

4.3.1 Commercial Screw-Driven Frame

For all preliminary analysis, an MTS Alliance RT/100 frame was used. The preliminary analysis included evaluation of as-received mechanical properties and evaluation of aging kinetics. Unless otherwise indicated, the uniaxial tensile tests on this screw tensile frame were performed in the same manner. Testing was performed at room temperature on samples machined transverse to the rolling direction with a strain rate of $8.3x10^{-4}$ s^{-1} and evaluated over a 50.8 mm gage length.

4.3.2 In-Situ Tensile Frame

A research objective was to design an in-situ straining apparatus to assist in recording Lüders topographies for uniaxial tension. The in-situ frame improved upon earlier methods used to create and record Lüders topography by keeping the applied load constant, and reduced possible aging during testing.[52] Earlier results[52] involved repeated cycles of straining followed by profilometry, then re-gripping prior to additional straining. The in-situ frame was designed and manufactured by the author (Figure 4.10). It was designed to maximize the viewable area of the tensile sample gage section and used standard sized (203.2 mm long) uniaxial tensile samples. Engineering drawings and bills of material are included in Appendix A. The in-situ frame was attached to an automated two-dimensional stage under the profilometer. For this reason it was designed to be light in weight to avoid overloading the automated stage motors. The capabilities of the frame include a crosshead displacement of 24.5 mm, and 6.6 kN maximum load. Displacements were monitored by a 50.8 mm (2 in) 50 % extensometer connected between the connection block and the crosshead of the apparatus. A displacement control program was also written by the investigator using LabView 7.1, and can be found in Appendix B. The displacement steps can be controlled via the user interface. The system can be fully automated and interfaces directly to the optical profilometer.

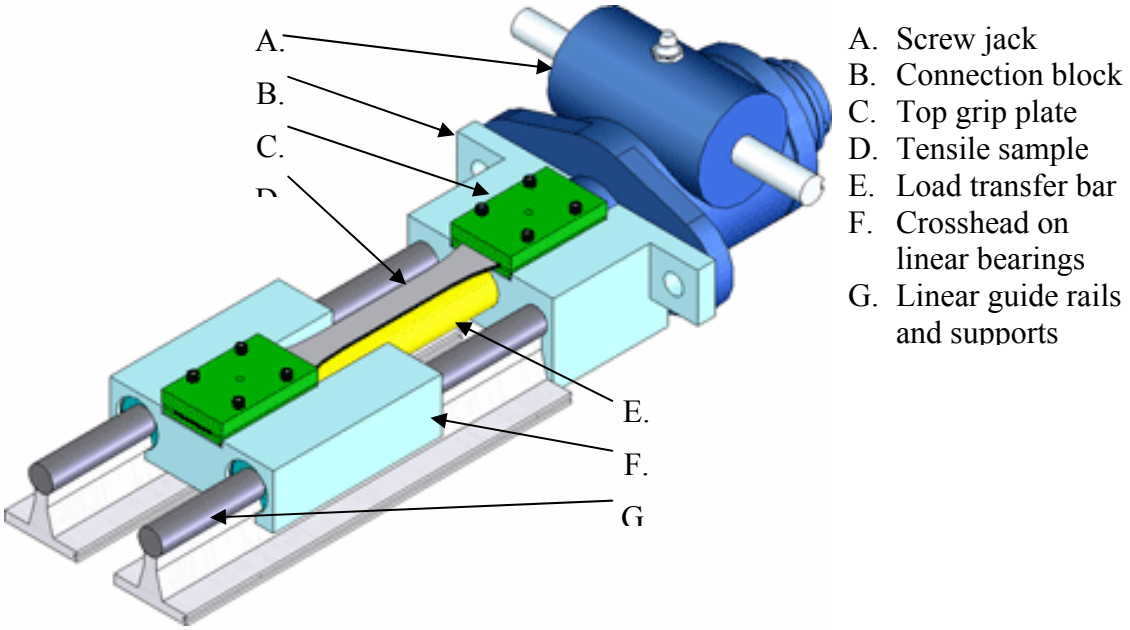

Figure 4.10 Isometric view of 6.6 kN load capable for use in combination with WYKO NT2000 optical profiler.

4.3.3 Methods to Obtain Topography Data In-Situ

A research objective was to create and record Lüders band topographies in-situ under uniaxial tension conditions. The in-situ frame was attached to an automated two-dimensional stage under the profilometer. Uniaxial tensile samples with StressCoat™ applied (Figure 4.8) were inserted into the in-situ frame, and the grips were tightened. The movable stage allowed the profilometer lens to be positioned over any area of interest on the tensile sample, including any Lüders bands that may be identified.

Two different observation methods were used to evaluate Lüders bands. The first was a static positioning method; the second was a dynamic positioning method. The static positioning obtained topography data for evolution of a single Lüders band with strain. The dynamic positioning method characterized multiple Lüders bands near the onset of the formation.

In the static positioning method, a single area of interest was located on the surface of the sample and remained in view throughout the test. The single area was selected either before any strain was imposed on the material, or selected once

StressCoat™ indicated the location of a Lüders band. Strain was then increased incrementally. At the conclusion of each strain increment, topographic data were collected. The crosshead displacement increment was 0.038 mm (~750 με) at the onset. The increment remained at this value until StressCoat™ indicated that the gage length had been fully deformed by non-uniform yielding. After this point, as the total strain increased, the increment of strain was also increased. The maximum strain imposed in any one of these tests was 6 % strain.

The dynamic positioning method also involved incrementally straining the tensile samples. The sample was strained at a constant crosshead velocity until StressCoat™ indicated a Lüders band was formed. The in-situ frame was located so the profilometer could view the location of the new band. Topographic data were then collected. The sample was strained more until another new Lüders band was formed. The process was repeated by moving the profilometer to the new location and taking topography data. The amount of strain imposed in each increment was variable but recorded. Straining and data collection continued until Lüders bands had covered the gage length of the sample. This was usually marked by the StressCoat™ cracking to the point where new non-uniform yielding could not be distinguished.

4.4 Biaxial Tension

All materials were strained with a Marciniak style die and stretch forming press. The press was originally designed and built by Buford [69] to accommodate a standard MTS test frame, shown in Figure 4.11. A 101.6 mm (4 in) circular Marciniak punch (Figure 4.12) was used in conjunction with circular upper and lower dies, with lock-beads at a diameter of 152.4 mm (6 in).

Biaxial tension analysis involved several strain paths. These strain paths included a balanced biaxial, two near plane strain, and two drawing strain paths.

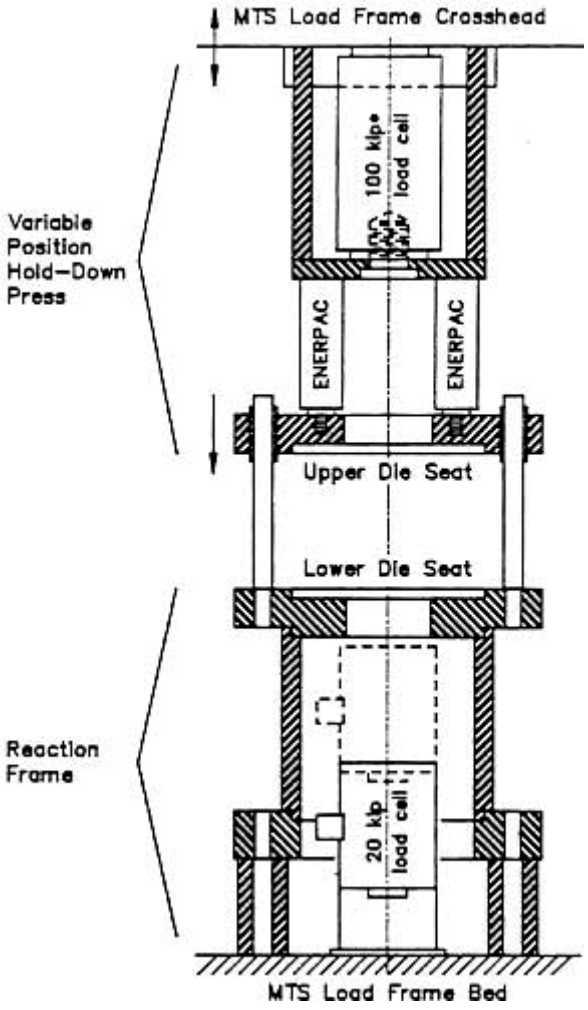

Figure 4.11 Stretch forming press originally designed and built by Buford.[69]

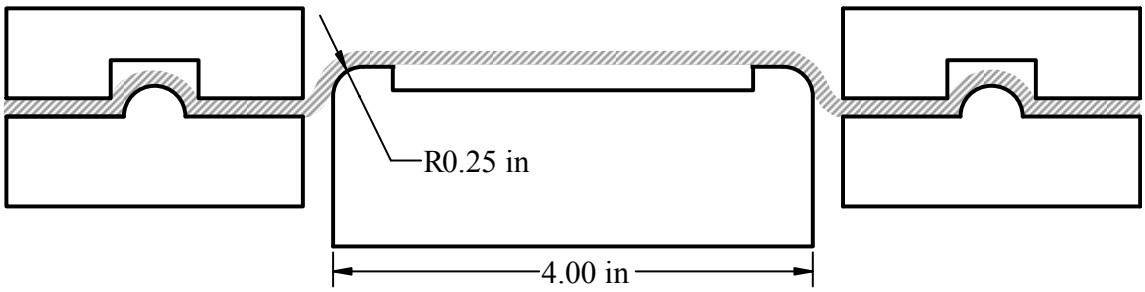

Figure 4.12 Sectioned view of 101.6 mm (4 in) diameter circular Marciniak punch used in biaxial tension stretch forming (not to scale).

4.4.1 Strain Ratio Evaluation

Before the final biaxial test specimen dimensions were chosen, the correlation between sample width and resulting strain path was explored using the Marciniak forming press. This exploration allowed for the determination of imposed major and minor strains as well as the corresponding strain ratios defined as the ratio of the major to minor strain. The major and minor strains were determined using the change in size of a nominal 50.8 mm (2 in) diameter circle scribed about the center of the sample. It was assumed that the development of strain was linear, and the strain ratio for a given width was the same no matter the amount of plastic deformation imposed. This assumption was necessary because the strain resolution was insufficient to characterize directly the strain ratios for the low strains of interest to yielding behavior. The samples were deformed to a punch depth of 12.5 mm, which corresponded to a major strain of approximately 12 % strain. The correlation between strain ratio and sample width is seen in Figure 4.13. The negative values of strain ratio represent drawing operations, the positive values are biaxial stretch forming, and where the trend crosses the x-axis is the point of plane strain. In this study with the Marciniack forming press, plane strain occurs at a sample width of about 134.6 (5.3 in). Samples with larger widths are constrained by the lock beads around the whole circumference and thus experience stretching.

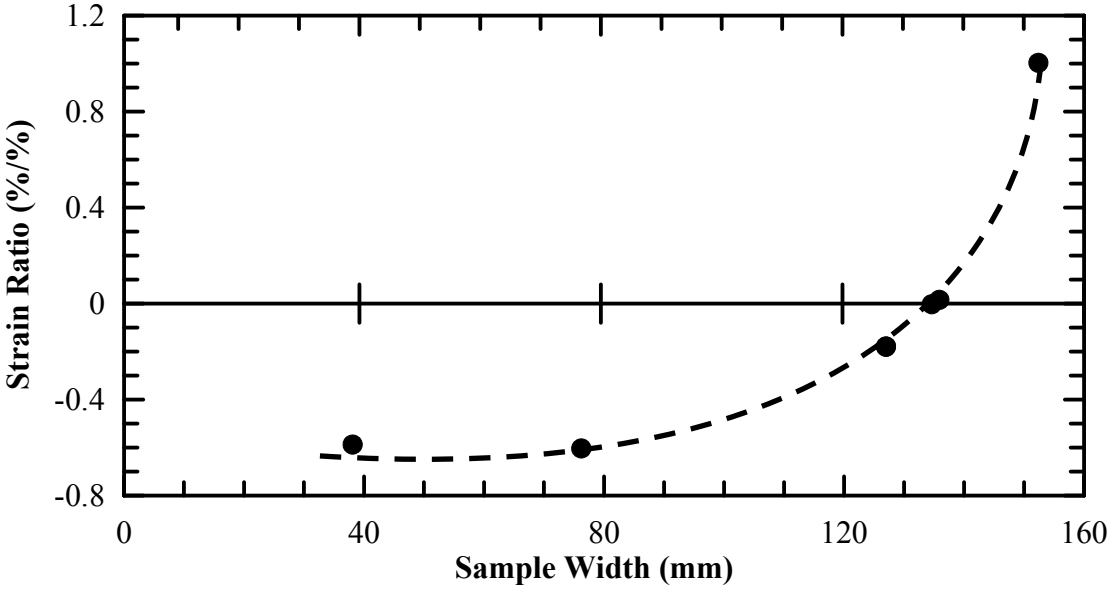

Figure 4.13 Strain ratio as a function of sample width used in strain path analysis. Samples were deformed to a major strain of approximately 12 % strain.

4.4.2 Testing Technique

All biaxial tension samples were prepared in the same manner. For lubrication, four polyethylene sheets, coated with a light oil, were placed over the punch and lower die. Next, the sample was placed over the polyethylene sheets, with StressCoat™ oriented downward, and the sample was centered over the punch. The upper die was lowered so it rested on the sample. A minimum holding force of 1.4 MN was applied to the dies using an external hydraulic pump. The holding force formed the sample over the lock-bead. The punch was pressed into the sample from below to a specified punch depth. Deformation was displacement controlled at a rate of 2.54 mm/s (0.1 in/s). The punch was then returned to its starting position, and the sample was removed.

To determine the desired punch depth, samples were deformed to various punch depths, and the strain imposed by each depth was recorded. As previously stated, a small punch depth was used so that the strain in the material would be below the Lüders strain in terms of the Von Mises equivalent to the tensile YPE.

The tests performed in the balanced biaxial strain path consisted of BH210 GI samples with 1.0 % YPE and 203.2 mm specimen widths. Additionally, the high-YPE EG material with 7.3 % YPE was used in technique development of the balanced biaxial test method. Because of the large YPE, the high-YPE EG material developed very noticeable surface imperfections and verified when techniques were capable of producing Lüders bands. Strains between 0.25 % and 0.50 % were imposed on the high-YPE EG material, to verify techniques and produce Lüders bands. Strains from 0.3 % to 1 % were imposed on the BH210 GI material. BH210 EG and BH210 GA materials were not tested because Lüders band formation was not observed in the BH210 GI material at these strain levels in balanced biaxial strain.

There were six test conditions in the strain path near plane strain. These conditions comprised three materials (BH210 EG, BH210 GA, and BH210 GI), one YPE level (1.0 %), and two gage widths (134.9 mm and 135.4 mm). Plane strain samples (of all three BH210 materials with 1.0 % YPE) were formed with a consistent punch depth of 1.3 mm which imposed a major strain of 0.4 %.

In addition to the conditions defined in the project objectives, twelve drawing conditions were also tested. The extra conditions used the same three materials and same YPE level (1.0 %) as the plane strain tests, but used two different widths (76.2 mm and 101.6 mm) in two orientations (longitudinal and transverse). The addition of further tests samples allowed for a comparison of possible Lüders band geometry change with changes in strain ratio. A constant punch displacement of 0.9 mm was used to deform the drawing samples.

4.4.3 Method of Topographic Measurement

Lüders topography was recorded on biaxial tension samples only after removal from the test frame. Topographic measurement of all post-formed samples was performed on the side not covered with StressCoat™. For consistency, surface topography data were obtained at the same five locations on each of the plane strain and drawn samples (Figure 4.14). Consistent locations allowed for automatic stage movement between locations. Additionally surface imperfections were not identifiable with the naked eye in all

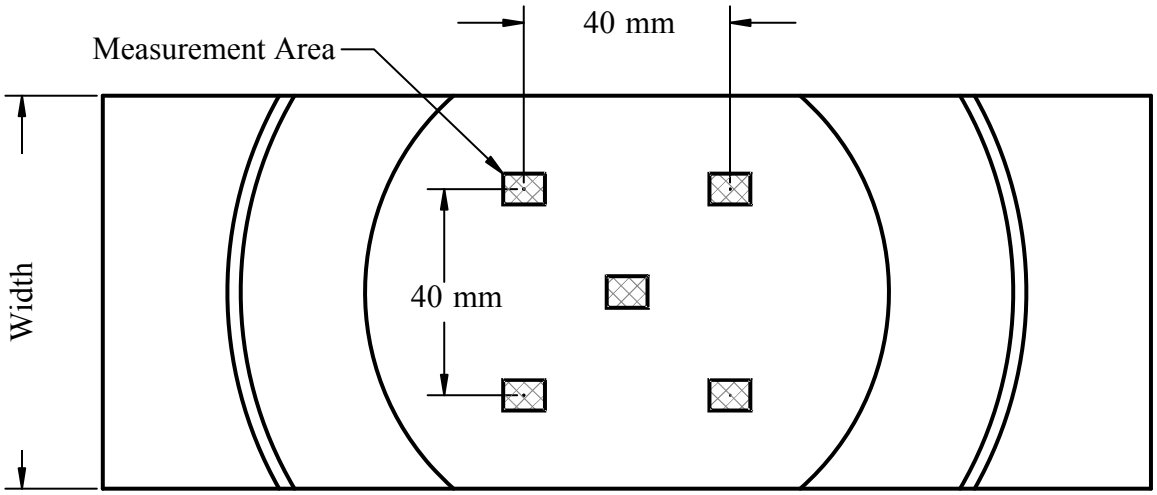

Figure 4.14 Schematic location of surface topography measurements on biaxial samples. Specimen widths are 76.2 mm, 101.6 mm, 134.9 mm, and 135.4 mm.

samples, adding to the difficulty in finding a location which provided Lüders band topography. These five positions on the sample were the center of the sample and the corners of a square, 40 mm on a side, centered on the sample. The corner points were chosen because all Lüders bands in these regions are oriented in the same direction, making them easier to identify.

4.5 Analysis of Lüders Band Topography

Essential to achieving the research objectives was the ability to locate, record, and analyze Lüders band topography. Techniques were developed to aid in these steps. The following sections describe the processes to obtain three-dimensional profiles, optical differences between the research materials' coatings, Lüders band identification techniques, and processing of the three dimensional data.

4.5.1 Recording Topography with the Optical Profilometer

A WYKO NT-2000 three-dimensional optical profilometer was used in this study to record topographic surface data. In addition to the hardware, the manufacturer provided Vision32* software which provided a means to analyze topographic data. For this investigation, a 1.5x objective lens was used in conjunction with a 0.5x magnification field of view, resulting in a single scan observable area of 8.083 mm by 6.146 mm. The profilometer records light intensities on a CCD camera, 716 pixels wide by 480 pixels tall. The illumination source produces coherent white light for normal operations. Two light filters are available for different measurement operations. The best measurements occur when the objective lens is perpendicular to the sample surface.

The Vision32 software allows for the manipulation of recorded topographic data. Very low spatial frequencies can be removed from the data. These frequencies include a dominant tilt plane and dominant cylinder radius. Removing these frequencies allow for higher frequencies, such as waviness, roughness and Lüders band formations to become the more dominant features. Various settings of Vision32 used for analysis are presented in Appendix C.

Topographic data can be represented in several ways, including a contour view. The contour view represents the surface on a two dimensional x-y plane with variations in surface height (z direction) represented as changes in color or shade. A linear "trace" can be made across the surface of the data, giving variations in surface height relative to the position along the trace. An example contour plot (topography) and two-point trace are provided in Figure 4.15 from the as-received LC GI material (6.0 % YPE). The width of the trace can be changed; increasing the width averages out features covered by the trace, as shown in Figure 4.16. The local depression shown in the thin trace (arrowed position in Figure 4.16) is nearly removed in the wider trace due to the averaging. This option provides an effective means of characterizing step heights, which may occur at a Lüders band front.

* Vision32 for NT-2000 version 2.303 SMU4 build 5

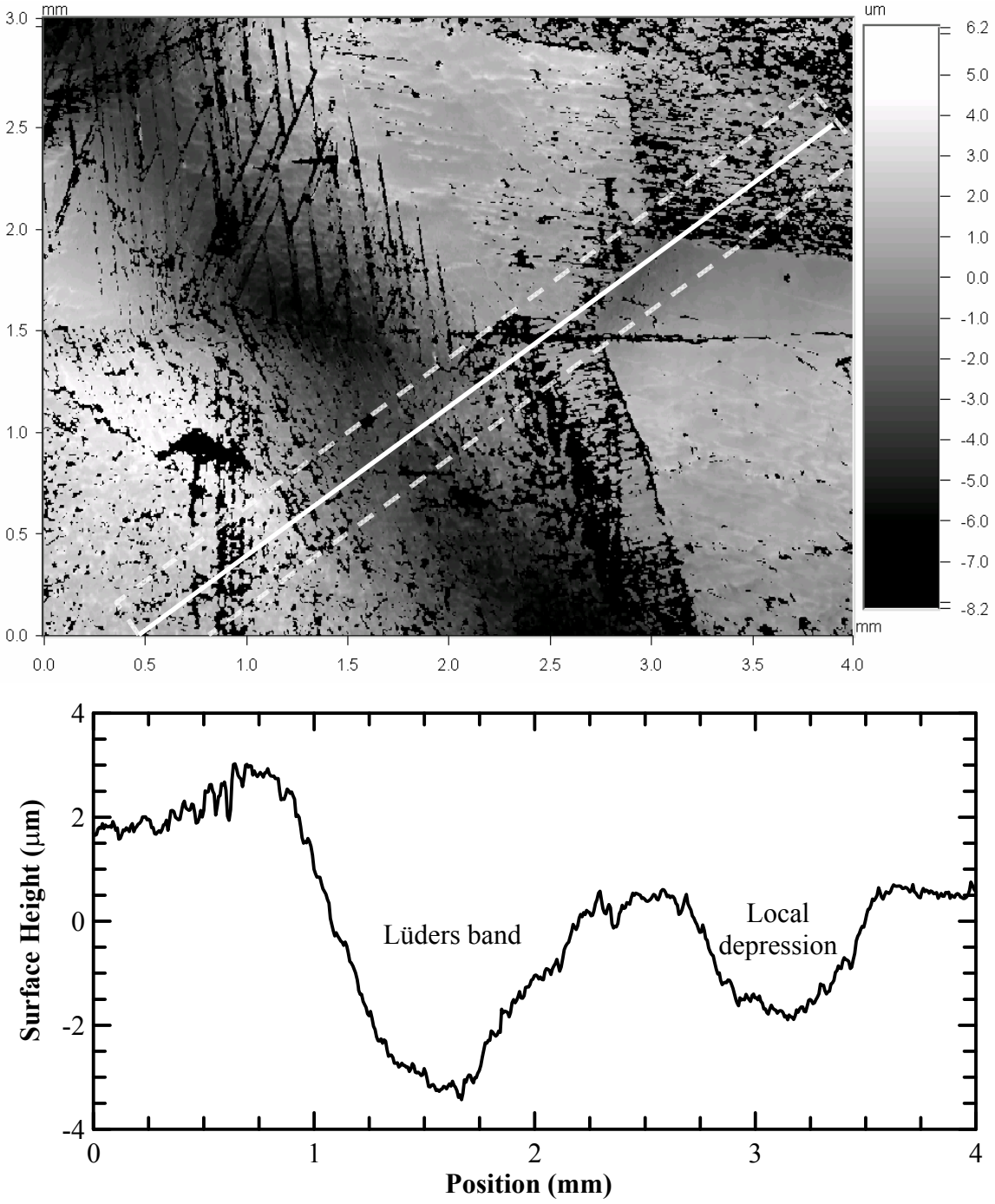

Figure 4.15 Contour plot and corresponding two-dimensional surface trace of Lüders band formed in as-received LC GI (6 % YPE). Trace shown contour plot in white, outlined by trace width. Tensile axis is horizontal in contour plot.

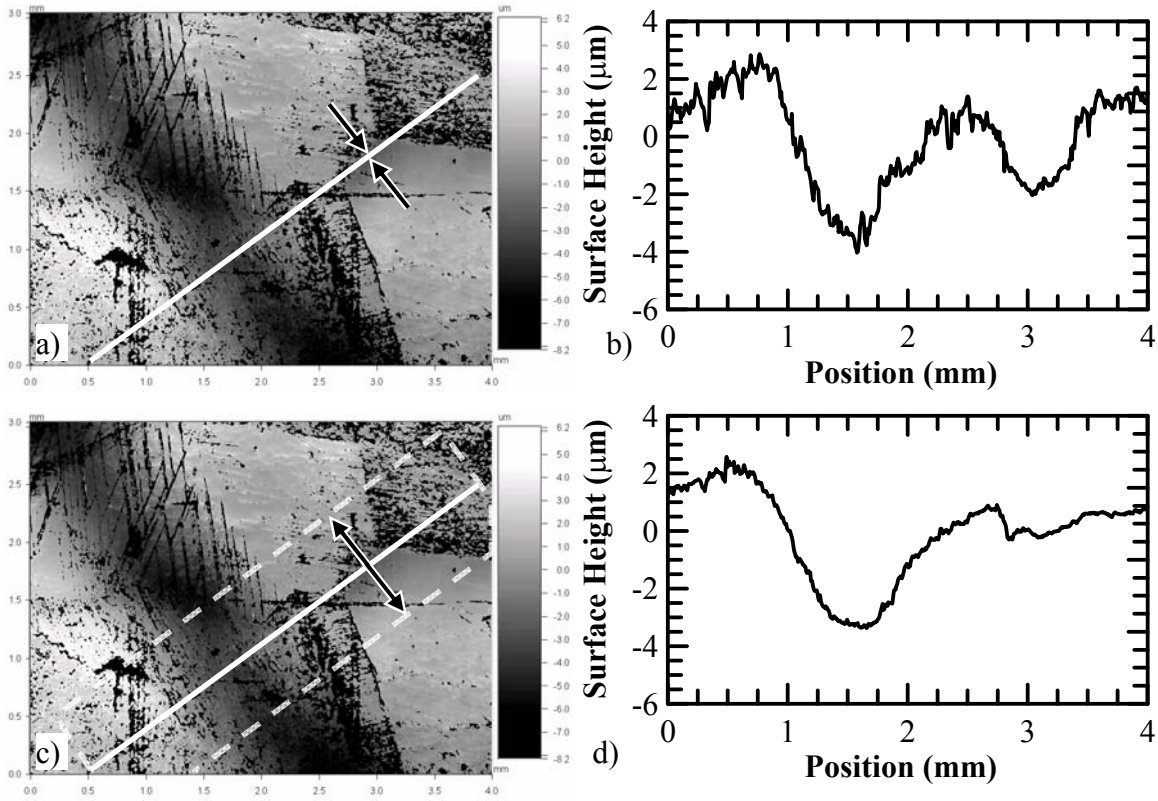

Figure 4.16 The width of the two-dimensional trace (shown on the contour views, indicated by arrows) affects the appearance of the two-dimensional profile (right); a) the contour view b) two-dimensional trace shown in a, c) same contour with a wider trace, d) two-dimensional trace shown in c. From similar representation by Humble.[52] Tensile axis is horizontal in contour plots.

4.5.2 Profilometry Differences between Coating Types

The surface finish of each material affected the quality of data obtained, i.e. number of pixels recorded. The NT-2000 is equipped with a CCD camera, 716 pixels wide by 480 pixels tall. For every scan the maximum number of data points it can obtain is 343,680. Factors exist which reduce the number of data points recorded. Three of these factors are (1) the surface not being in the vertical scan range (either too high or too low), (2) the brightness or contrast of the interferometric fringe is not large enough for the software to detect the height of the surface at that pixel, and (3) the slope of the surface

does not reflect sufficient light back to the lens. A single scan of the as-received surface of each material was measured to illustrate these differences. The same settings were used to measure these surfaces as were used in measuring the deformed surfaces. The comparison of the data obtained from each material is shown in Table 4.4. The BH210 EG data was not spread out evenly but clustered, generating large voids in the profile. With such small and clustered coverage the confidence in obtaining a Lüders band and not just a local surface depression is therefore reduced.

Table 4.4 Surface data coverage from as-received material surfaces

Material	Pixels with data	Data Coverage (%)
BH210 EG	24692	7.2
BH210 GA	226828	66.0
BH210 GI	299597	87.2
LC GI	310070	90.2

4.5.3 Identification of the Presence of a Lüders Band

A referencing technique was used to assist in the location of the Lüders bands, in addition to using StressCoat™. The technique ensured that the band's topography was in the area where surface height was being measured. Lüders bands appeared macroscopically as linear features on all materials. A reference mask was laid down next to the feature indicated by StressCoat™ and extended into the uncoated area (Figure 4.17). The reference mask was much larger in height than the surface and was out of the vertical scan range. On topographic images, the reference appeared as a black area without data. The sample was positioned under the lens and a topographic image was taken. The reference mask was then removed and a second image was taken. The comparison of the referenced and non referenced areas can be seen in Figure 4.18.

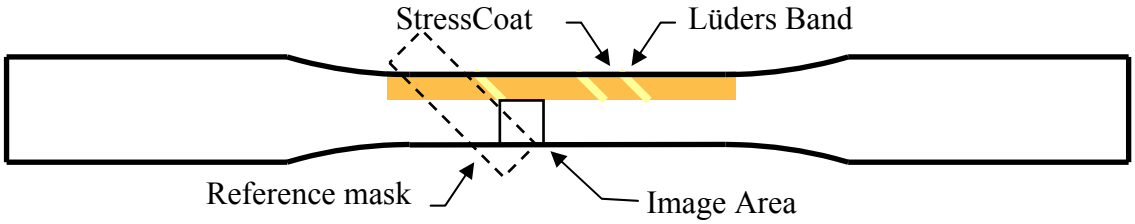

Figure 4.17 Illustration of Lüders band and referencing technique used in recording topography.

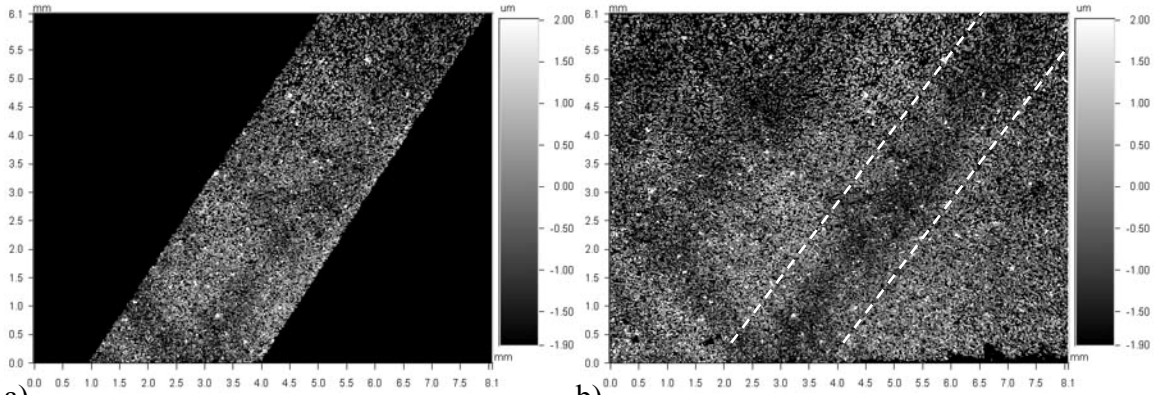

Figure 4.18 Lüders band topography measurements on BH210 GA; a) referenced region used to identify Lüders band, b) same area with reference mask removed. Tensile axis horizontal in contour plot.

4.5.4 Measurement of Lüders Band Characteristic Geometry

A two-dimensional trace was recorded from each topographic image obtained. The trace was oriented perpendicular to the perceived Lüders band. When Lüders band topography was not highly distinct, the trace was taken perpendicular to the reference mask edge. From the two-dimensional trace, three points were used to describe the band, a left edge and right edge and the maximum depth. From these three points, a band's width and depth were determined. The equations describing the width and depth of the bands are:

$$\text{Width (mm)} = \sqrt{(x_2 - x_1)^2 + \left(\frac{y_2 - y_1}{1000}\right)^2} \qquad [4.5]$$

$$\text{Depth (mm)} = \frac{\left|(x_2 - x_1)\left(\frac{y_1 - y_b}{1000}\right) - (x_1 - x_b)\left(\frac{y_2 - y_1}{1000}\right)\right|}{\sqrt{(x_2 - x_1)^2 + \left(\frac{y_2 - y_1}{1000}\right)^2}} \qquad [4.6]$$

where the values x_1, y_1, x_2, y_2, x_b, and y_b are shown in Figure 4.19 on a trace from as-received LC GI material (6.0 % YPE) previously shown in Figure 4.15. The right and left "edge" points were selected at a peak in the roughness at a horizontal position which marked a substantial decrease in surface height. The bottom point was measured at the lowest vertical position between the two edge points. The width is the distance between two points in Cartesian geometry, and the depth is the distance from a point to a line which intersects two other points. These types of calculations took account for local variations in slope on which Lüders bands formed. These variations were not able to be removed with the "tilt" feature of the Vision32 software. The occurrence of large local variations was rare on BH210 samples, but very common on LC GI samples (as illustrated in Figure 4.19). Both equations took into account unit conversion.

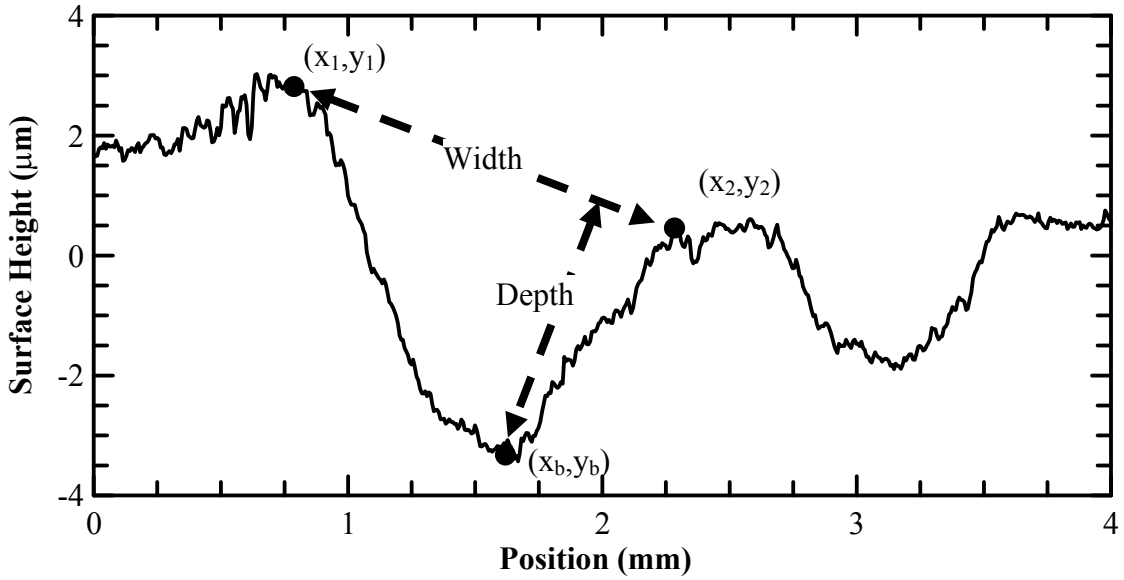

Figure 4.19 Locations of interest on a Lüders band to describe its characteristic geometry by equations of width and depth, Equations [4.5] and [4.6] respectively. Lüders band observed on as-received LC GI material (6.0 % YPE).

5.0 RESULTS AND DISCUSSION

Lüders bands were created and their surface topographies were examined to improve understanding of surface changes experienced during non-uniform yielding. The changes in topography were quantified by a characteristic geometry of Lüders band width and depth. Furthermore, the geometry was correlated to YPE which was re-introduced using artificial aging.

The evolution of Lüders band characteristic geometry with strain was examined in four Lüders bands in the BH210 GA. These bands were created by in-situ uniaxial straining with four BH210 GA samples, one band per sample for each level of YPE.

Thirty samples were uniaxially strained in-situ to determine Lüders band characteristic geometry near nucleation, which approximately defined the point of Lüders band maximum depth. These samples included all four test materials with variations in YPE and specimen orientation.

Lüders band characteristic geometries in biaxial tension samples were also determined. Several strain conditions were examined including balanced biaxial, two drawing strain paths, and two strain paths very close to plane strain. Results for all test conditions are presented in the following sections.

5.1 YPE Return in Longitudinal and Transverse Orientations

The three BH210 materials (EG, GA, and GI) were commercially temper-rolled prior to receipt to remove YPE. The LC GI material was temper-rolled at CSM, with a reduction of 1.9 %. For the LC GI samples, the temper rolling direction was parallel to the “tensile” axes for both the longitudinal and transverse oriented samples.

Artificial aging was used to introduce YPE into test samples. The evolution of YPE with aging time is shown with stress-strain curves in Figures 5.1 through 5.8. Transverse samples are shown in the odd numbered figures and longitudinal samples are shown in even numbered figures. It is assumed that the YPE values in these stress-strain

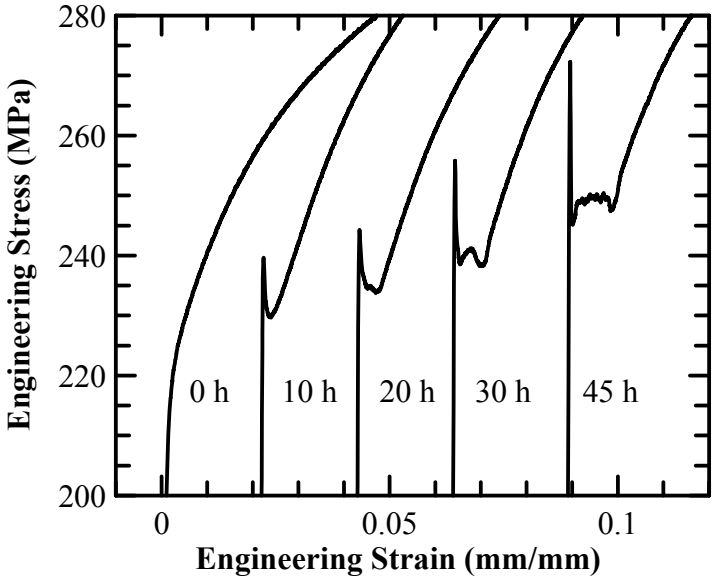

Figure 5.1 Stress-strain curves emphasizing yield points of BH210 EG transverse samples artificially aged at 150 °C for time indicated. Curves displaced for clarity.

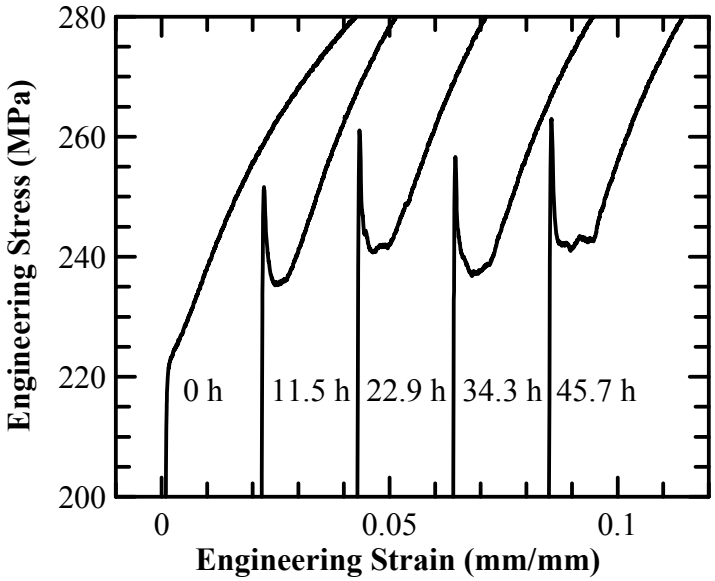

Figure 5.2 Stress-strain curves emphasizing yield points of BH210 EG longitudinal samples artificially aged at 150 °C for time indicated. Curves displaced for clarity.

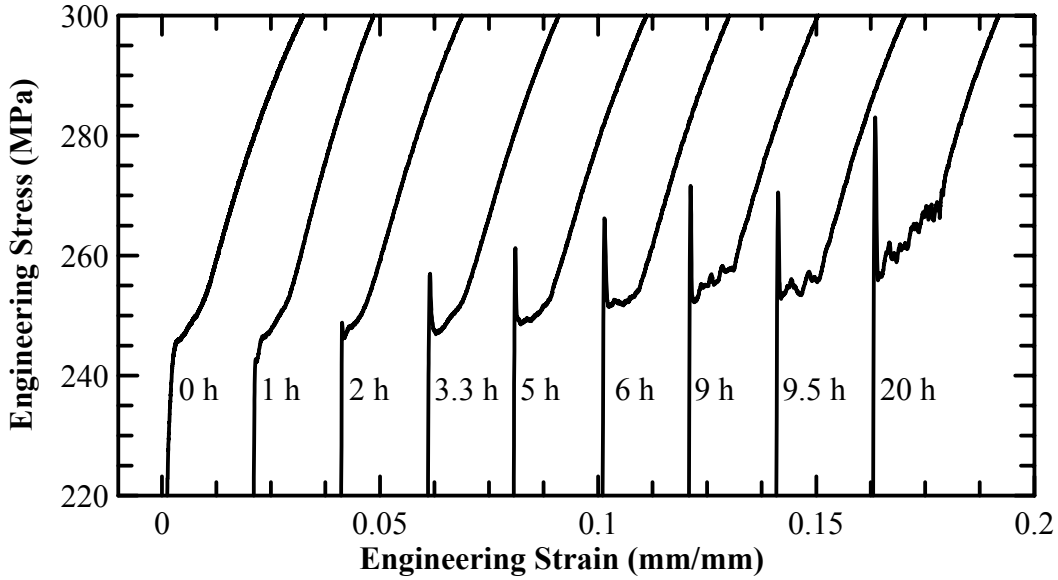

Figure 5.3 Stress-strain curves, emphasizing yield points of BH210 GA transverse samples artificially aged at 100 °C for time indicated. Curves displaced for clarity.

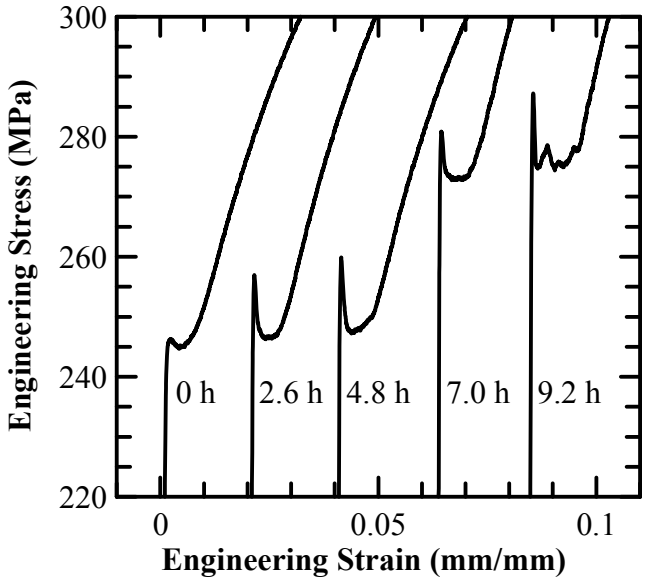

Figure 5.4 Stress-strain curves emphasizing yield points of BH210 GA longitudinal samples artificially aged at 100 °C for time indicated. Curves displaced for clarity.

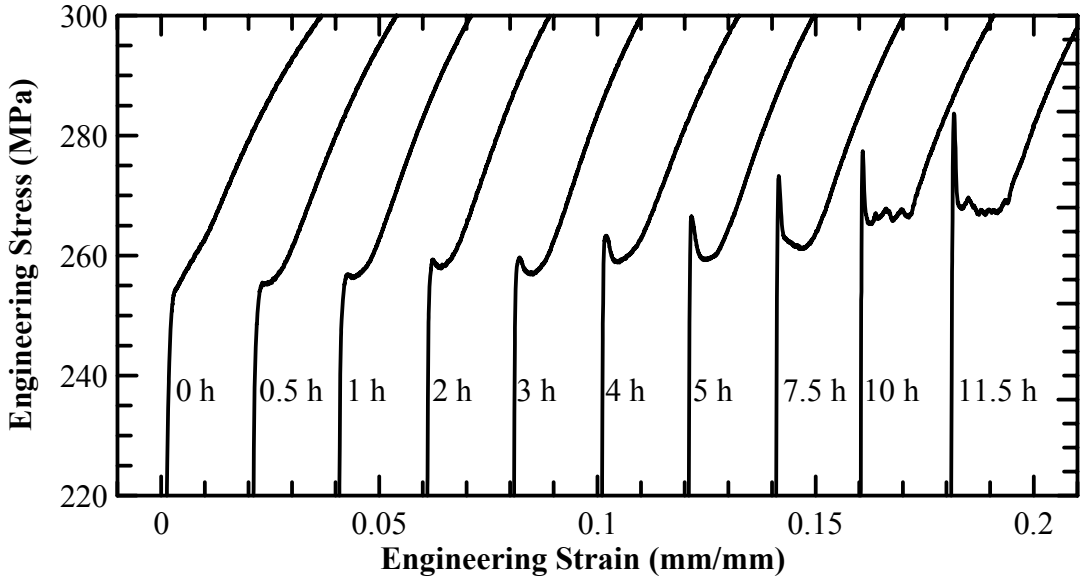

Figure 5.5 Stress-strain curves emphasizing yield points of BH210 GI transverse samples artificially aged at 150 °C for time indicated. Curves displaced for clarity.

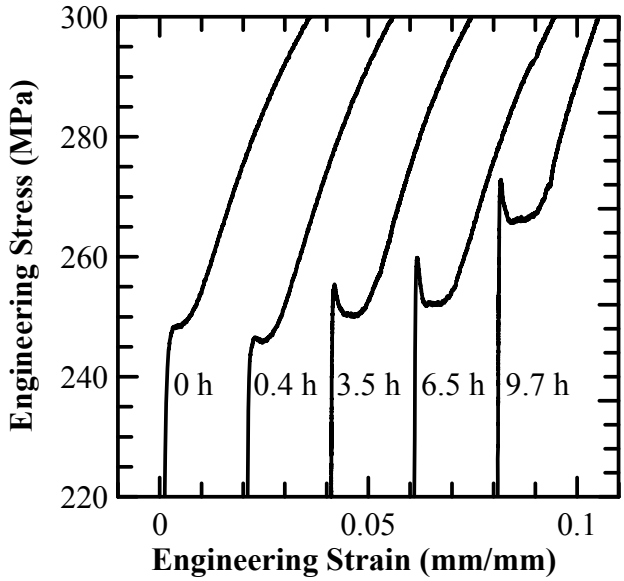

Figure 5.6 Stress-strain curves emphasizing yield points of BH210 GI longitudinal samples artificially aged at 150 °C for time indicated. Curves displaced for clarity.

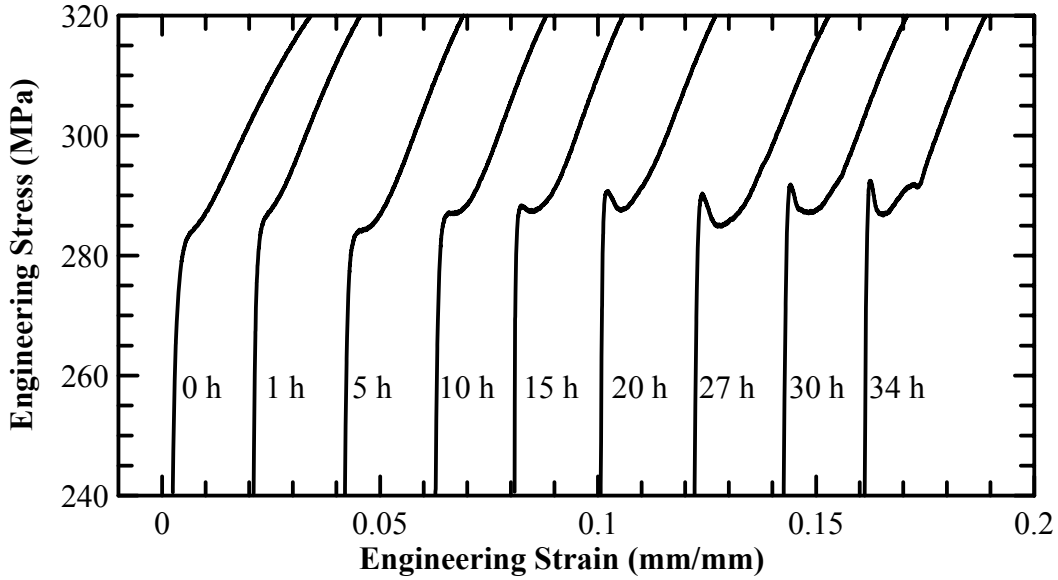

Figure 5.7 Stress-strain curves emphasizing yield points of LC GI transverse samples artificially aged at 100 °C for time indicated. Curves displaced for clarity.

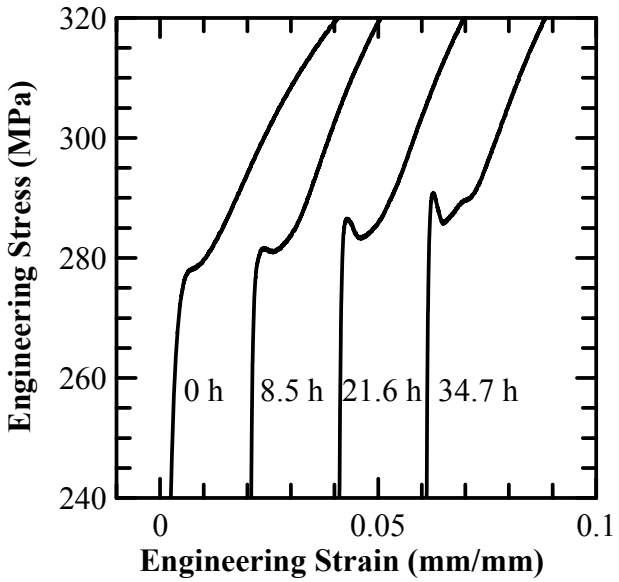

Figure 5.8 Stress-strain curves emphasizing yield points of LC GI longitudinal samples artificially aged at 100 °C for time indicated. Curves displaced for clarity.

curves are representative of the YPE developed in test samples with identical processing conditions.

Figures 5.1 through 5.8 show expected increases in YPE, upper yield stress, and lower yield stress with increasing aging time. The increases in YPE and LYS have been observed by several investigators[14,68] and are attributed to Cottrell atmospheres pinning dislocations. The increase in upper yield point is predicted by Hahn's model[19] due to the decreased number of mobile dislocations due to enhanced pinning with increased static strain aging.

Transverse samples were used to correlate aging time to YPE development (Figures 5.1, 5.3, 5.5, and 5.7). These correlations were shown earlier with Equations 4.1 through 4.4. From these equations, appropriate aging times were determined to generate the desired values of YPE (0.25 %, 0.50 %, 0.75 %, and 1.00 %). Both longitudinal and transverse samples were aged for identical times. The amount of YPE developed in longitudinal samples was determined from the stress-strain curves (Figures 5.2, 5.4, 5.6, and 5.7) and the results are presented in Table 5.1, compared to the desired YPE value produced in transverse orientation samples.

Table 5.1 Longitudinal sample YPE produced by artificial aging of as-received material

Transverse YPE (%)	BH210 EG YPE (%)	BH210 GA YPE (%)	BH210 GI YPE (%)	LC GI YPE (%)
0.00	0.00	0.50	0.44	0.00
0.25	0.53	0.64	0.51	-
0.50	0.64	0.67	0.81	0.52
0.75	0.74	0.72	0.87	0.70
1.00	0.94	0.98	0.99	0.84

The amount of YPE return versus aging time for all materials is shown in Figure 5.9a transverse orientation and Figure 5.9b longitudinal orientation. Linear least-squares fits were applied to each material/orientation condition. A fit versus time to the 2/3 power was also applied to the data (not shown) to compare with theoretical models. For the materials, temperatures, and YPE levels of interest here, the linear fit provided a better

description of the relationship between YPE return and aging time. It should be noted that the linear fits did not include the 0 h aging condition, but focused on YPE return after the material was considered to have YPE. Rate of YPE return (as shown by the slopes of the

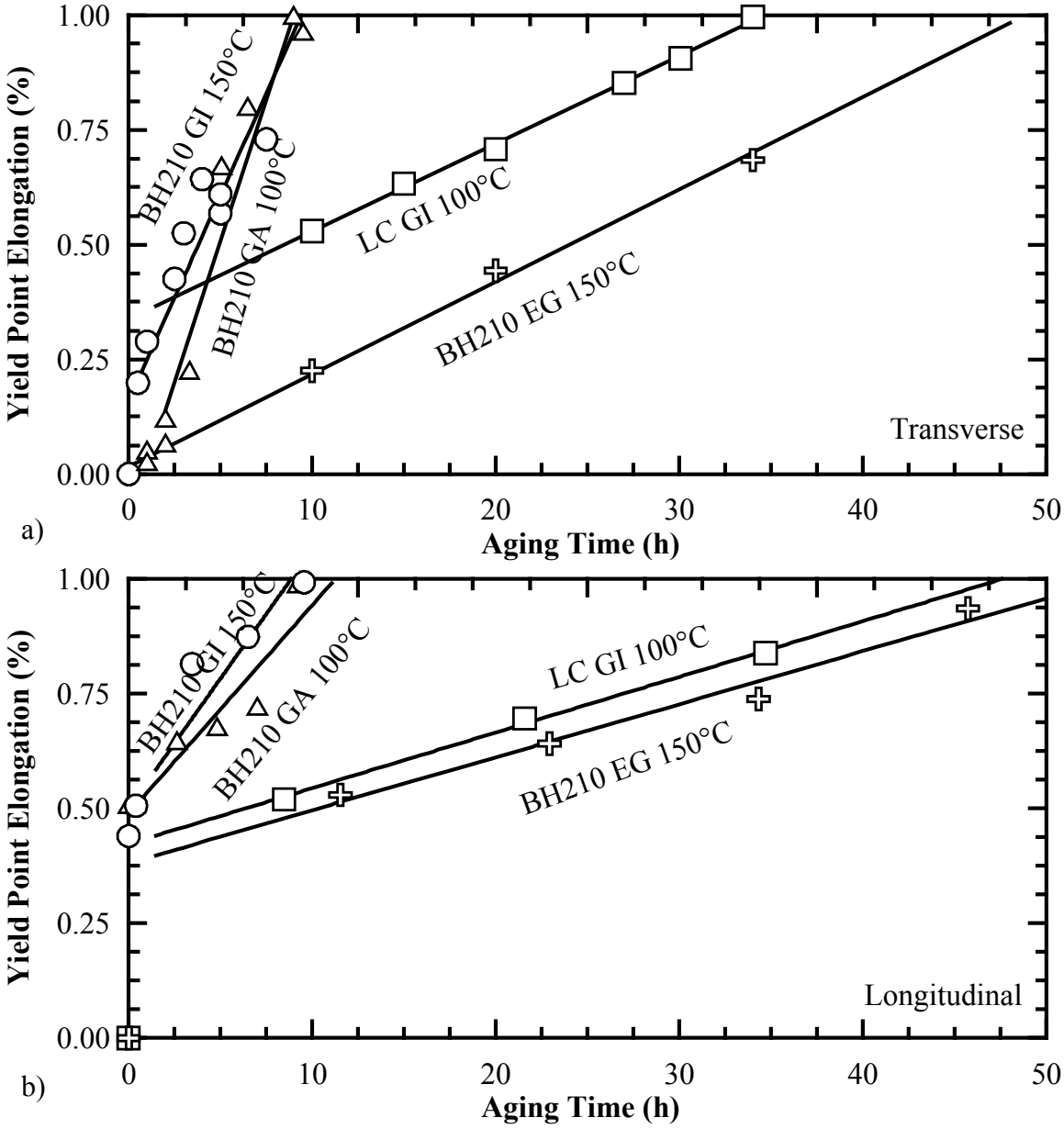

Figure 5.9 Yield point elongation development as a function of aging time. YPE determined from stress-strain curves in Figures 5.1 through 5.8. Materials and aging temperatures indicated. Least-squares linear fit plotted with data. a) transverse orientation; b) longitudinal orientation.

linear fits) in transverse oriented samples was somewhat greater than in longitudinal oriented samples, for the conditions tested.

Including the 0 h aging condition shows behavior that may appear to be discontinuous; YPE remains zero until a point where, by definition, YPE exists and may already have substantial value. This is further illustrated through examination of the 0 h aging condition with longitudinal orientation in Figure 5.9.

The "definition" of YPE, used in its determination becomes critical to material evaluation especially at the as-temper-rolled 0 h condition. The YPE definition was reviewed in Section 2.2. The criterion for having a YPE is that a material must exhibit a zero-slope at or near yielding. Without a point of zero-slope, the material has no YPE and with a zero-slope the material has some value of YPE. From the unaged stress-strain curves in Figures 5.2 and 5.8, BH210 EG and LC GI samples yielded continuously, without a zero-slope condition in their stress-strain curves. A zero-slope condition exists in the stress-strain curve of BH210 GI (Figure 5.6). Because of this zero-slope, BH210 GI has YPE and it is found to be 0.4%. BH210 GA had a noticeable load drop in its stress-strain curve, and a resulting YPE of 0.5%. Both BH210 GI and BH210 GA have YPE levels at the 0 h aging condition in the longitudinal direction that could be of concern in sensitive applications.

StressCoat™ was applied to all eight sample materials/orientations in the as-temper-rolled 0 h aging condition. Samples were then uniaxially strained, and the progression of StressCoat™ cracking was recorded with a video camera. From the images recorded, the cracking pattern indicated uniform deformation on all samples, even those which by definition have YPE. Further investigation would be warranted, possibly at lower crosshead speeds and with a higher resolution camera. In these videos, at the strain rate used (8.3×10^{-4} s^{-1}) the speed of cracking StressCoat™ is fast (~8 s to fully crack StressCoat™ in the gage section), and difficult to film.

With increasing aging time, there is a transition of yielding behavior in the stress-strain curves (Figures 5.1 through 5.8). This transition affects the surface response of materials in the form of non-uniform yielding and Lüders band formation. Additionally the YPE, used as a description of the extent of the non-uniform yielding, is also affected.

An exploration of this transition and its effects are an important factor in providing understanding between the easy to measure value of YPE and the surface response.

Analyzing the detailed relationship between surfaces at low strains less than 0.25% (e.g. in this transition range) was outside the current of the research plan. Additionally, the straining equipment designed for this project was not built with a load transducer, load data were not obtained directly when studying surface deformations in-situ. Nonetheless, a closer inspection of the transition behavior is worthwhile, and will be commented on using stress-strain data obtained in the pursuit of the overall project objectives.

From a classic yielding phenomenon perspective, the formation of a Lüders band occurs at the first load drop in the stress-strain curve. It follows that in the transition between two yielding responses, one with a load drop and one without a load drop, is a yielding response with a region of zero-slope. This transition curve is shown in Figure 5.10.

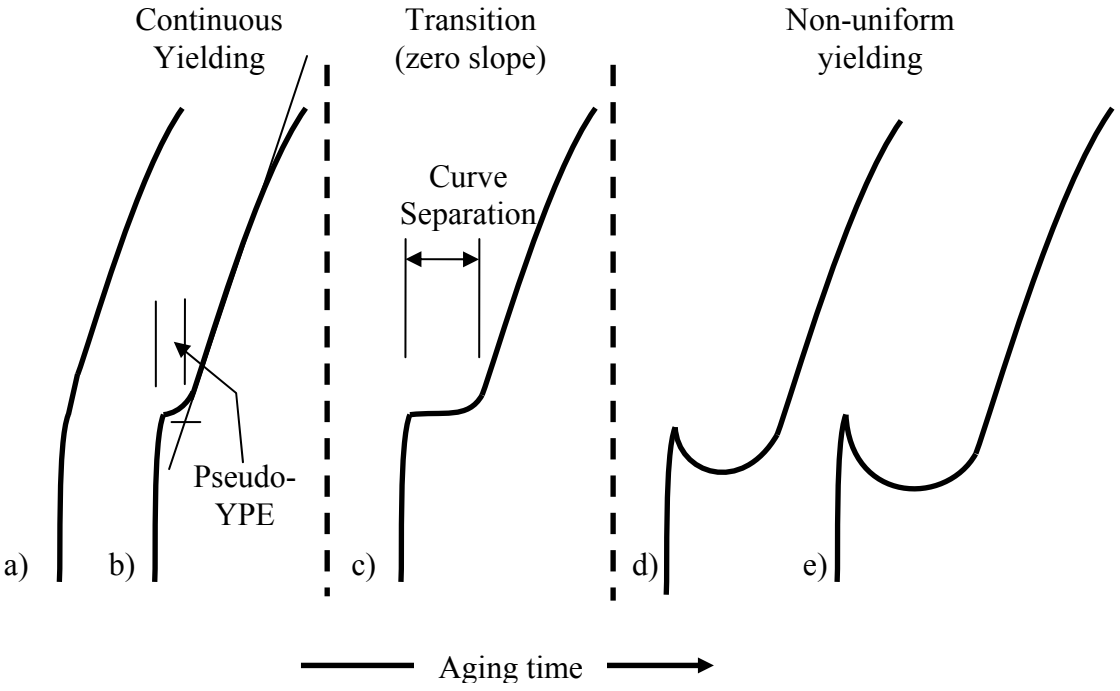

Figure 5.10 Schematic representation of the transition of stress-strain curves from continuous yielding to non-uniform yielding behavior with increased aging time; a) "roundhouse" yielding, b) development of pseudo YPE, c) region of zero slope obtained d) yield drop occurs e) increased YPE.

From the aging results presented above there is a suggestion of the existence of additional, complicating factors to this transition. An as-temper-rolled material can exhibit a fully "roundhouse" type stress-curve (Figure 5.1, 0 h, schematically Figure 5.10a) which is expected to yield continuously. A transition occurs in stress-strain behavior due to static strain aging. The continuous work hardening regime begins to shift to a higher strain and "separate" from the yield point.[†] An intermediate region of increasing strain hardening rate with increasing strain develops. This region will be hereafter referred to as "pseudo-YPE" to distinguish from "true" YPE (involving a zero-slope condition or yield drop).The pseudo-YPE can be observed in the zero-hour aging condition of Figures 5.2, 5.3, 5.5, 5.7 and 5.8 (schematically Figure 5.10b). Increasing aging time further produces a possible critical point, the zero-slope condition, shown in Figure 5.5, 0.5 h and Figure 5.6, 0 h. This point is "critical" in the sense that literature has repeatedly stated non-uniform yielding initiates at a load drop. At the condition containing the zero-slope condition, a region of the stress-strain curve remains constant, with variations in load on the order of the resolution of the load transducer. Increases in aging times increase the amount of yield drop, YPE, UYS etc., as previously indicated in this section.

A BH210 GI sample with a stress-strain curve assumed to be very similar to Figure 5.5 (0.5 h condition) had its surface topography recorded during yielding. This stress-strain curve contained the zero-slope condition, which is the possible transition point between continuous yielding and non-uniform yielding. It was believed at the time, that the sample did undergo discontinuous yielding. The manner in which the StressCoat™ cracked had characteristics which support both continuous and non-uniform sample deformation. Continuous deformation was indicated by StressCoat™ cracking in a dispersed, but random pattern (Figure 5.11a). Non-uniform deformation was indicated by short cracks forming in a linear pattern across the sample width (Figure 5.11b). The cracking pattern in this sample consisted of a large dispersion of random cracks with some well defined linear formation. The Lüders bands in the recorded topographies were not very prominent and were so obscured by local roughness of the coating that the

[†] This phenomenon can also result from temper rolling using the rolling of LC GI as evidence. LC GI was temper-rolled to a sufficient but non-ideal amount, and showed this phenomenon in both the longitudinal and transverse orientations.

possibility exists that the sample may have yielded continuously. Samples with more distinct yield drops in their stress-strain behavior exhibited well defined Lüders band topographies.

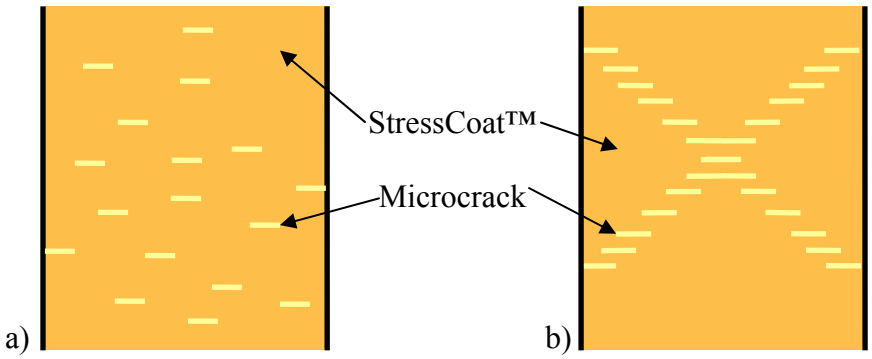

Figure 5.11 StressCoat™ crack formation on gage section of samples for: a) continuous yielding b) non-uniform yielding (tensile axis vertical).

It would be worthwhile in future studies to vary the YPE in several samples near YPE levels which produce a zero-slope condition to determine if the zero-slope is the delineation between continuous yielding and non-uniform yielding. Such a study would benefit from removing the coating and polishing the sample to reduce "noise" in the surface characterization.

A progressive transition in stress-strain behavior may indicate a progressive transition from fully continuous yielding to discontinuous yielding. It is unknown if there is local deformation within the material or at the surface in materials without a clear load drop. The shape of curvature in the pseudo yield point region is reminiscent of the TRIP yielding phenomenon. There may be possible parallels drawn, understanding that no phase transformation occurs in these materials. The surface response to pseudo YPE and associated (possibly discontinuous) microscopic yielding phenomena still needs to be determined. If localized deformation exists on the surface, the way YPE should be defined could be impacted. For this reason this transition region should be the subject of a future directed study, to verify or invalidate the current measure of non-uniform surface yielding.

5.2 Evolution of Lüders Bands with Strain in Uniaxial Tension

The evolution of Lüders band geometry with strain was documented in four BH210 GA samples. The characteristic geometry of concern was the Lüders band width and depth. Compared to other materials used in this investigation, the bands formed on BH210 GA were the most readily identifiable with the optical profilometer. Samples were aged to the desired YPE levels of 0.25 %, 0.50 %, 0.75 % and 1.00 % and then uniaxially strained. As strain was increased, surface topography was recorded at a single specimen location at multiple strain increments. Straining utilized the in-situ straining device designed for this project. The use of the straining device allowed each series to be completed within 1.5 h. Previous investigation[52] performed similar topography evolution measurements with maximum testing times on the order of 24 h. Concerns were raised about static strain aging occurring during the previous work. The use of the in-situ machine in this investigation reduced concerns of substantial strain aging during testing, as well as specimen alignment issues associated with the removal of the specimen from the grips after each strain increment.

In the following sections, steps taken to analyze the topography data are described and the resulting evolution of Lüders band topography with strain is presented.

5.2.1 Profilometry Analysis of Lüders Band Topography

Several steps were taken to analyze the effect of strain on Lüders band topography. First, Lüders band three-dimensional topography was recorded with increasing strain. Next, the Lüders band location was determined in the three-dimensional topographies. A linear surface trace, oriented perpendicular to the Lüders band was obtained for all topographies, by examining the topography with the largest and most evident band depth. The trace provided a two-dimensional profile, which is surface height as a function of position along the trace. The trace coordinates were noted, and the same trace location was used in the other topographies collected from the same sample. These profiles were compared to each other to determine the evolution of Lüders band geometry with strain. These steps will be illustrated using a BH210 GA sample with 1.00 % YPE. Further evolutionary details for this sample are given in the next section.

Topographic data from the same sample area at three different strain levels were chosen to illustrate stages of Lüders band development. Several visual aids are used in figures showing contour plots and two-dimensional traces (Figure 5.12 through 5.14). The center of the trace location is indicated with a white line in the contour plot (part a of each figure). The corresponding two-dimensional profile of the trace is shown in part b of each figure. The traces are 0.8 mm wide and the two-dimensional profiles shown are the average of the underlying topographic data.

Figure 5.12 shows the sample topography prior to the formation of a Lüders band. Although the overall gage strain of the sample is 0.05 % (as measured by the crosshead and subsequent conversion), this area of the sample has not yielded. Figure 5.13 shows a Lüders band detected with StressCoat™ as described in Section 4.5.3. Its position has been outlined with dashed lines. The gage strain in this figure is 0.31 %. At this strain, the depth of Lüders band is at its maximum, (shown in the next section). Figure 5.14 shows the same area after the sample was strained to 1.73 %. The Lüders band which was readily visible in Figure 5.13 is no longer apparent (Figure 5.14) after straining through the YPE.

5.2.2 Lüders Band Topography Changes with Strain

Selected samples were deformed in uniaxial tension to observe changes in Lüders band topography with strain. For each sample, a fixed trace location was used to follow the evolution of the band. The two-dimensional profiles of three YPE conditions are shown in Figures 5.15, 5.17, and 5.19, one figure for each YPE level. A smoothing function[‡] was used to make these profiles clearer. In three additional figures (Figures 5.16, 5.18, and 5.20), the locations of the surface traces are shown in an example profile. The profiles for the 0.75 % YPE condition are not shown. Two sequential locations were used to monitor surface change on this sample. The first location did not capture a Lüders band, and data recorded in the second location did not provide additional insight in to Lüders band evolution.

[‡] The smoothing function is a linear filter[70] governed by $f(x_n) = (x_{n-2} + 2x_{n-1} + 3x_n + 2x_{n+1} + x_{n+2})/9$. For final measurements of Lüders band geometries, only original topographies were analyzed.

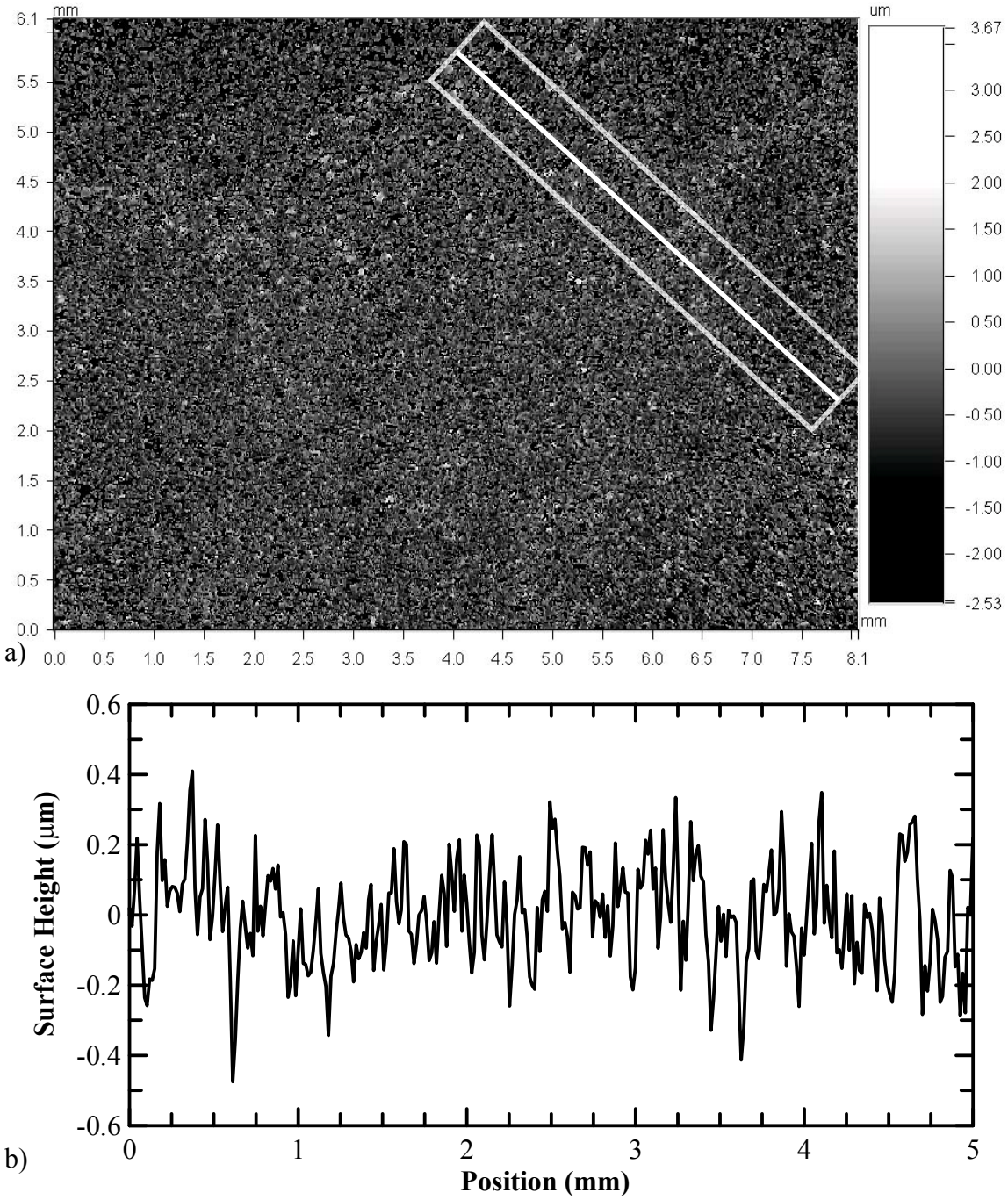

Figure 5.12 Topography of sample prior to Lüders band formation; a) three-dimensional topography contour view, b) two-dimensional surface topography corresponding to trace in contour view represented as a white line with outlined trace area. BH210GA, 1.00 % YPE, gage strain 0.05 % (trace 5). Tensile axis horizontal is in contour plot.

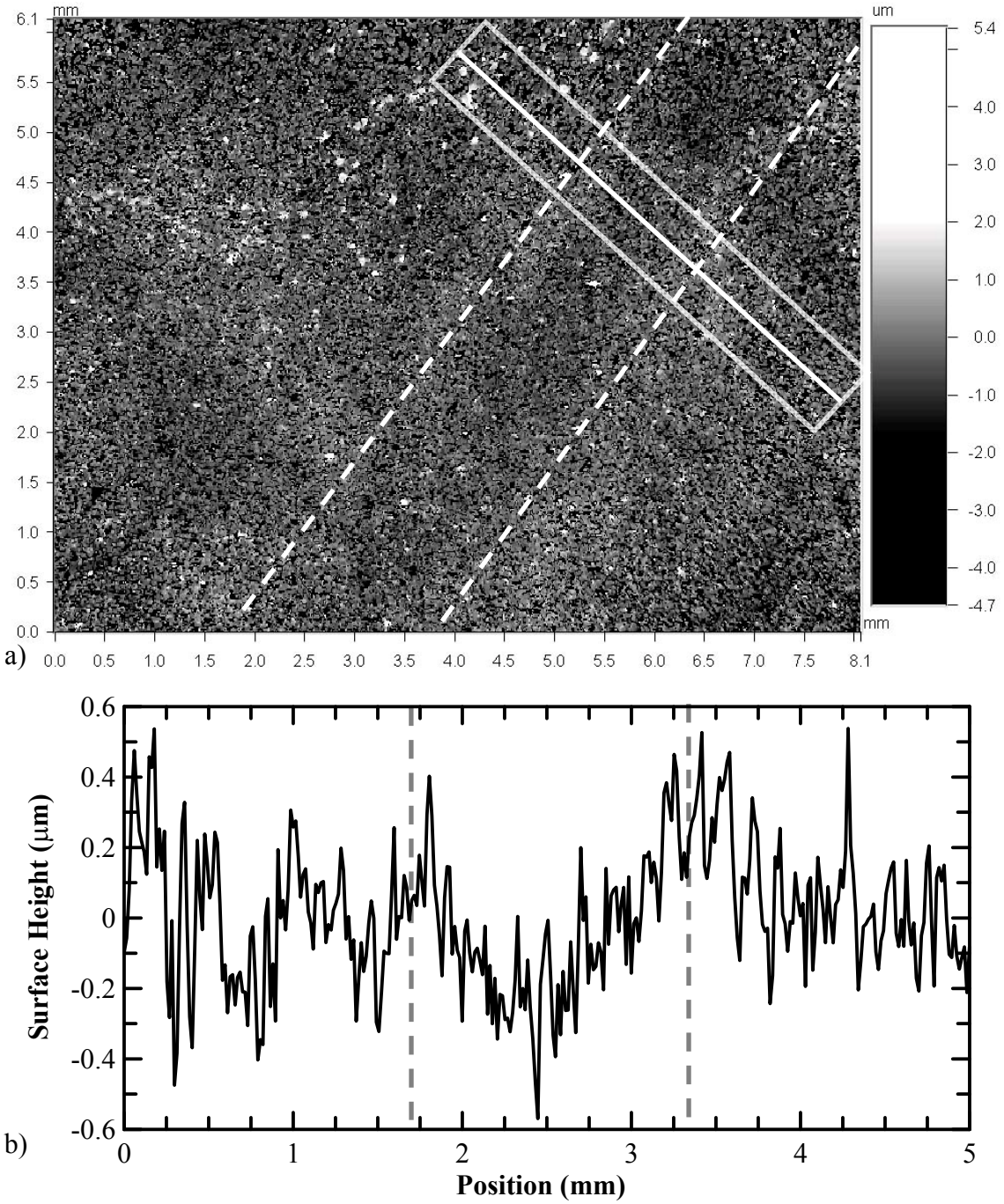

Figure 5.13 Topography of sample containing a formed Lüders band (outlined by dashed lines); a) three-dimensional topography contour view, b) two-dimensional surface topography corresponding to trace in contour view represented as a white line with outlined trace area. BH210GA, 1.00 % YPE, gage strain 0.31 % (trace 15). Tensile axis is horizontal in contour plot.

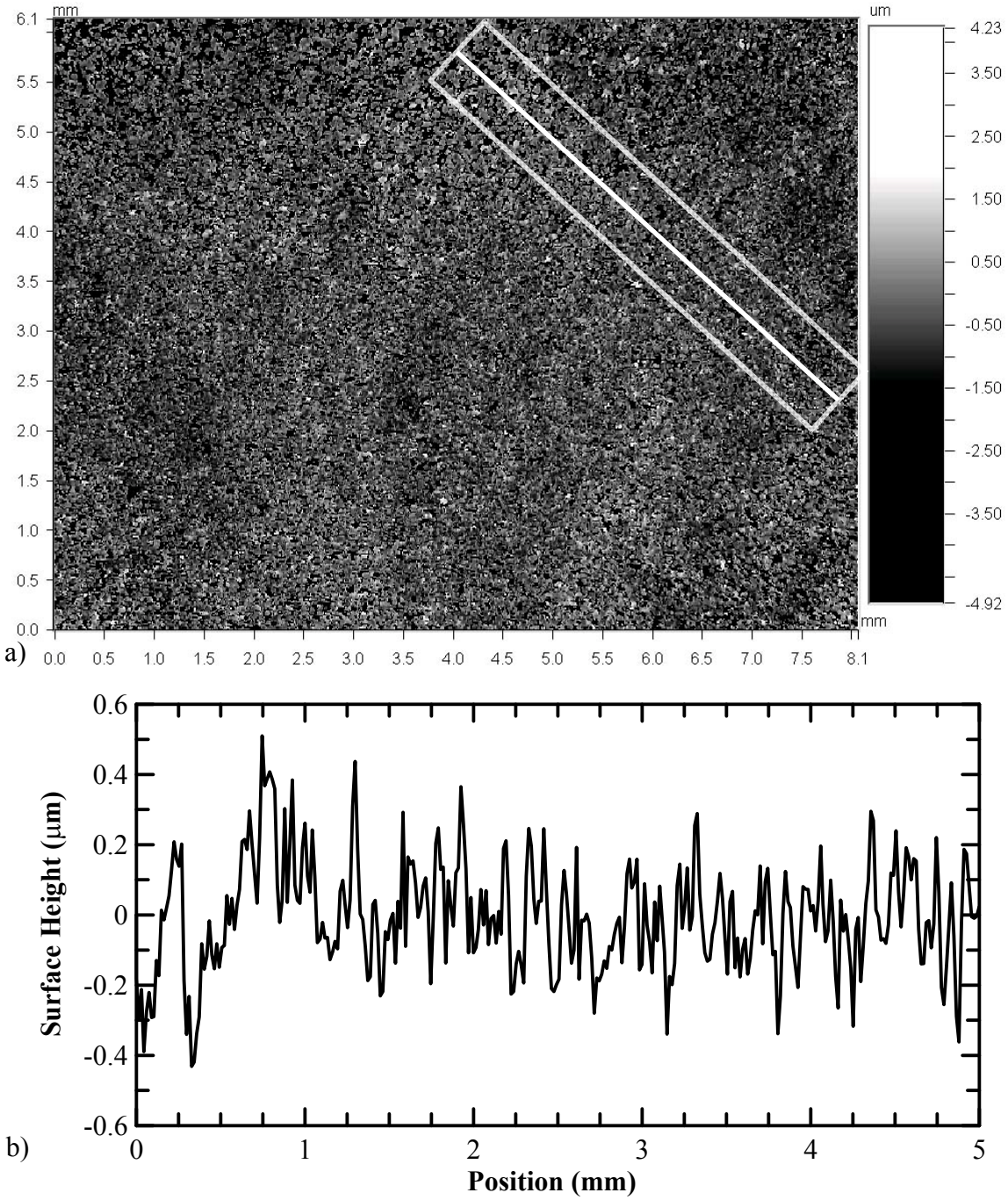

Figure 5.14 Topography of sample containing Lüders band after straining; a) three-dimensional topography contour view, b) two-dimensional surface topography corresponding to trace in contour view represented as a white line with outlined trace area. BH210GA, 1.00 % YPE, gage strain 1.73 % (trace 36). Tensile axis is horizontal in contour plot.

To improve clarity in figures showing surface profile changes with strain, the following adjustments to the data were performed: the profiles were shifted along the position axis to align common features, they were displaced vertically so as to not overlap, dashed reference lines were added to show the location of the Lüders band (shown with solid line segments at the trace containing the maximum depth), and some traces were suppressed. A trace was suppressed when it did not vary distinctly from one of its neighbors, and therefore would not provide additional insight. On the figures, these trace number and corresponding gage strain for each profile are given.

For each figure showing topography profile changes with strain (Figures 5.15, 5.17, and 5.19) there was one profile which demonstrates a condition of "maximum severity". The point of maximum severity was suggested by Humble[52] to be a condition of maximum Lüders band depth, and consequently the condition most readily visible to the naked eye. In the current investigation, topographies recorded at or near strain levels which produced the largest Lüders band depth gave the best indication of the presence of a Lüders band. From these topographies, shown in Figures 5.15, 5.17, and 5.19, the locations of two-dimensional topography traces were determined using Equations 4.5 and 4.6, and are indicated. In these figures, the profile two-dimensional topographies are not smoothed, and the dimensions of the Lüders bands are given.

In Figure 5.15, surface traces for BH210 GA with 0.25 % YPE are shown. Variations between profiles are subtle. The nucleation of the Lüders band occurs between traces 4 and 5, indicated by a slightly lower portion in the center of the indicated area. The point of largest depth can be seen in trace 9 (0.18 % strain). The band location was verified at this strain by a combination of cracking by StressCoat™ and the masking technique discussed in Section 4.5.3. The depth of this band remains relatively constant between traces 5 and 21. The calculation of depth is very dependent on the features of the coating at the edges of the Lüders band. The forms of the profiles remain relatively unchanged between 5 and 9 and again between traces 12 and 21. Figure 5.16 gives the three-dimensional contour plot of trace 9. Lüders band topography at this YPE level is difficult to observe in the contour plot. At this YPE level, the formation and propagation of a Lüders band is difficult to monitor accurately, because of very gradual changes in profiles.

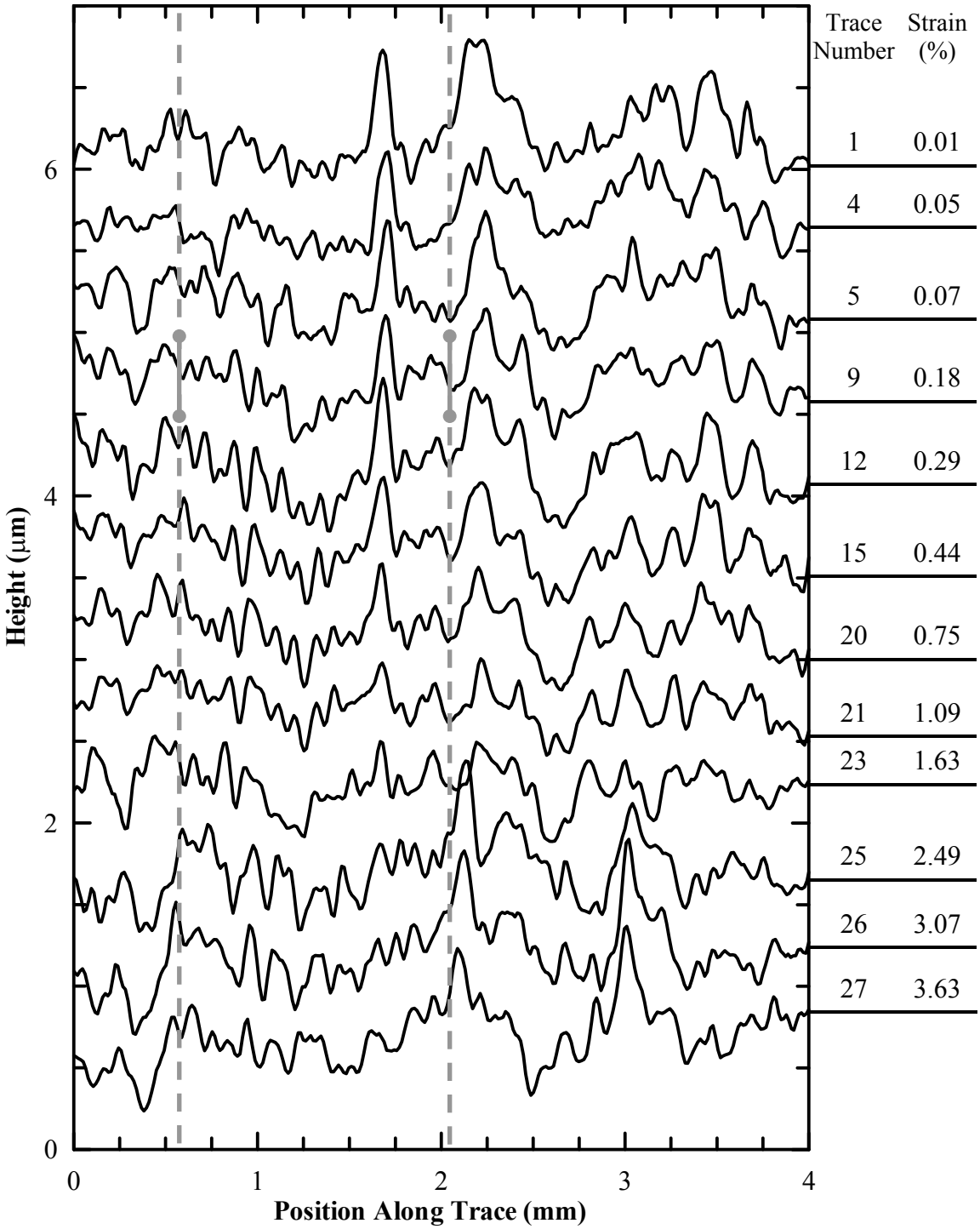

Figure 5.15 Two-dimensional surface traces on BH210 GA, 0.25 % YPE sample surface. Traces are from a common location, with increasing strain. Trace number and gage strain are indicated on right.

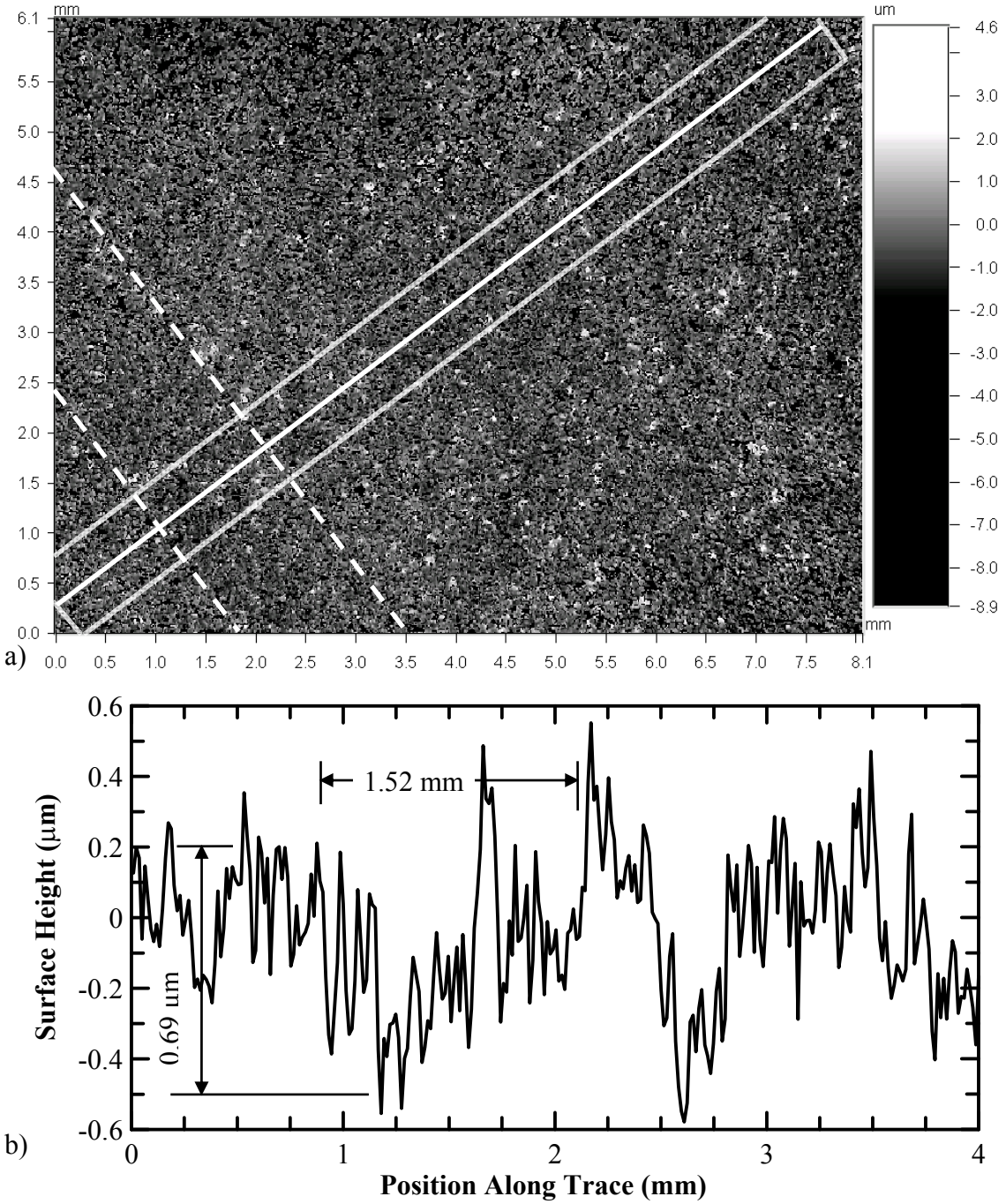

Figure 5.16 Topography of BH210GA sample with 0.25 % YPE containing a formed Lüders band (outlined by dashed lines); a) three-dimensional topography contour view, b) two-dimensional surface topography corresponding to trace in contour view represented as a white line with outlined trace area. Trace 9, gage strain 0.18%. Tensile axis is horizontal in contour plot.

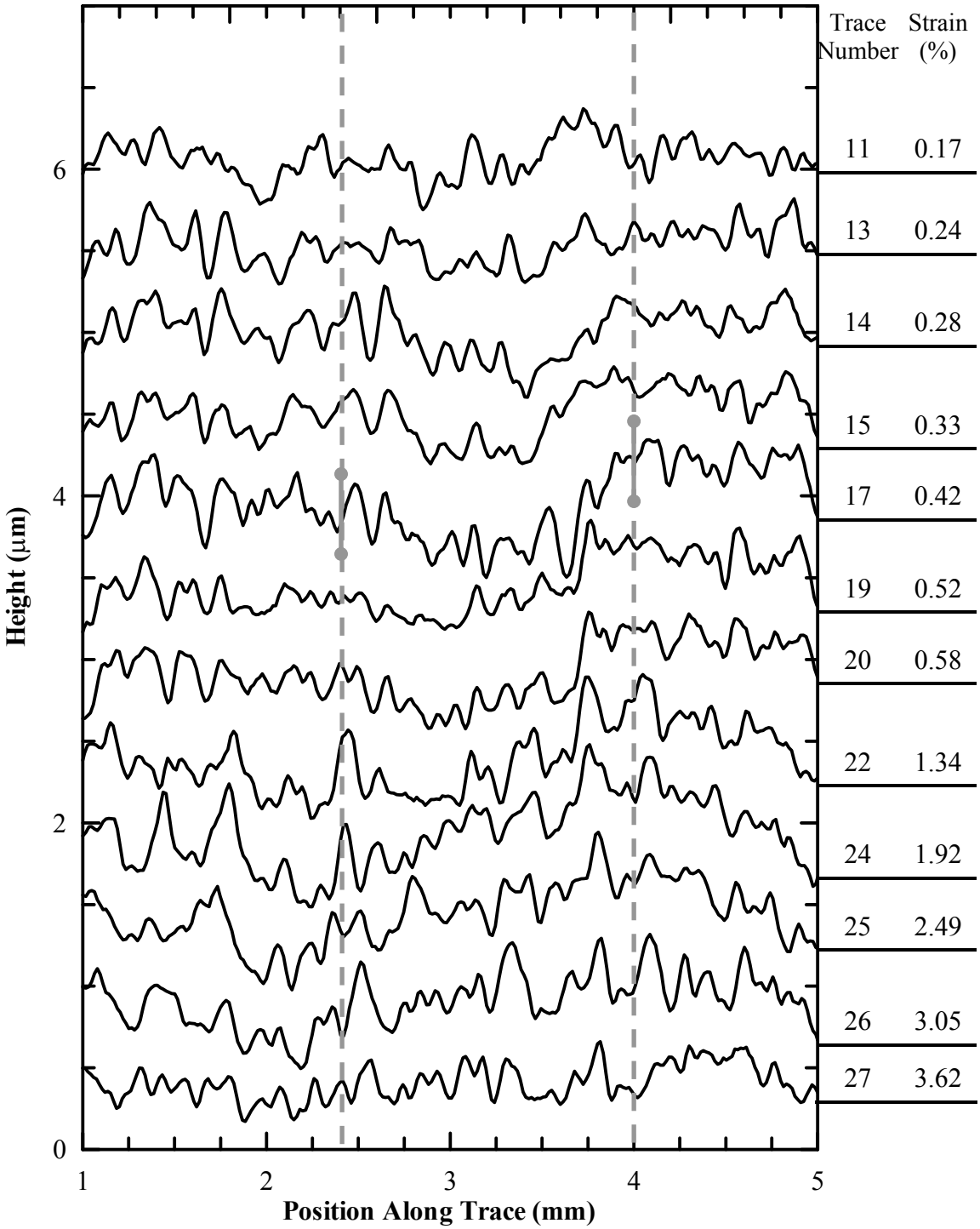

Figure 5.17 Two-dimensional surface traces on BH210 GA 0.50 % YPE sample surface. Traces are from a common location, with increasing strain. Trace number and gage strain are indicated on right.

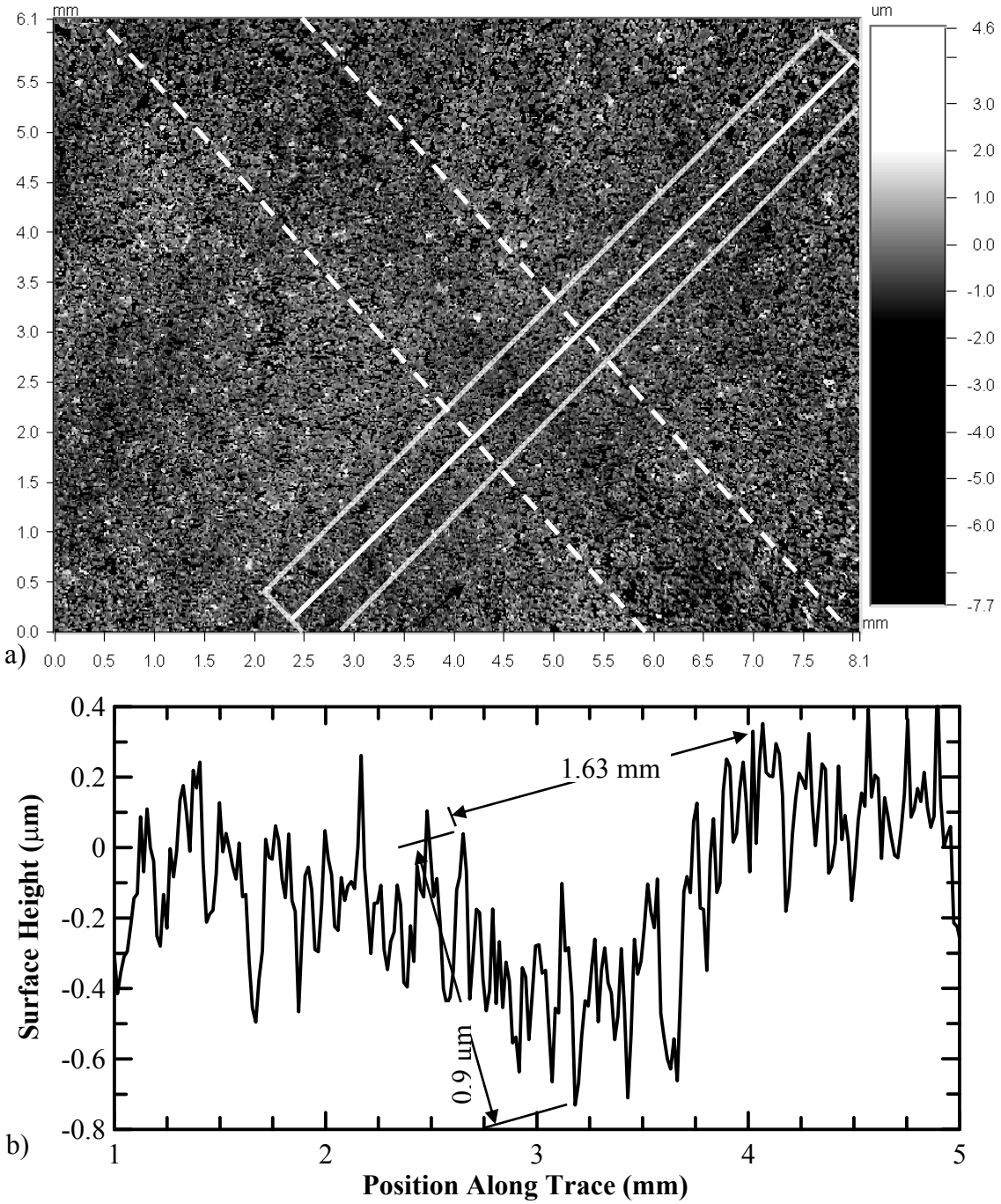

Figure 5.18 Topography of BH210GA sample with 0.50% YPE containing a formed Lüders band (outlined by dashed lines); a) three-dimensional topography contour view, b) two-dimensional surface topography corresponding to trace in contour view represented as a white line with outlined trace area. Trace 17, gage strain 0.42 %. Tensile axis is horizontal in contour plot.

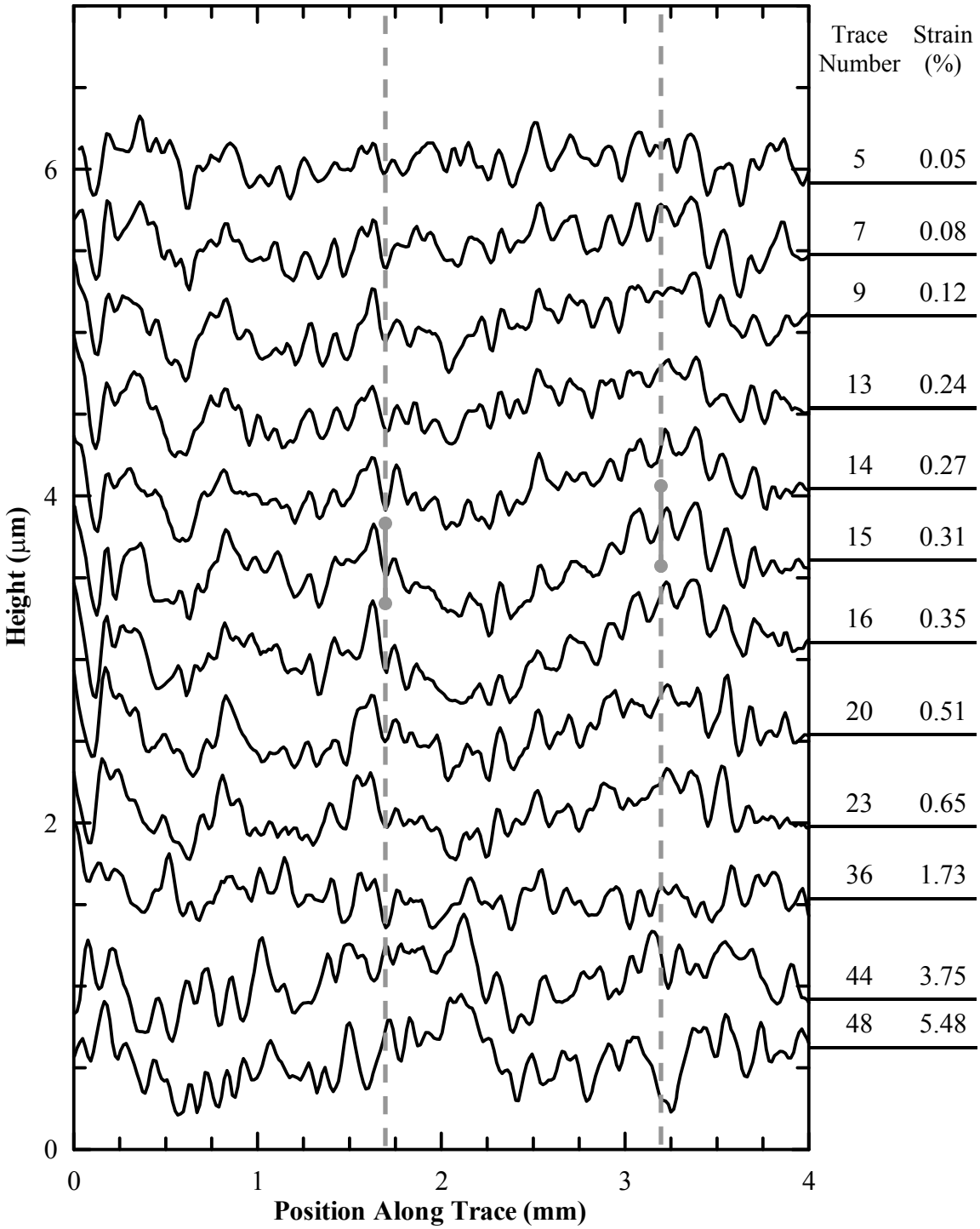

Figure 5.19 Two-dimensional surface traces on BH210 GA 1.00 % YPE sample surface. Traces are from a common location, with increasing strain. Trace number and gage strain are indicated on right.

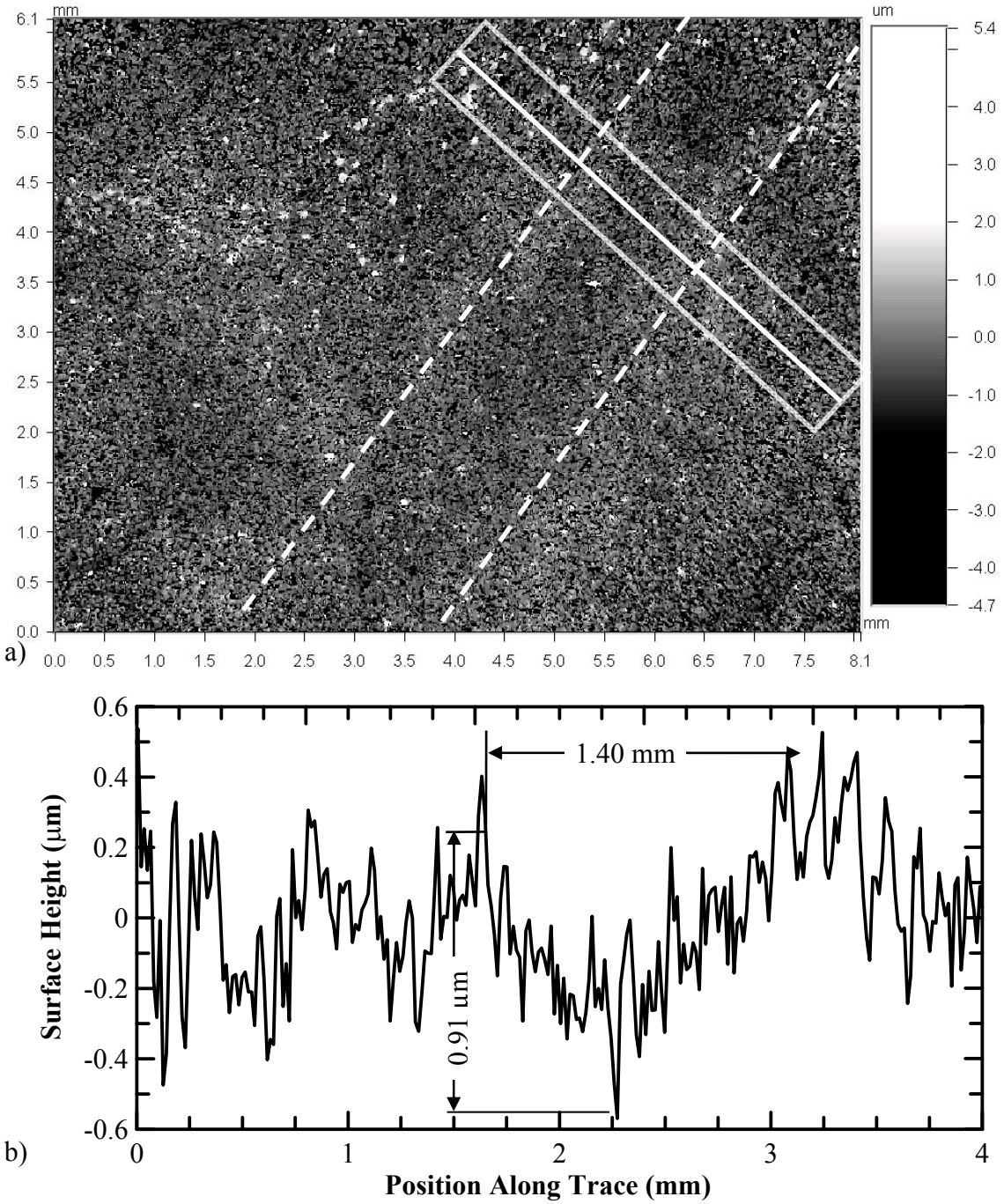

Figure 5.20 Topography of BH210GA sample with 1.00% YPE containing a formed Lüders band (outlined by dashed lines); a) three-dimensional topography contour view, b) two-dimensional surface topography corresponding to trace in contour view represented as a white line with outlined trace area. Trace 15, gage strain 0.31 %. Tensile axis is horizontal in contour plot.

In Figure 5.17, surface traces for BH210 GA with 0.50 % YPE are shown. Trace 0 was recorded at 0 % strain. Traces 1-10 were recorded at the same location as trace 0. It was noticed that the band front nucleated outside this location and the imaging area was moved between traces 10 and 11 to intercept the moving Lüders band front. Trace 11 was located ahead of the front, which was indicated by StressCoat™. Nucleation of the Lüders band occurred between traces 13 and 14. The band location was verified during trace 15 by a combination of cracking by StressCoat™ and the masking technique discussed in Section 4.5.3. The point of largest depth can be seen in trace 17 at a gage strain of 0.42 %. At increased strains, the Lüders band depth decreases, and at 3 % strain, is nearly flat i.e. comparable to the overall roughness. The contour plot of trace 17 is shown in Figure 5.18.

In Figure 5.19, surface traces for BH210 GA with 1.00 % YPE are shown. The Lüders band nucleated between traces 13 and 14. The point of largest depth can be seen in trace 15. With increasing strain, the prominence of the Lüders band decreases; the depth decreases and the band flattens out. The imaging area was fixed during the entire test sequence. The contour plot of trace 15 is shown in Figure 5.20 at a gage strain of 0.31 %.

Table 5.2 provides a summation of the maximum depth and the corresponding Lüders band width at that depth for each sample tested. The determinations of depths are very dependent on the points of selection, e.g. how much "noise" resulting from the coating was included. The uncertainty in these depths is approximately 0.2 μm. An overall increase in maximum depth with increasing YPE is indicated by the data. There is no clear effect of YPE apparent in terms of Lüders band width. Humble's findings also indicated both an increase in depth and unchanging width with increasing YPE.[52] The maximum depths of the Lüders bands occurred close to their onset, e.g. within 0.15 % strain. The prominence of the Lüders band appearance seems to decrease with increasing strain. The band depth seems to reduce as the topography flattens out. Other features within the coating's roughness, not associated with the Lüders bands, become prominent. The average roughness values for the BH210 GA material are also given in Table 5.2 for the unstrained condition. The roughness of the material is expected to increase further with strain.[71] These roughness values are substantial compared to the Lüders band depth.

Table 5.2 Summary of Lüders band characteristic geometry at most severe condition

YPE (%)	Maximum Depth (μm)	Width at Maximum Depth (mm)	Trace number	Roughness at 0 % Strain (μm)	Gage Strain (%)
0	-	-	-	-	-
0.25	0.6	1.5	9	0.60	0.18
0.50	0.9	1.6	17	0.57	0.42
1.00	0.9	1.4	15	0.54	0.31

5.3 Analysis of Multiple Lüders Bands in Uniaxial Tension

The second method of determining Lüders band geometry allowed for the evaluation of multiple band geometries on each sample. On each sample, between 3 and 15 distinguishable Lüders bands were formed and their topographies were characterized by obtaining the width and depth of the bands. Thirty samples were examined, each representing a condition defined within the test matrix.

The Lüders band locations were determined using StressCoat™. The bands were measured at the same strain where StressCoat™ first indicated their formation, i.e. just after nucleation. This state of deformation was chosen because research by Humble,[52] and results from previous sections indicated that maximum band depth is achieved at strains very near to those which cause nucleation of the Lüders bands. The crosshead was manually stopped when Lüders bands became apparent. Because the samples remained under load, a period of stress relaxation followed the stopping of the crosshead. For some samples, during this stress relaxation, the region of non-uniform yielding (indicated by StressCoat™) was noticed to increase in width, indicating further propagation. Observations of Lüders band propagation during stress relaxation are consistent with literature.[38]

In some instances, especially the BH210 GA samples with larger YPE, the topographies of multiple bands could be observed in a single scan area (e.g. Figure 5.18). Figure 5.21 gives one example of the surface topographies recorded for each material. At least one recorded Lüders band is present in each scan area. The intersection of crossing Lüders bands increases the measured depth by at least a factor of two. Therefore, depth

measurements were taken at positions which only captured single Lüders bands. The variation in the measured surfaces, due to roughness can be an influential factor in the interpretation in surface geometries. The mean roughness of as-received samples, and roughness of surfaces with Lüders bands (featured in Figure 5.21) are given in Table 5.3; the Lüders bands were not excluded from the roughness values. The roughness values of LC GI are misleading because of very long wavelength, high amplitude changes in surface, which could not be removed with Vision32 software. When sampling small regions which could be filtered, the LC GI as-temper-rolled surface roughness is 0.5 μm. The uncertainty in the depth measurements was considered to be related to the surface roughness amplitude at the points used to calculate the two "edges" and the bottom of the Lüders band, and was estimated from surface profiles.[§] From a propagation-of-error analysis (error being the surface roughness amplitude at the points chosen), the depth uncertainty was 1.0 μm, 0.2 μm, 0.6 μm, and 0.2 μm for BH210 EG, GA, GI and LC GI, respectfully. The uncertainty in measuring the width is caused by the local variations in the trace masking of the left and right edges of the Lüders band. This uncertainty was on the order of the spatial wavelength of the roughness, between 0.1 and 0.2 mm for all materials.

Because multiple bands were recorded on a single sample, each condition had a range of Lüders band depths and widths. The resulting data set was narrowed by inspecting all three-dimensional topographies containing Lüders bands. Topographies with "well formed" Lüders bands, i.e. linear depressions extending across the observable topography, were included in the analysis. The characteristic geometries (i.e. depth and width) of Lüders bands with "well formed" topographies for all materials are shown in Figures 5.22 and 5.23 as a function of YPE and specimen orientation. The Lüders band depths are shown in Figure 5.22 while the widths are shown in Figure 5.23. The YPE for each condition was based on the stress-strain curves described in Section 5.1. Using Figures 5.22 and 5.23 the relationship between YPE development and the key variables will be discussed in the following sub-sections.

[§] A thirtieth-order polynomial was fit to each surface profile. The deviation from the recorded surface height to the polynomial fit for each data point was summed, then divided by the total number of data points. A high order polynomial fit was used to closely follow topography which included the presence of Lüders bands.

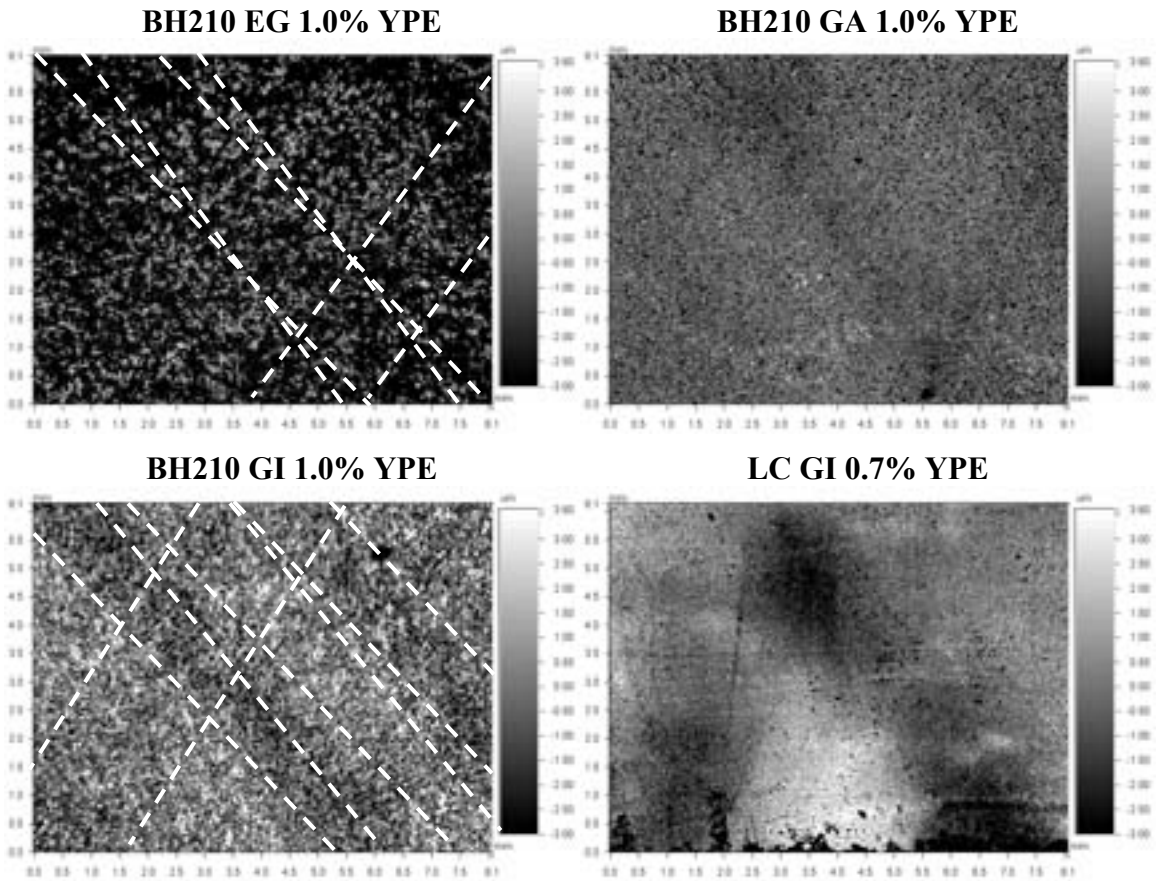

Figure 5.21 Contour plots of tested materials strained to form Lüders bands. Three-dimensional topographies were recorded after nucleation, and location of bands was indicated with StressCoat™. Dashed lines border Lüders bands in each scan area. Tensile axis horizontal in contour plots.

Table 5.3 Single scan roughness of materials

Material	R_a, as-received surface (μm)	R_a, surface with Lüders band (μm)
BH210 EG	0.9	1.1
BH210 GA	0.6	0.6
BH210 GI	1.4	1.2
LC GI	1.2	1.1

5.3.1 Comparison of Materials

In the analysis of specimens developing multiple Lüders bands, there were differences among the test materials. With respect to Lüders band depths (Figure 5.22), BH210 EG had the most scatter and the largest overall depth values at each YPE level. It is believed that the greater depth in BH210 EG may be an artifact of the low total amount of data collected in topography scans. For this same reason, it is also believed to be the least reliable dataset among the materials. BH210 GA had the least scatter overall, and the smallest values of Lüders band depth.

For the materials which obtained 0.25 % YPE, the recorded Lüders band depths were very close to or less than their respective average unstrained surface roughness. It is possible that these Lüders bands would appear invisible, their topography "lost" in the local variations of the surface. This could possibly influence the acceptable YPE criteria in surface critical components.

The Lüders band widths for all materials were very similar, most falling within the 1 mm to 2.5 mm range. This assessment excludes two large values from LC GI, which will receive special consideration in a later section.

In comparing the results of different steels, it should be noted that the sample materials were produced by different manufacturers using different alloying and processing approaches, and that single (rather than multiple) coils were examined. Thus, it is not yet possible to conclude that observed differences are characteristic of the full class of materials represented by the different steels. Nonetheless, a slightly reduced Lüders band depth in the galvannealed coating in comparison to the two pure zinc coatings is interesting, and may related to the higher hardness of the GA coating as well as a somewhat different temper rolling response, although further work would be needed to examine these aspects.

5.3.2 Orientation Effect on Lüders Band Geometry

The scatter present in the longitudinal and transverse datasets for the materials and YPE levels tested obscure any small differences that may exist between the longitudinal and transverse directions for either Lüders band widths or depths.

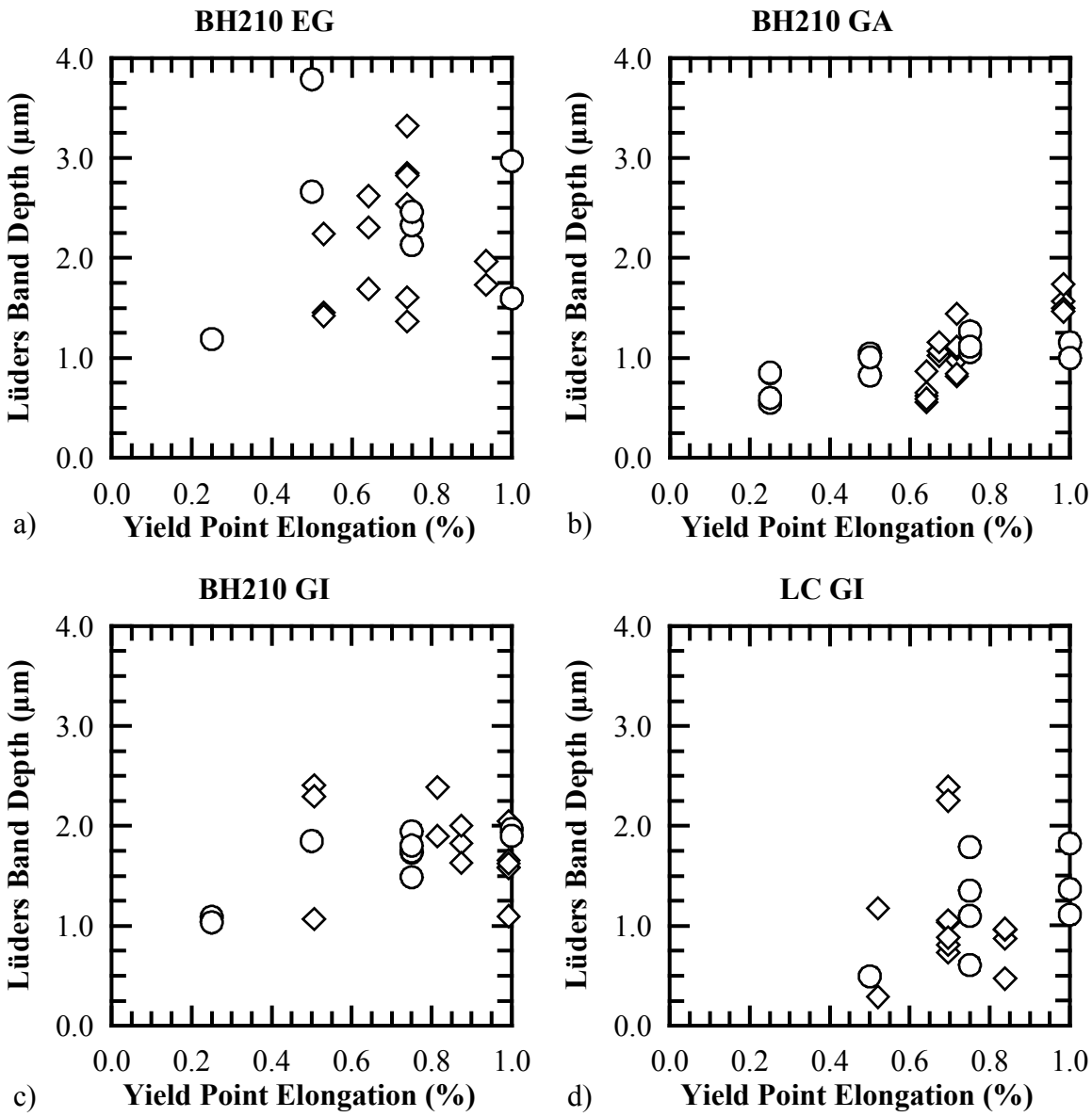

Figure 5.22 Variation of recorded band depth with YPE for the four test materials. ∽ Longitudinal, ▭ Transverse; a) BH210 EG, b) BH210 GA, c) BH210 GI, d) LC GI.

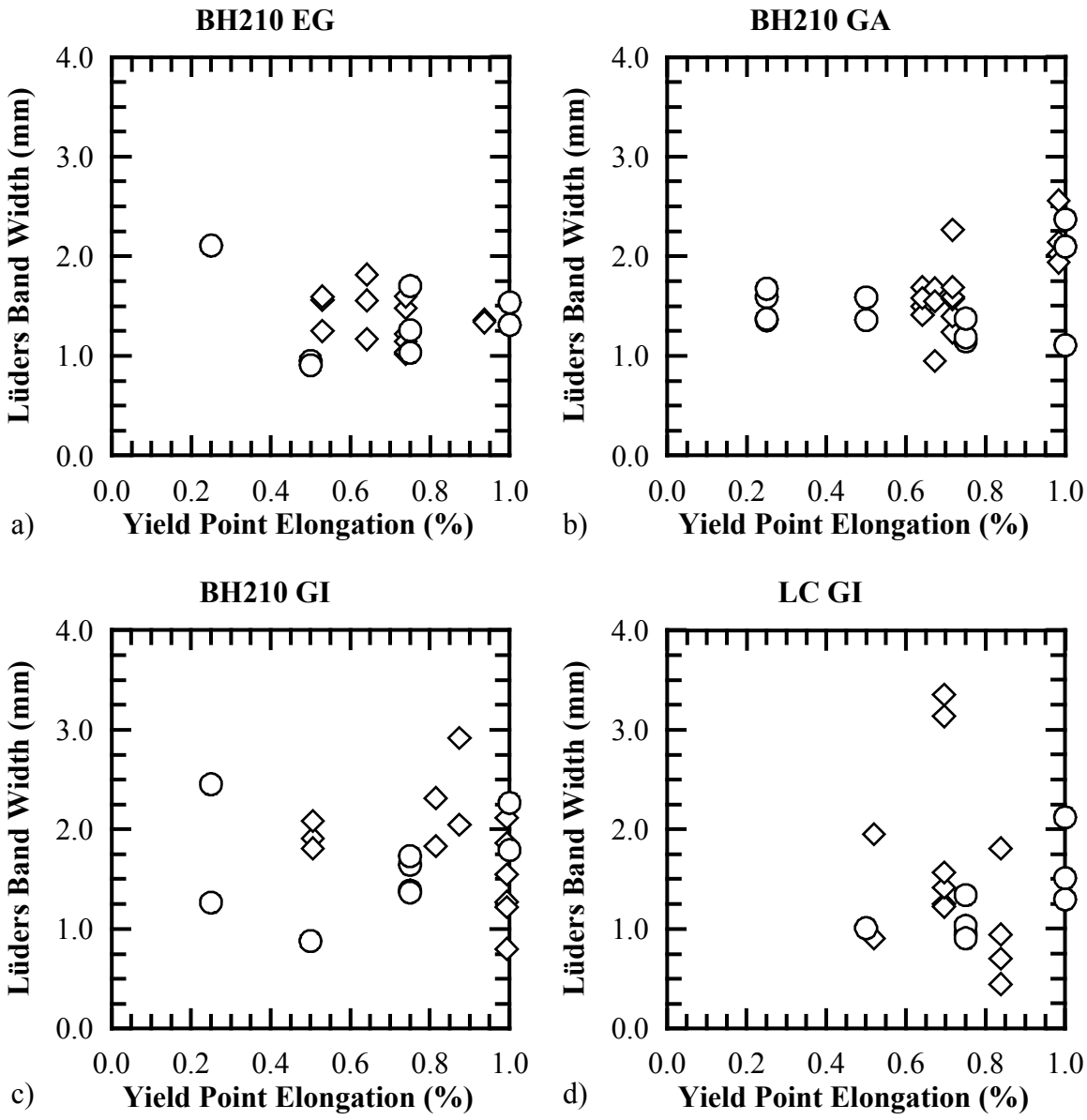

Figure 5.23 Variation of recorded band width with YPE for the four test materials. ⌇ Longitudinal, ⌸ Transverse; a) BH210 EG, b) BH210 GA, c) BH210 GI, d) LC GI.

5.3.3 YPE Effect on Lüders Band Geometry

Based on the behavior of BH210 GA, BH210 GI and LC GI for both orientations, there is a general increase in Lüders band depth with increasing YPE. For samples with transverse orientation, which had YPE levels between 0.25 % and 1.00 %, the depths in all four materials increased up to YPE levels of approximately 0.7 % and then appear unchanged up to 1.00 % YPE. Lüders band depths for samples with longitudinal orientation did not exhibit a consistent trend over the measured YPE range (0.50 % to 1.00 %). BH210 GA (longitudinal) is an exception, which indicated an average depth increase with increasing YPE.

For both orientations, average Lüders band widths remain unchanged with increasing YPE for all materials. The exceptions are BH210 GA longitudinal and LC GI transverse which increase with increasing YPE, but only have data at higher YPE levels.

5.3.4 Thickness Effect on Lüders Band Geometry

It was expected that an increase in sample thickness should increase the dimensions (at least the depth) of a Lüders band. The reasoning is this: assuming an isotropic material with a rectangular cross-section and volume conservation during plastic deformation, if the gage length increases by 1 % the width and thickness would reduce by 0.5 %. It can be further assumed that this deformation can be localized relative to the length of the sample, and would then represent a single formed Lüders band. Using the localized strain argument and relating original and final thickness with strain reduction, the reduction in thickness at the Lüders band should be directly proportional to the original thickness of the material.

Using the above reasoning, doubling the thickness should double the depth of the Lüders band. The BH210 materials were about 0.7 mm thick while the LC GI material was 1.4 mm thick. From the data presented in Figure 5.22, the depths of the Lüders bands in the LC GI material are very similar to the BH210 materials, not twice as large. Similarly, the Lüders band widths also do not double in size (Figure 5.23), although this behavior is less surprising.

Some evidence of increasing width and depth with increasing thickness is shown by two large value points in the LC GI material. In addition to being significantly greater in both depth and width compared to other LC GI data points, these points were obtained from topographies with the most "well formed" Lüders band. One of these topographies was shown previously in (Figure 5.21, LC GI). They were obtained from the same sample, 0.7 % YPE longitudinal condition. Both the width and depth of these bands were nearly twice as large as the Lüders band widths and depths in other LC GI YPE/orientation conditions, but still fell within the range of dimensions recorded on samples half their thickness.

5.3.5 Comparison of Methods to Obtain Lüders Band Geometry

Direct comparisons can be made between the Lüders band characteristic geometries (widths and depths) for the two observation methods using results obtained from BH210 GA transverse tensile samples. The "maximum severity" characteristic geometry found during evolution (Table 5.2) can be compared to the "average" characteristic geometry of the multi-band analysis for respective YPE levels. These characteristic geometries are reproduced in Table 5.4. In most cases, the multiple Lüders band measurement approach recorded band depths greater than those observed in the evolution measurements. If the visual severity of a Lüders band is related to its depth, the multiple Lüders band measurement approach appears to give appropriate geometry data.

Table 5.4 Lüders band characteristic geometry comparison between two topography capturing methods using BH210 GA material

	Geometry from evolution of a single band		Geometry from multi-band analysis	
YPE (%)	Maximum Depth (μm)	Width at Maximum Depth (mm)	Average Depth (μm)	Average Width (mm)
0.25 %	0.64	1.6	0.71	1.5
0.50 %	0.90	1.3	0.96	1.5
1.00 %	0.91	1.4	1.05	1.9

5.4 Discontinuous Yielding In Balanced Biaxial Strain Paths

Two materials were tested in balanced biaxial tension in order to analyze the surface topography of Lüders bands formed in this strain path. These materials were BH210 GI and a high-YPE EG material (not associated with BH210 EG). The high-YPE EG material was used in order to develop analysis techniques and determine feasibility of generating discontinuous yielding in biaxial tension. This material developed a YPE in uniaxial tension of 7.3 % (with well developed Lüders bands) when aged at 150 °C for 43.5 hr.

For all biaxial tests the plastic strain imposed on the samples was calculated using the change in dimension of scribed circles (50.8 mm in diameter). The strain is reported in terms of principal surface strains rather than Von Mises (effective) strain.

5.4.1 High-YPE EG Material

StressCoat™ was activated (i.e. microcracked) during balanced biaxial deformation of the high-YPE EG material (with 7.3 % YPE). The activated areas, indicating local deformation, are shown photographically and schematically in Figures 5.24 and 5.25 for imposed strains of 0.25 % and 0.5 % respectfully. Strain lines were present on the reverse sides of the sample in the corresponding locations to StressCoat™ cracking. In biaxial testing, at approximately 0.03 % plastic strain, StressCoat™ was activated in the center of the test material. Increasing strain (through 0.5 % plastic strain) further developed the StressCoat™. The pattern of development did not reflect the classical stretcher strain appearance, a cross hatched pattern. On the high-YPE EG surface, local deformations appear to be linear running diametrically across the surface. Increases in strain increased the area covered by localized deformation but the bands did not develop in any distinctive pattern.

5.4.2 BH210 GI Material With 1 %YPE

BH210 GI steel sheets were aged to 1.0 % YPE. Principal plastic surface strains between 0.25 % and 0.8 % were imposed on the samples. At these strain levels, no

samples produced local deformation as indicated by StressCoat™ (Figure 5.26). Visual observations on the reverse side of the samples were also unable to identify any non-uniform deformation. It was reasoned that the presence of discontinuous yielding would not be observed in the other BH210 materials with 1.00 % or less YPE. Therefore, no other materials, or YPE levels were evaluated in balanced biaxial strain.

At a major plastic strain of 0.8 %, the effective strain was greater than the 1.00 % YPE. The material was strained beyond the point where Lüders bands might have finished propagating across the surface. This implies that at an industrially significant YPE level of 1.00 % YPE, small balanced biaxial strains may not produce Lüders bands on sample surfaces.

A possible reason for the lack of Lüders band formation at low plastic strain is the physical constraint placed on the samples. In discontinuous yielding material elongates significantly more perpendicular to the Lüders band, compared to the length. In a true balanced biaxial tension, there are no in-plane directions which can alleviate this

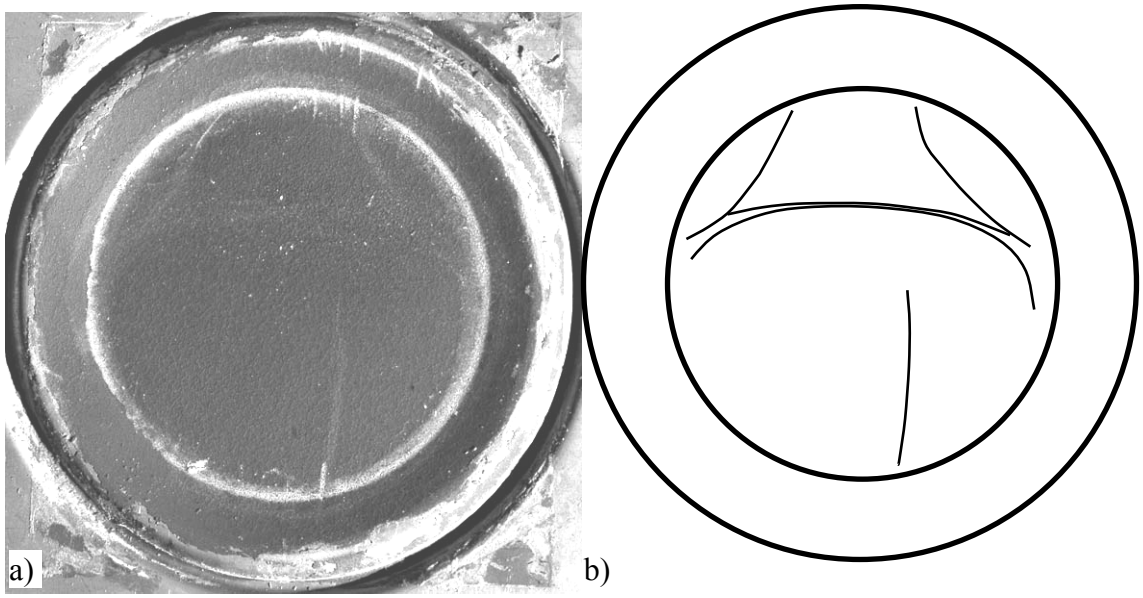

Figure 5.24 High-YPE EG material after biaxial deformation, with underside of sample shown. 7.3 % YPE, $\varepsilon_1=\varepsilon_2=0.25$ %; a) photograph of sample with microcracked StressCoat™ seen as lighter regions, b) schematic representation of regions of microcracked StressCoat™ (dark lines). 0.5x magnification.

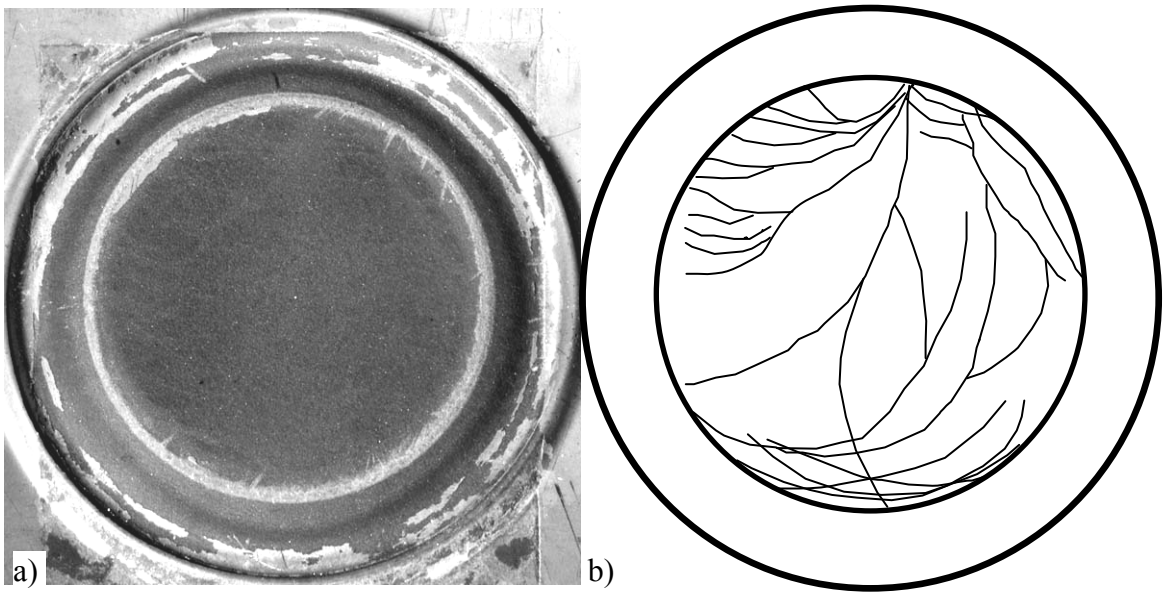

Figure 5.25 High-YPE EG material after biaxial deformation, with underside of sample shown. 7.3 % YPE, $\varepsilon_1=\varepsilon_2=0.5$ %; a) photograph of sample with microcracked StressCoat™ seen as lighter regions, b) schematic representation of regions of microcracked StressCoat™ (dark lines). 0.5x magnification.

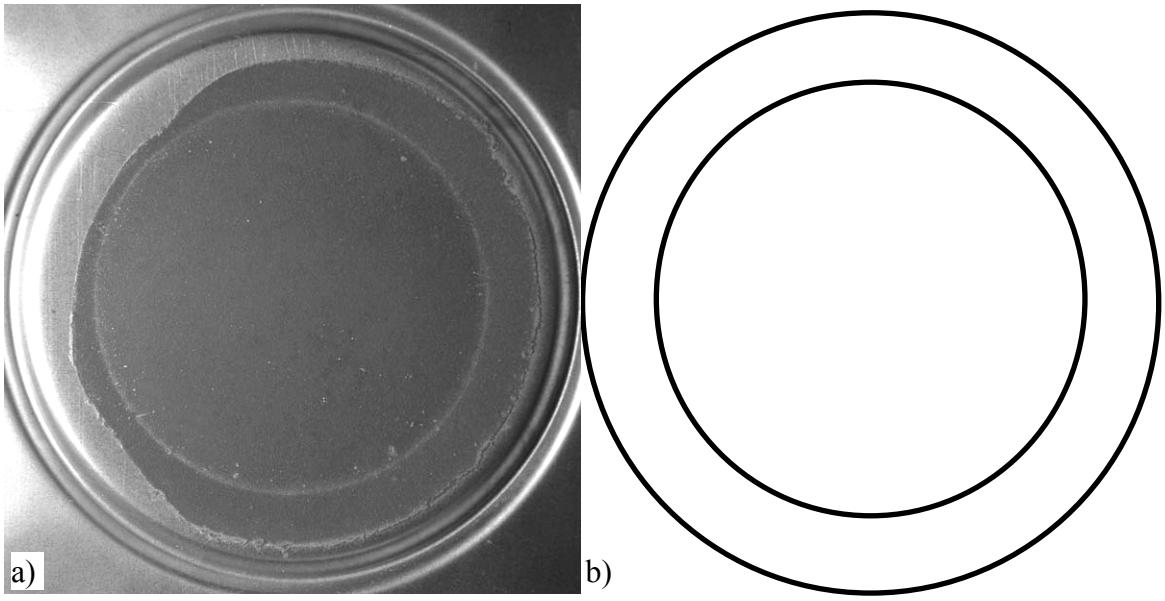

Figure 5.26 BH210 GI material after biaxial deformation, with underside of sample shown. 1.0 % YPE, $\varepsilon_1=\varepsilon_2=0.3$ %; a) photograph of sample, microcracked StressCoat™ would be seen as lighter regions, b)schematic representation of regions of microcracked StressCoat™, no regions of discontinuous yielding were found. 0.5x magnification.

discontinuous distortion. Further exploration is necessary to determine YPE or strain level thresholds, and the mechanism responsible for keeping the material yielding continuously.

5.5 Analysis of Lüders Band Characteristics in Non-Balanced Biaxial Tension

Two series of tests were conducted to achieve the objective of analyzing the surface topography of Lüders bands formed in non-balanced biaxial tension. The first series of tests produced strain paths which can be considered drawing (in addition to the uniaxial tension states that are also a drawing mode). The second series of tests produced strain paths near plane strain. Multiple strain paths were considered in order to identify if varying strain path affects Lüders band geometry. An illustration of sample widths after forming is shown in Figure 5.27.

For both series of tests, all three BH210 materials were used. All samples were aged to produce a 1.00 % YPE condition (in uniaxial tension). The LC GI material was not included because the Marciniak sample dimensions were larger than the capacity of the laboratory rolling mill, and subsequently the material could not be temper-rolled to remove the initial YPE that was present in the as-received condition for this portion of the work.

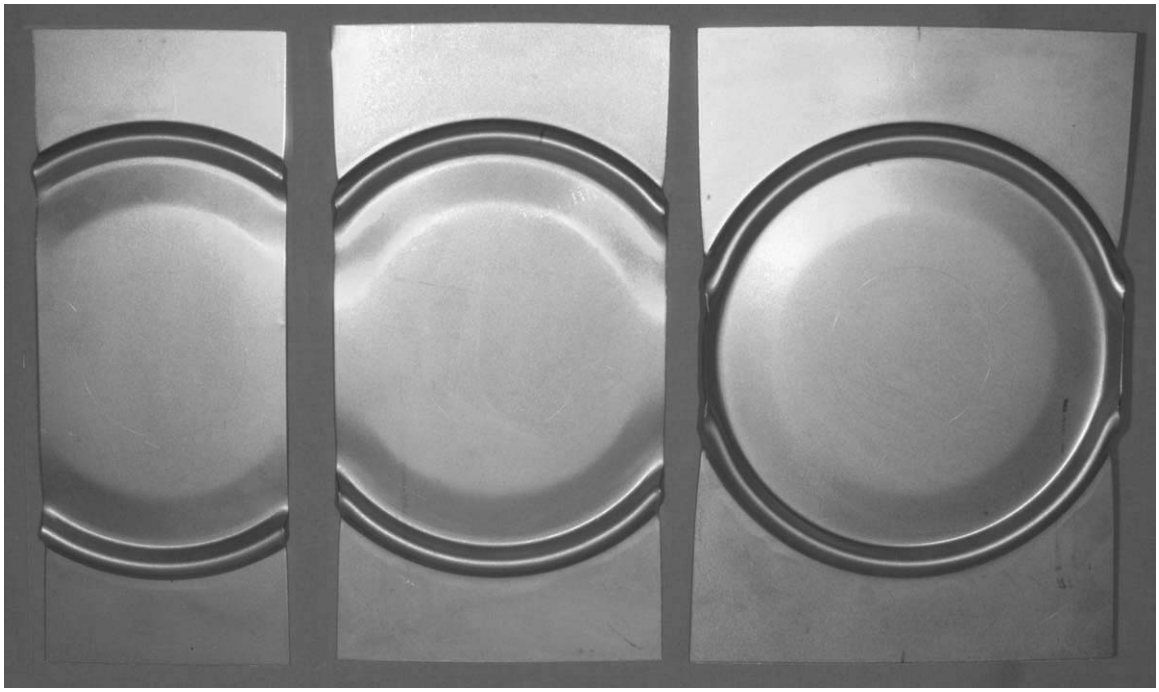

Figure 5.27 Non-balanced biaxial samples as formed. a) 76.2 mm wide, b) 101.6 mm wide, c) 134.9 mm.

5.5.1 Drawing Strain Paths

Two sample widths were used in the drawing strain states, 76.2 mm and 101.6 mm. Punch depth was kept constant for all samples (0.9 mm). The drawing strain paths produced non-uniform yielding in a classic stretcher strain crosshatched pattern in both sample widths (Figure 5.28). The measured principal strains for all drawing conditions are given in Table 5.5. Uncertainty in measurement of strain was relatively large (one-quarter to one-half the measured strain) for the small plastic strains imposed.

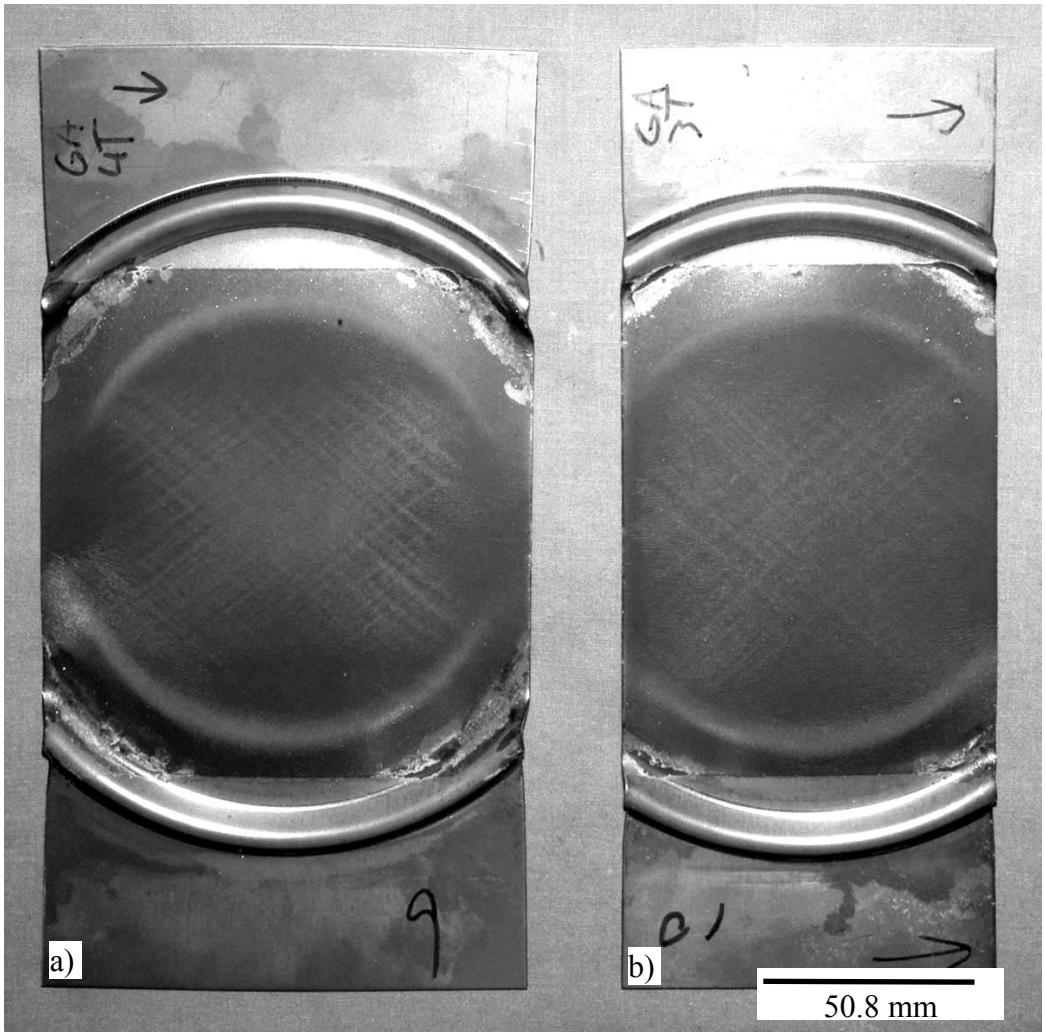

Figure 5.28 BH210 GA samples after drawing deformation microcracked StressCoat™ seen as lighter linear crosshatched pattern. a) 101.6 mm wide, 1.0 % YPE, ε_1= 0.5 % ε_2=-0.4 %, punch depth 0.9 mm; b) 76.2 mm wide, 1.0 % YPE, ε_1= 0.4 % ε_2=-0.5 %, punch depth 0.9 mm.

Measurements of surface topography were taken at five locations on the as-deformed sample surface. Lüders bands present in these topographies were analyzed. The characteristic geometries (depth and width) of these measured bands are given in Tables 5.5 through 5.7. Relationships between Lüders band geometry and strain ratio will be further discussed in a later section.

5.5.2 Strain Paths near Plane Strain

Two sample widths were chosen for each BH210 material to analyze the formation of Lüders bands very near to plane strain (134.9 mm and 135.4 mm). The sample widths were chosen based on an empirical relationship of strain ratio to sample width (shown previously in Section 4.4.1). This initial strain ratio relationship was developed with samples undergoing 12 times more punch displacement than those tested at small strains to produce Lüders band topography, so that the strains could be accurately measured. A consistent punch depth of 1.3 mm was used to deform all samples to produce Lüders band topography at low strains. The post-deformation strains measured for each test material are given in Table 5.9. On average, a 0.3 % major strain and a -0.3 % minor strain was measured. Although it was anticipated that these materials would exhibit plane strain, at these small deformations it is not clear that plane strain conditions were obtained.

The Lüders bands generated on the near plane strain samples were observed to form in the classical cross hatched patterns of stretcher strains (Figures 5.29 through 5.31). Lüders bands formed on BH210 EG (Figure 5.29) were more widely spaced and fewer in number than those bands formed on BH210 GA and BH210 GI (Figure 5.30 and Figure 5.31 respectively).

Measurements of surface topography were taken at five locations on the as-deformed sample surface. Lüders bands present in these topographies were analyzed. The characteristic geometries (depth and width) of these measured bands are given in Tables 5.9 through 5.11. Variation in Lüders band geometries was small when comparing the two sample widths for each material. This result is not surprising given the small variation between the sample widths and similar strain ratios. The influence of strain ratio on Lüders band geometry will be examined in the next section.

Table 5.5 Deformation of materials with drawing strain paths

Material	Sample Width (mm)	Orient.	Major Eng. strain, ε_1 (%)	Minor Eng. Strain, ε_2 (%)	Effective Strain (%)	$\varepsilon_1/\varepsilon_2$ True (%/%)
BH210 EG	76.2	Long.	0.4 ± 0.2	-0.3 ± 0.2	0.4 ± 0.2	-0.6 ± 0.6
		Trans.	0.5 ± 0.2	-0.4 ± 0.2	0.5 ± 0.2	-0.8 ± 0.5
	101.6	Long.	0.6 ± 0.2	-0.6 ± 0.2	0.7 ± 0.2	-1.0 ± 0.5
		Trans.	0.4 ± 0.2	-0.6 ± 0.2	0.7 ± 0.2	-1.5 ± 0.8
BH210 GA	76.2	Long.	0.9 ± 0.2	-0.5 ± 0.2	0.9 ± 0.2	-0.5 ± 0.3
		Trans.	0.4 ± 0.2	-0.5 ± 0.2	0.5 ± 0.2	-1.1 ± 0.8
	101.6	Long.	0.4 ± 0.2	-0.6 ± 0.2	0.6 ± 0.2	-1.4 ± 0.9
		Trans.	0.5 ± 0.2	-0.4 ± 0.2	0.5 ± 0.2	-0.8 ± 0.5
BH210 GI	76.2	Long.	0.5 ± 0.2	-0.4 ± 0.2	0.5 ± 0.2	-0.9 ± 0.6
		Trans.	0.4 ± 0.2	-0.3 ± 0.2	0.4 ± 0.2	-0.9 ± 0.8
	101.6	Long.	0.5 ± 0.2	-0.6 ± 0.2	0.6 ± 0.2	-1.2 ± 0.6
		Trans.	0.5 ± 0.2	-0.5 ± 0.2	0.5 ± 0.2	-1.0 ± 0.6

Table 5.6 Lüders band profile dimensions of BH210 EG (1.00 % YPE) in drawing strain path

Sample Width (mm)	Orientation	Width (mm)	Depth (μm)
76.2	Long.	0.9	2.1
		1.1	2.0
		1.3	2.8
		1.1	1.1
		1.2	2.1
76.2	Trans.	0.8	2.7
		1.3	2.5
		0.9	1.9
		1.2	2.7
101.6	Long.	1.0	2.0
		1.4	1.8
		1.3	2.2
		1.7	3.0
		1.0	1.8
		0.9	2.8
		1.4	1.9
101.6	Trans.	1.1	1.8
		1.0	3.7
		1.0	2.3
		1.2	2.8
		1.3	2.7

Table 5.7 Lüders band profile dimensions of BH210 GA (1.00 % YPE) in drawing strain path

Sample Width (mm)	Orientation	Width (mm)	Depth (μm)
76.2	Long.	1.6	1.6
		1.7	1.4
		1.6	1.1
		1.0	1.1
		1.1	0.9
		1.4	1.2
		1.4	1.2
		1.1	1.1
		1.1	1.0
		1.3	1.1
76.2	Trans.	0.9	0.9
		1.1	1.0
		1.0	1.1
		1.0	0.8
		1.0	0.8
		1.0	0.9
		1.1	0.9
101.6	Long.	1.6	1.4
		1.3	1.7
		1.5	1.5
		1.1	1.4
		1.7	1.8
		1.5	1.2
		1.4	1.3
101.6	Trans.	0.9	1.2
		1.4	1.5
		1.0	1.5
		1.6	1.2
		1.0	1.4

Table 5.8 Lüders band profile dimensions of BH210 GI (1.00 % YPE) in drawing strain path

Sample Width (mm)	Orientation	Width (mm)	Depth (μm)
76.2	Long.	1.3	1.8
		1.3	1.4
		1.1	1.7
		1.3	1.6
		1.3	1.5
76.2	Trans.	1.4	1.8
		1.5	1.8
		1.1	1.8
		0.9	2.3
		1.3	1.8
		1.3	1.7
		1.9	1.7
		1.0	1.6
101.6	Long.	1.4	1.3
		1.1	1.9
		1.2	1.4
		2.0	2.1
		1.4	2.3
		1.3	2.0
		1.5	2.4
		1.5	2.4
101.6	Trans.	1.3	1.4
		1.1	1.4
		1.4	1.7
		1.6	1.3

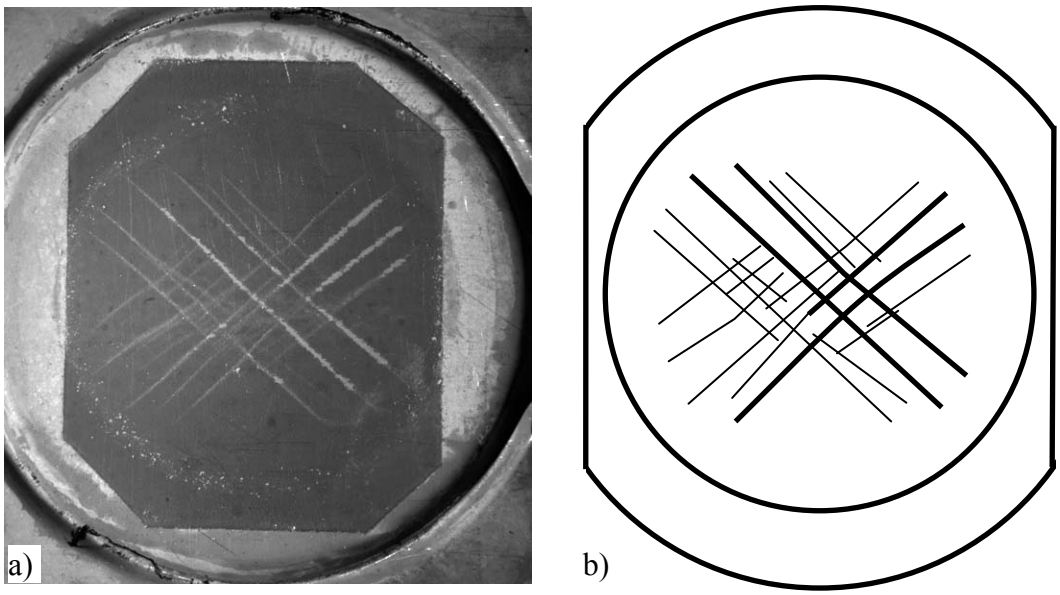

Figure 5.29 BH210 EG material post drawing deformation, with underside of sample shown. 134.9 mm wide, 1.0 % YPE, ε_1= 0.3 % ε_2= -0.3 %, punch depth 1.3 mm; a) photograph of sample, with microcracked StressCoat™ seen as lighter linear crosshatched patterns, b) schematic representation of regions of microcracked StressCoat™ (dark lines). 0.5x magnification

a) 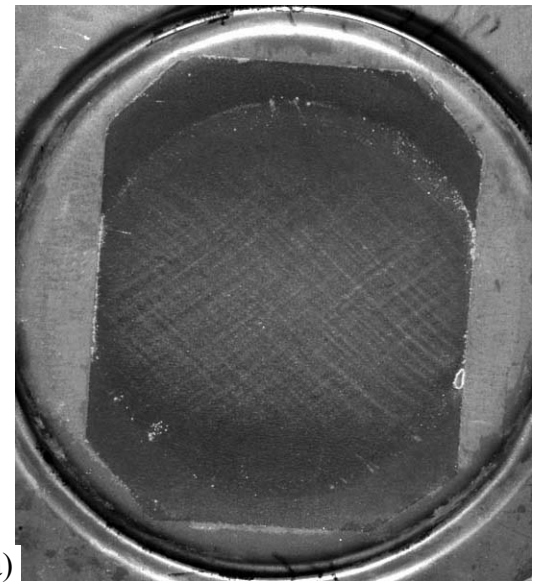 b) 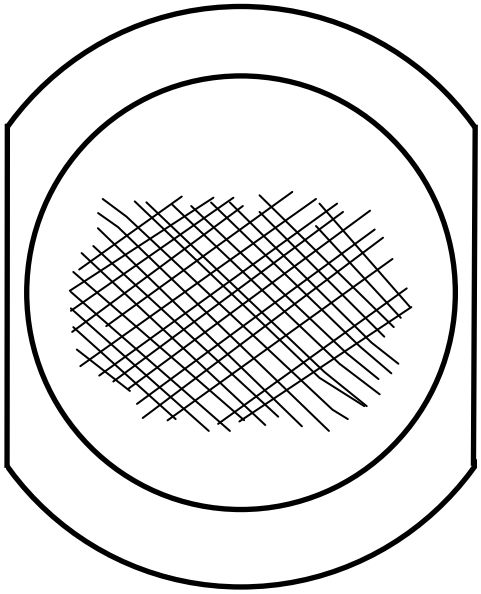

Figure 5.30 BH210 GA material post drawing deformation, with underside of sample shown. 134.9 mm wide, 1.0 % YPE, ε_1= 0.4 % ε_2= -0.3 %, punch depth 1.3 mm; a) photograph of sample, with microcracked StressCoat™ seen as lighter linear crosshatched patterns, b) schematic representation of regions of microcracked StressCoat™ (dark lines). 0.5x magnification

a) 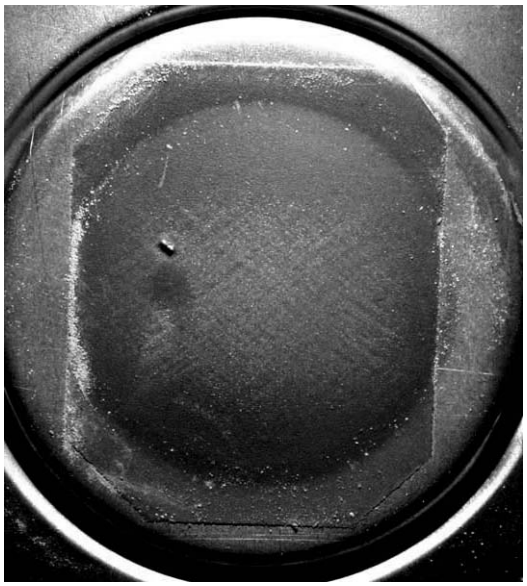 b) 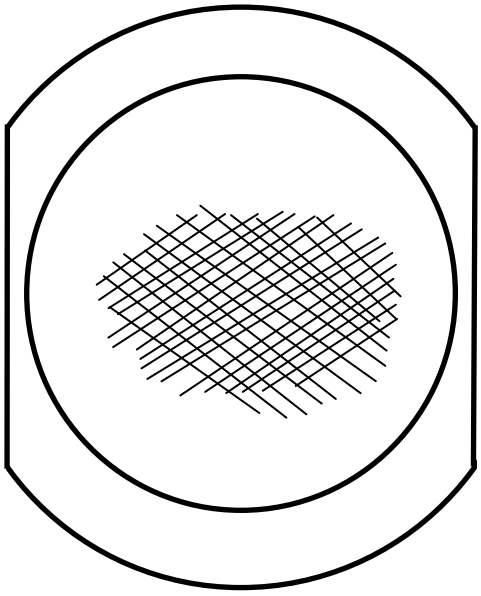

Figure 5.31 BH210 GI material post drawing deformation, with underside of sample shown. 134.9 mm wide, 1.0 % YPE, ε_1= 0.3 % ε_2= -0.5 %, punch depth 1.3 mm; a) photograph of sample, with microcracked StressCoat™ seen as lighter linear crosshatched patterns, b) schematic representation of regions of microcracked StressCoat™ (dark lines). 0.5x magnification

Table 5.9 Deformation of materials through plane strain

Material	Sample Width (mm)	Major Eng. Strain, ε_1 (%)	Minor Eng. Strain, ε_2 (%)	Effective Strain (%)	$\varepsilon_1/\varepsilon_2$ (%/%)
BH210 EG	134.9	0.3 ± 0.2	-0.3 ± 0.2	0.3 ± 0.2	-0.8 ±0.9
	135.1	0.3 ± 0.2	-0.4 ± 0.2	0.4 ± 0.2	-1.3 ±1.1
BH210 GA	134.9	0.3 ± 0.2	-0.5 ± 0.2	0.7 ± 0.2	-0.6 ±0.3
	135.4	0.7 ± 0.2	-0.5 ± 0.2	0.5 ± 0.2	-1.8 ±1.4
BH210 GI	134.9	0.4 ± 0.2	-0.3 ± 0.2	0.4 ± 0.2	-0.6 ±0.6
	135.4	0.3 ± 0.2	-0.2 ± 0.2	0.3 ± 0.2	-0.8 ±1.0

Table 5.10 Lüders band profile dimensions of BH210 EG (1.00 % YPE) in strain path near plane strain

Sample Width (mm)	Orientation	Width (mm)	Depth (μm)
134.9	Trans.	1.1	4.2
135.4	Trans.	1.4	4.0
		1.1	3.1
		1.1	3.6
		1.5	2.6

Table 5.11 Lüders band profile dimensions of BH210 GA (1.00 % YPE) in strain path near plane strain

Sample Width (mm)	Orientation	Width (mm)	Depth (μm)
		1.34	1.01
		1.45	0.97
		1.83	1.14
		1.20	0.94
134.9	Trans.	1.29	0.99
		1.37	0.65
		1.69	0.86
		1.30	0.74
		0.92	0.82
		1.01	0.76
		1.26	1.27
		1.53	1.13
135.4	Trans.	1.38	1.25
		1.06	0.79
		1.76	0.63
		1.19	0.95

Table 5.12 Lüders band profile dimensions of BH210 GI (1.00 % YPE) in strain path near plane strain

Sample Width (mm)	Orientation	Width (mm)	Depth (μm)
134.9	Trans.	1.6	1.3
		1.3	1.3
		1.1	1.2
		1.7	1.0
135.4	Trans.	1.6	1.3
		1.7	1.1
		1.5	1.6
		1.9	2.00
		1.3	1.4
		1.2	1.9
		1.5	1.7

5.5.3 Relationship of Lüders Band Geometry to Strain Ratio

Sample widths were increased with the intention of decreasing the resulting strain ratio ($\varepsilon_1/\varepsilon_2$), although there may be considerable uncertainty associated with the strain ratio obtained at low strains. Uniaxial tensile samples experienced a strain ratio of -0.6 ± 0.1 with a major strain varying from zero up to 10 %. The difference between strain ratio and sample width is presented in Figure 5.32. Comparisons of Lüders band geometry (depth and width) between the five sample widths, for each material and 1.00 % YPE, indicate little difference between them. This is reasonable based on the possibility that the strain ratios experienced by the materials may not have varied greatly between the sample geometries. Figure 5.33 gives the relationship between Lüders band depth and the original sample width. Figure 5.34 gives the relationship between Lüders band depth and the original sample width. There are two notable observations. First, the Lüders band depths in the near plane strain BH210 EG samples are noticeably larger compared to other BH210 EG specimen widths (Figure 5.33). This difference may be a consequence of the limited number of data recorded in these topographies, increasing scatter. Second, the Lüders band widths for the BH210 GA uniaxial samples (both

orientations) are significantly larger than for other BH210 GA sample widths (Figure 5.34). These results do not suggest a substantial effect of strain path on Lüders band topography.

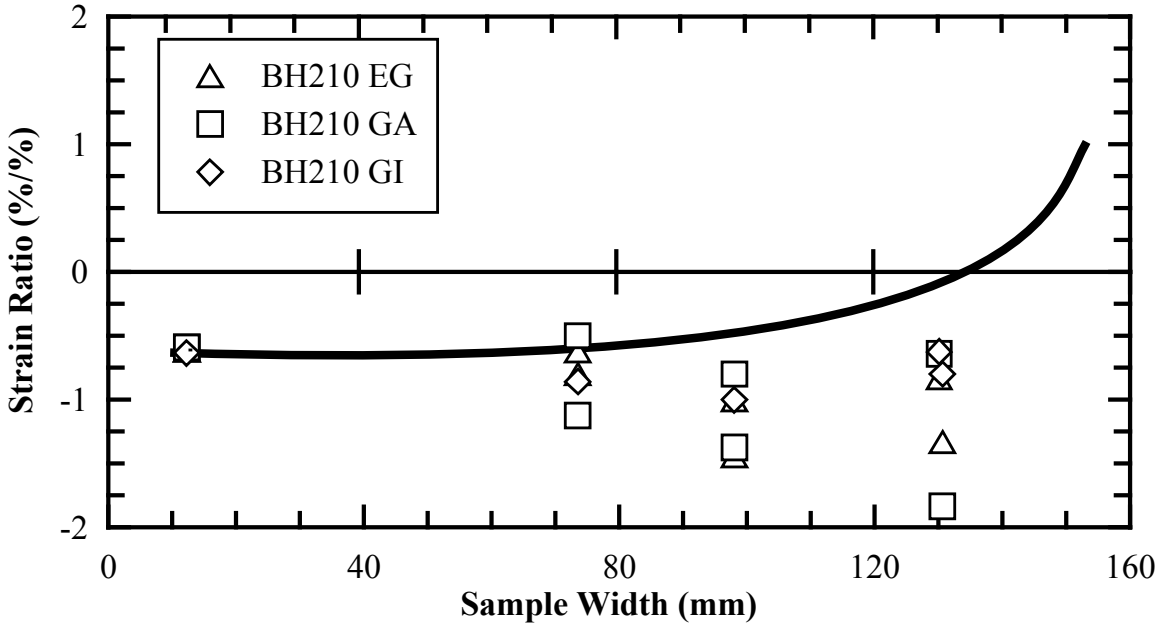

Figure 5.32 Strain ratio versus sample width; predicted strain ratio curve (solid line) is based on greater punch displacements (shown in Figure 4.13), material strain ratios were measured from test samples creating Lüders bands.

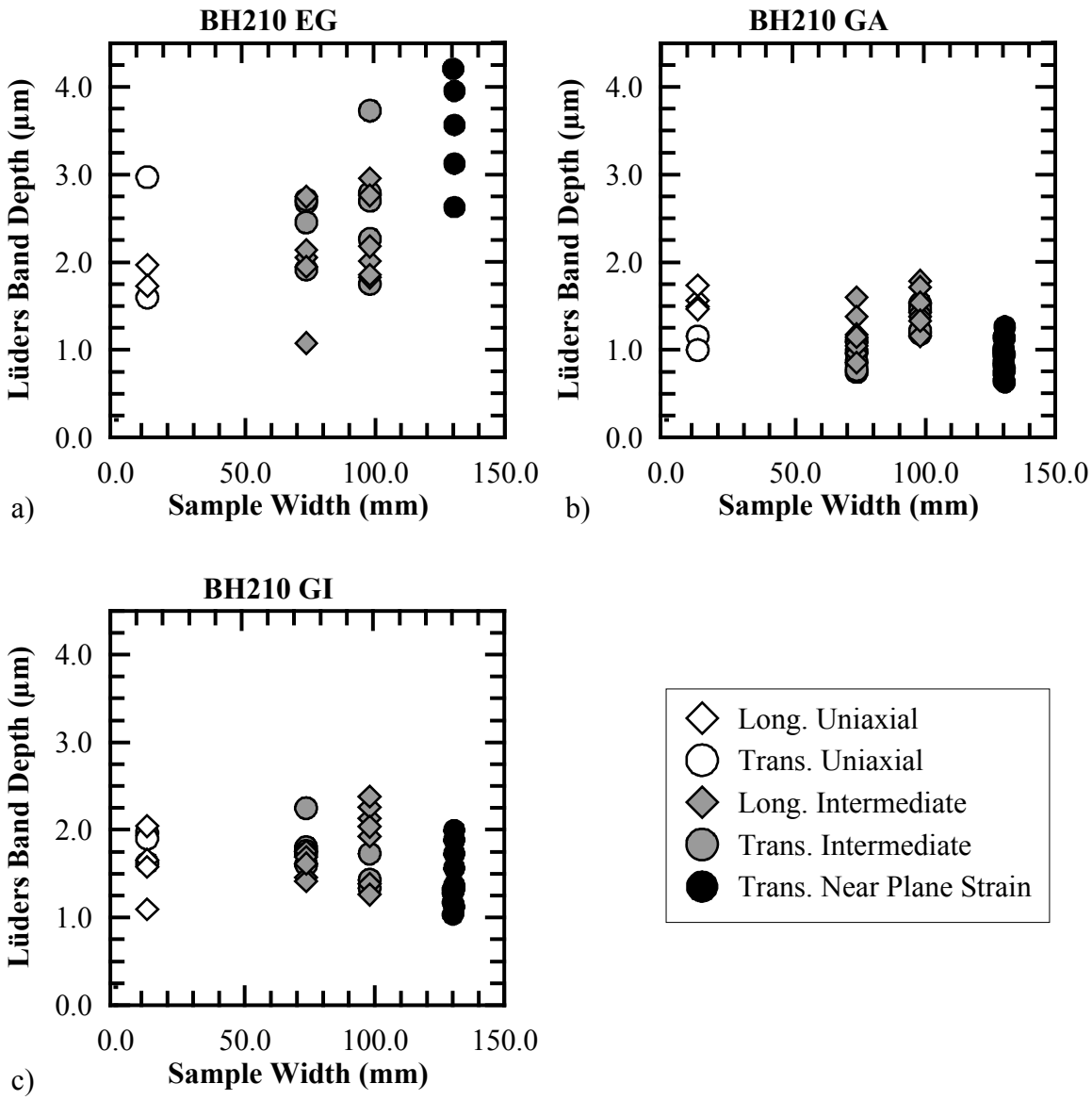

Figure 5.33 Lüders band depth versus sample width for uniaxial tension, intermediate strain ratios (strain ratios which can be considered drawing), and ratio near plane strain. a) BH210 EG, b) BH210 GA, c) BH210 GI.

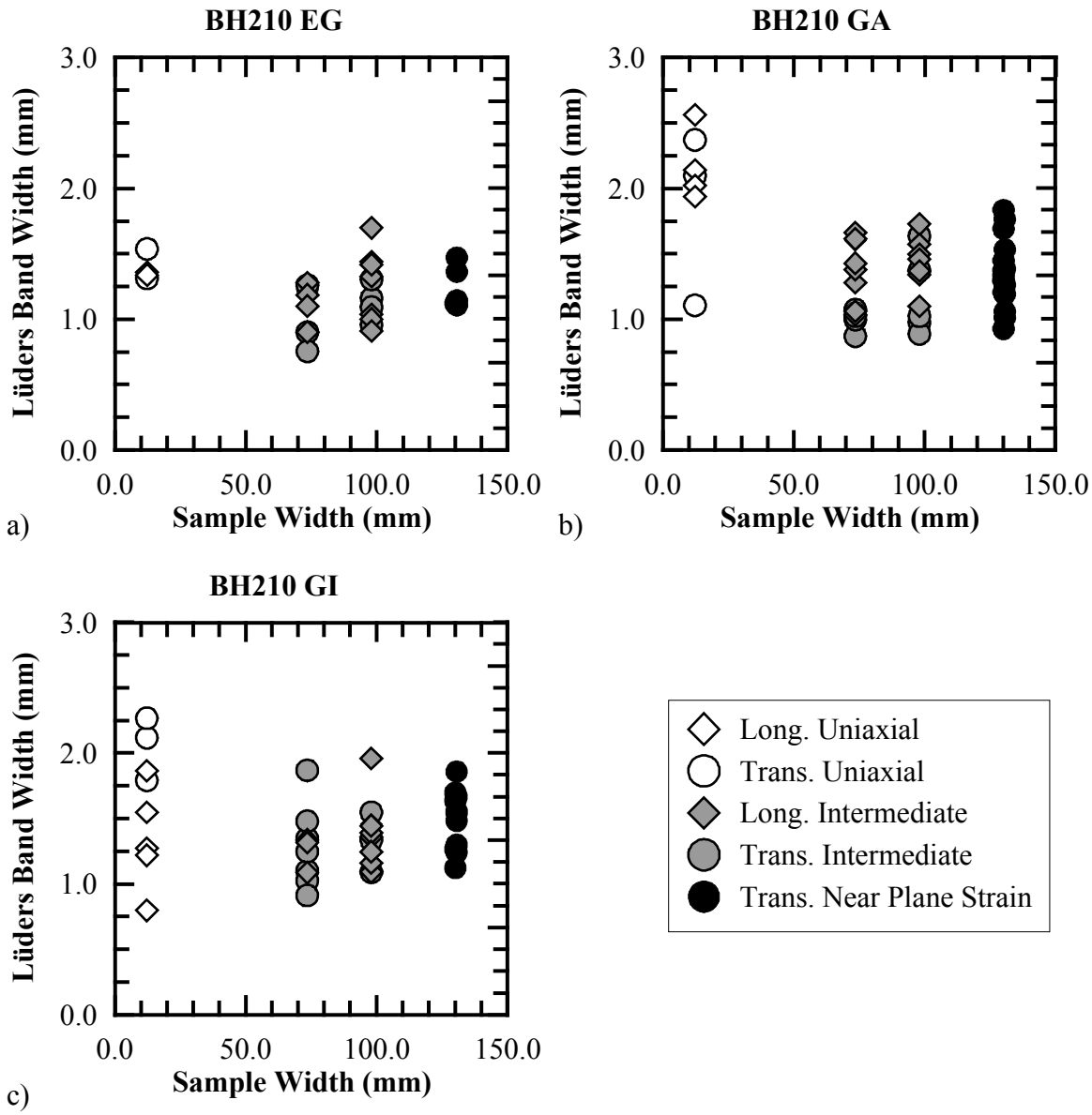

Figure 5.34 Lüders band width versus sample width for uniaxial tension, intermediate strain ratios (strain ratios which can be considered drawing), and ratio near plane strain. a) BH210 EG, b) BH210 GA, c) BH210 G

6.0 SUMMARY AND IMPLICATIONS

The intent of the project was to evaluate Lüders band topography on coated sheet steel, and provide additional understanding of Lüders band formation. The evaluation involved a quantitative determination of the band geometry i.e. width and depth as affected by several industrially relevant variables (coating types, YPE amount, sample orientation, thickness, and surface strain ratio). It was found that the influence of these variables on the Lüders band geometry is relatively small in most instances. An exception is the increase of Lüders band depth with increasing YPE, which agrees with previous work.[52] Additionally, a much different response in balanced biaxial deformation was found.

The roughness of the zinc-based coatings caused the Lüders band profiles to be obscured somewhat in terms of visual observation and topography measurements (i.e. in comparison to earlier work on polished surfaces). It was noted that the coatings had similar roughness amplitudes as the Lüders band depths. The roughness of the coating also helps to make the bands less visible to the unaided eye.

The generation of predictive trends of a "typical" Lüders band would best incorporate larger variations in YPE since the ability to discriminate small differences was shown to be an issue in the present study. Thus YPE levels from 0 % to as much as can be obtained in the first stage of aging could be of benefit in any further fundamental studies. The range of YPE levels chosen for this investigation is industrially important, but the addition of higher YPE values would help understand the relationship between steel characteristics and Lüders band geometry. In one instance, by using a large value YPE sample the trend between increasing YPE and increasing Lüders band depth becomes more apparent. In Figure 6.1 three data sets for maximum depth, as determined by Lüders band evolution, are plotted. The first data set is from assessment of Lüders band depths on polished samples in a previous study,[52] the second data set is from the current study of BH210 GA, and the third datum (star) is from the LC GI material in an as-received condition (with 6.0 % YPE). The data were normalized by sample thickness. A projection of least-squares fits from the studies of lower-YPE materials defines a

region which also contains the high YPE datum. This correlation supports the linear relationship between YPE and the maximum Lüders band depth.

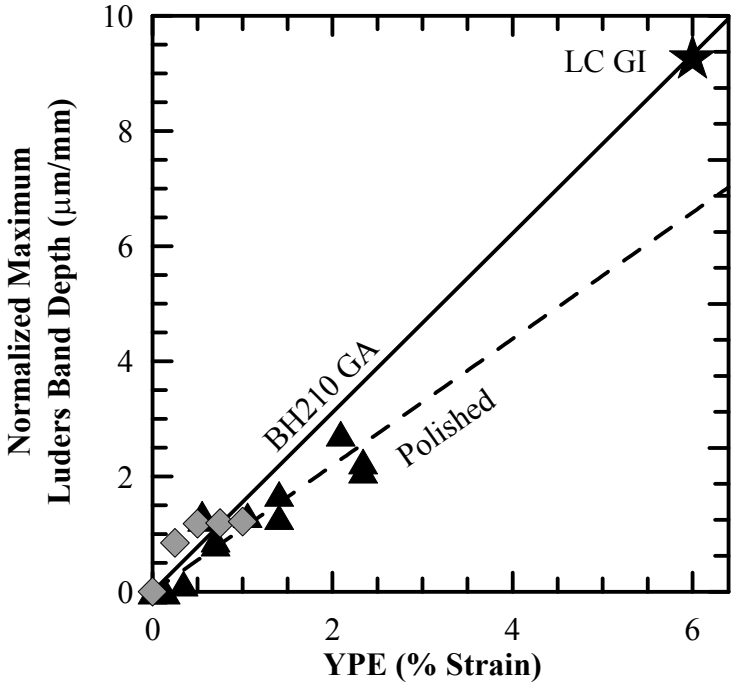

Figure 6.1 Maximum Lüders band depth as a function of YPE. Polished material was shipped as a bake-hardenable grade sheet, coating was removed and samples were polished.[52] Lüders band depths have been normalized by sample thickness.

An observation from the present study which may deserve additional follow-up is the absence of discontinuous yielding in sheet subjected to small deformations in balanced biaxial stretching. This observation appears not to have been reported previously, and may be related to the constraint involved in this deformation state, whereby strain localization is difficult under balanced biaxial conditions.

It is also worthwhile to consider the current results within the context of earlier work assessing severity of surface imperfections on automotive exposed surfaces. Figure 6.2 shows results from previous studies of Choi[72] and Humble,[52] obtained using the same profilometry instrumentation employed in the current study, albeit with a higher magnification objective lens. (The higher magnification lens is capable of greater lateral

resolution, but measures smaller areas of the specimen.) In the work of Choi, commercially produced sheet steels with surface imperfections of interest to industry were evaluated before and after laboratory application of a multilayer automotive paint system. The figure shows the depth and width of these imperfections before painting, and their visibility after painting (based on shading of the diamonds). Imperfections having depths greater than 5 μm are excluded from the figure to focus attention on smaller features. Also included in Figure 6.2 are data from Humble showing measured Lüders band depths and widths, obtained for one sheet steel using polished specimens.

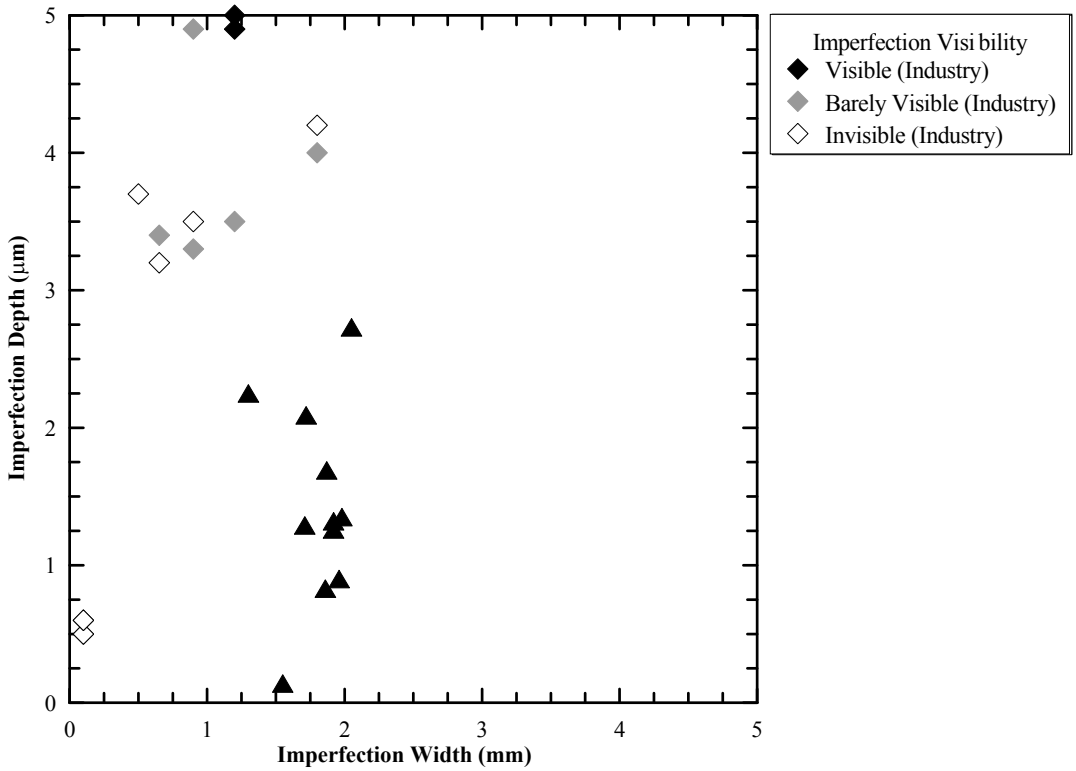

Figure 6.2 Surface geometry of imperfections and visibility after painting, from previous studies. Shaded diamonds indicate visibility (after painting) of surface imperfections on industrially produced coils, with imperfection depths and widths plotted on the axes shown (from Choi[72]). Maximum Lüders band depths and corresponding widths (triangles) are shown from prior work of Humble[52] obtained using polished sheet steel.

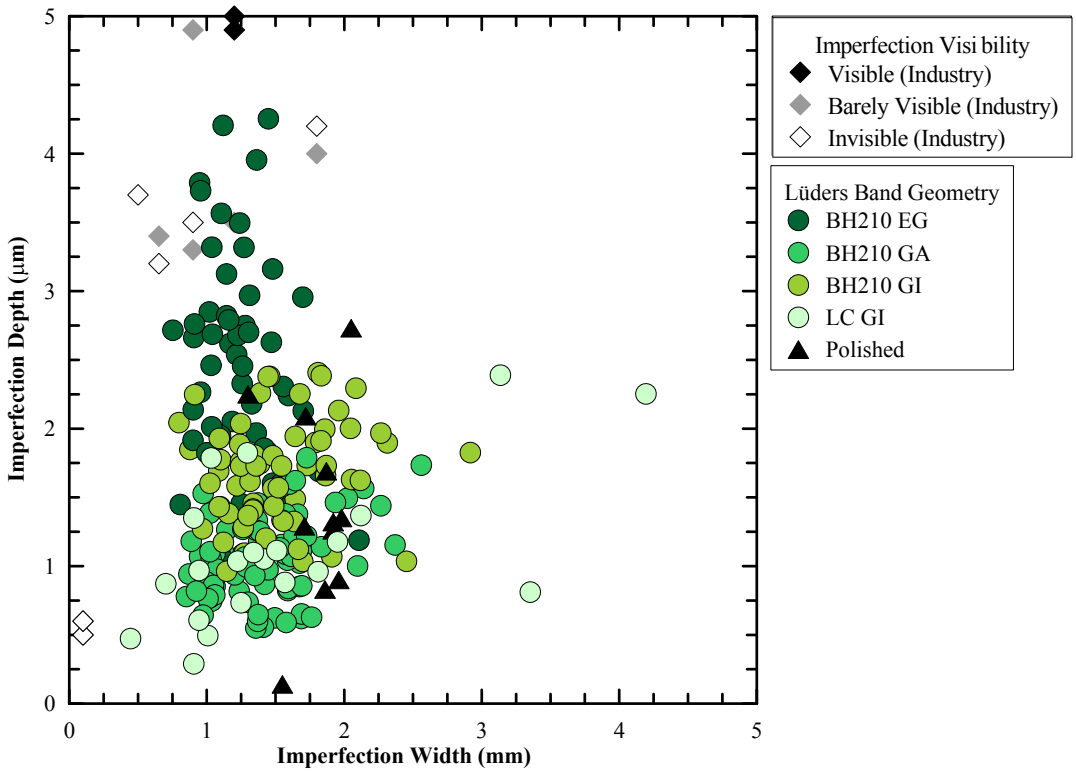

Figure 6.3 Lüders band geometries for materials tested in the current work, plotted along with the data shown from earlier work in Figure 6.2.

The results of Humble suggested that the characteristic geometries of Lüders bands are small relative to some other surface imperfections that are either completely invisible or barely visible after painting. These results provided motivation for current study using coated surfaces, multiple strain states, *in-situ* deformation, etc. In Figure 6.3, the Lüders band characteristic geometries measured in the current study are overlayed on the plot shown in Figure 6.2. While some individual data overlap, the figure nonetheless shows the general comparisons between the different steels, discussed earlier. More importantly, for these materials with YPE levels below about 1%, the apparent "amplitude" of Lüders topography is usually below about 3 μm, and is less than typically

would be associated with other surface imperfections on sheet steels that were both of interest to industry, and shown to be invisible or barely visible after painting. Thus, the results of the present work suggest that further industry consideration may be worthwhile, of the appropriate levels of maximum YPE for automotive sheet steels. Such considerations need to incorporate issues related to individual paint systems at different automobile assembly locations, and are thus not straightforward. Several opportunities also remain for further fundamental study of the discontinuous yielding phenomenon. (These are detailed in the student thesis that provided the data and analysis incorporated in the final project report.[73])

7.0 SPECIFIC CONCLUSIONS

- A computerized tensile stage designed to mount *in-situ* to a non-contacting three-dimensional optical profilometer was shown to provide a methodology to examine the change in Lüders band topography in-situ with increasing strain on coated sheets steels.
- Maximum Lüders band depth increases with increasing YPE while Lüders band width apparently remains unchanged with increasing YPE.
- Lüders band geometry was found to be insensitive to sample orientation (relative to rolling direction) and sample width in in-plane deformation.
- Deformation of several percent (greater than 3 % strain) reduces the prominence of Lüders bands as the characteristic surface imperfection, due to overall surface roughening
- Application of galvanized/galvannealed coatings and related roughness obscures the Lüders band topography somewhat at low YPE levels, due to the depth of the Lüders band being similar in size to the average roughness.
- Formation of Lüders bands does not occur when straining under balanced biaxial stretching conditions within the YPE for samples containing 1.0 % YPE.
- The maximum Luders band depth was below 5 μm (and usually below 3 μm) for the coated BH210 steels, and would be considered invisible or barely visible after painting, based on earlier studies in the authors' laboratories.

8.0 REFERENCES CITED

[1] H. Takechi, "Advances in Interstitial-Free, and Bake-Hardening Steel Sheets for Automotive Applications", Microalloying '95 Conf. Proc., ISS, pp. 71-80.

[2] A. Piobert, Mem De l'Artillerie, Vol. 5, 1842, pp 525, as reported by D.W. Moon, "Consideration on the Present State of Lüders Band Studies," Materials Science and Engineering, Vol. 8, 1971, pp. 235-243.

[3] W. Lüders, Dinglers Polytech Journal, Vol. 155, 1860 pp 18, as reported by D.W. Moon, "Consideration on the Present State of Lüders Band Studies," Materials Science and Engineering, Vol. 8, 1971, pp. 235-243.

[4] G.E. Dieter, Mechanical Metallurgy 3rd Edition, McGraw Hill, Boston, MA, 1986 p. 198.

[5] W. Sylwestrowicz and E.O. Hall, "The Deformation and Ageing of Mild Steel I," Proceedings of the Physical Society B, Vol. 64, 1951, pp. 495-502.

[6] E.O. Hall, Yield Point Phenomena in Metals and Alloys, Plenum Press, New York, 1970, pp. 71.

[7] Z. Marciniak and J.L. Duncan, The Mechanics of Sheet Metal Forming, Edward Arnold, London, 1992, pg. 35.

[8] ASTM E-8, "Standard Test Methods for Tension Testing of Metallic Materials," ASTM International, West Conshohocken, PA, 2004, pp. 62-84.

[9] A.H. Cottrell, B.A. Bilby, "Dislocation Theory of Yielding and Strain Ageing of Iron," *Proceedings*, Physical Society Sec. A., Vol. 62, 1949, pp. 49-62.

[10] W.C. Leslie, The Physical Metallurgy of Steels, Hemisphere Publishing Corporation, Washington, DC, 1981, pp. 142-186.

[11] D.V. Wilson and B. Russell, "Stress Induced Ordering and Strain Aging in Low Carbon Steels," Acta Metallurgica, Vol. 7, 1959, pp. 628-631.

[12] Y. Nakada and A.S. Keh, "Kinetics of Snoek Ordering and Cottrell Atmosphere Formation in Fe-N Single Crystals," Acta Metallurgica, Vol. 15, 1967, pp. 879-883.

[13] H.C. Rogers, "A Yield Point in Steel Due to Hydrogen," Acta Metallurgica, Vol. 2, 1954, p. 167; Vol. 4, 1956, p. 114; Vol. 5, 1957, p. 112, as reported by J. Gouzou, "Analysis of the Grain/Size Dependence of the Lower Yield Stress in Steel," Acta Metallurgica, Vol. 12, 1964, pp. 785-795.

[14] H.P. Tardif and C.S. Ball, "The Effect of Temper-Rolling on the Strain Aging of Low-Carbon Steel," Journal of the Iron and Steel Institute, Vol. 182, 1956, pp. 9-19.

[15] J. Gouzou, "Analysis of the Grain/Size Dependence of the Lower Yield Stress in Steel," Acta Metallurgica, Vol. 12, 1964, pp. 785-795.

[16] J.D. Baird, "Strain Aging of Steel - A Critical Review," Iron & Steel, Vol. 36, 1963, Part Ia pp. 186-192; Part Ib pp. 326-334; Part IIa pp. 368-374; Part IIb pp. 400-405.

[17] K. Yamazaki, T. Horita, Y. Umehara, and T. Morishita, "Manufacturing Condition and Automotive Use of Bake Hardenable Steel Sheets," Microalloying '88 Conference Proceedings, 1988, pp. 327-336.

[18] D.K. Matlock, B.J. Allen, and J.G. Speer, "Aging Behavior and Properties of Ultra-Low Carbon Bake-Hardening Steels," in Modern LC and ULC Sheet Steels for Cold Forming: Processing and Properties ed. by W. Bleck, Verlag Mainz, 1998, pp. 265-276.

[19] G.T. Hahn, "A Model For Yielding With Special Reference to the Yield-Point Phenomena of Iron and Related BCC Metals," Acta Metallurgica, Vol. 10, 1962, pp. 727-738.

[20] P.J. Worthington and E. Smith, "The Formation of Slip Bands in Polycrystalline 3% Silicon Iron in the Pre-Yield Microstrain Region," Acta Metallurgica, Vol. 12, 1964, pp. 1277-1281.

[21] W.E. Carrington and D. McLean, "Slip Nuclei in Silicon-Iron," Acta Metallurgica, Vol. 13, 1965, pp. 493-499.

[22] D.W. Moon and T. Vreeland Jr., "Dislocation Velocity in Single and Polycrystalline Silicon-Iron," Journal of Applied Physics, Vol. 39, 1968, pp. 1766-1770.

[23] D.V. Wilson, "Grain-Size Dependence of Discontinuous Yielding in Strain-Aged Steels," Acta Metallurgica, Vol. 16, 1968, pp. 743-753.

[24] J.C. Fisher, "Application of Cottrell's Theory of Yielding to Delayed Yielding in Steel," Transactions of the American Society of Metals, Vol. 47, pp. 451-462, 1955.

[25] T.L. Russell, D.S. Wood and D.S. Clark, "The Influence of Grain Size on the Yield Phenomenon in Steel," Acta Metallurgica, Vol. 9, pp. 1054-1063, 1961.

[26] E.O. Hall, "The Deformation and Ageing of Mild Steel: II Characteristics of the Lüders Deformation," Proceedings of the Physical Society B, Vol. 64, 1951, pp. 742-747.

[27] H. Fujita and S. Miyazaki, "Lüders Deformation in Polycrystalline Iron," Acta Metallurgica, Vol. 26, 1978, pp. 1273-1281.

[28] V.S. Anathan and E.O. Hall, "Macroscopic Aspects of Lüders Band Deformation in Mild Steel," Acta Metallurgica & Materilia, Vol. 39, 1991, pp. 3153-3160.

[29] D.E. Delwiche and D.W. Moon, "Orientation of Lüders Band Fronts," Material Science and Engineering, Vol. 7, 1971, pp. 203-207.

[30] W.M. Lomer, "The Yield Phenomenon in Polycrystalline Mild Steel," Journal of the Mechanics and Physics of Solids, Vol. 1, 1952, pp. 64-73.

[31] J. Zhang and Y. Jiang, "Lüders Band Propagation of 1045 Steel Under Multiaxial Stress State," International Journal of Plasticity, Vol. 21, 2005, pp. 651-670.

[32] J. Friedel, Dislocations, Pergamon Press, Oxford, 1964, as referenced by E.O. Hall, Yield Point Phenomena in Metals and Alloys, Plenum Press, New York, 1970, pg 32.

[33] V.S. Ananthan and E.O. Hall, "Surface Features of Microscopic Shear Bands at Lüders Fronts in Mild Steel," Scripta Metallurgica, Vol. 21, 1987, pp. 1699-1704.

[34] V.S. Ananthan and E.O. Hall, "Shear and Kink Angles at the Lüders Band Front," Scripta Metallurgica, Vol. 23, 1989, pp. 1075-1078.

[35] J. F. Butler, "Lüders Front Propagation in Low Carbon Steels," Journal of the Mechanics and Physics of Solids, Vol. 10, 1962, pp. 313-334.

[36] R. Iricibar and J. Mazza, "The Contribution of Creep to the Strain Profile of a Propagating Lüders Band Fron in Mild Steel," Scripta Metallurgica, Vol. 10, 1976, pp. 289-294.

[37] D.W. Moon, "Consideration on the Present State of Lüders Band Studies," Materials Science and Engineering, Vol. 8, 1971, pp. 235-243.

[38] K. Prewo, J. C. M. Li, and M. Gensamer, "Lüders Band Motion in Iron," Metallurgical Transactions, Vol. 3, 1972, pp. 2261-2269.

[39] E.W. Hart, "Uniaxial Strain Model for a Lüders Band," Acta Metallurgica, Vol. 3, 1955, pp. 146-149.

[40] R. Iricibar and J. Mazza, "Meaning of the Strain Profile of a Propagaing Lüders Band Front," Scripta Metallurgica, Vol. 9, 1975, pp. 1045-1050.

[41] I. Gupta and F. Garofalo, "Effect of Grain Size and Free Interstitials on Yield Stress, Flow Stress and Lüders Strain in Iron and an Iron-Titanium Alloy," Material Science and Engineering, Vol. 5, 1970, pp. 271-278.

[42] J.C. Fisher and H.C. Rogers, “Propagation of Lüders Bands in Steel Wires,” Acta Metallurgica, Vol. 4, 1956, pp. 180-185.

[43] R. Iricibar, J. Mazza, and A. Cabo, “On the Lüders Band Front in Mild Steel-I,” Acta Metallurgica, Vol. 25, 1977, pp. 1163-1168.

[44] R. Iricibar, G. Panizza, and J. Mazza, “On the Lüders Band Front in Mild Steel-II Elastic Plastic Analysis of the Front by The Finite Element Method,” Acta Metallurgica, Vol. 25, 1977, pp. 1169-1177.

[45] F. Garofalo, “Effect of Grain Size and Cross-Head Velocity on the Lower Yield Strength During Inhomogeneous Discontinuous Yielding in Iron and Steel,” Metallurgical Transactions, Vol. 4, 1973, pp. 1557-1561.

[46] J.F. Butler, “Effect of Lüders Front Number on the yield Point of Iron,” Acta Metallurgica, Vol. 10, 1962, pp. 258-259.

[47] H. Conrad and G. Stone, “The Effect of Stress on the Lüders Band Velocity in Niobium,” Journal of the Mechanics and Physics of Solids, Vol. 12, 1964, pg. 139, as reported by D.W. Moon, “Consideration on the Present State of Lüders Band Studies,” Materials Science and Engineering, Vol. 8, 1971, pp. 235-243.

[48] D.J. Verel and A.W. Sleeswyk, “Lüders Band Propagation at Low Velocities,” Acta Metallurgica, Vol. 21, 1973, pp.1087-1098.

[49] D.W. Moon, “Strain Distribution Through a Propagating Lüders Band Front,” Scripta Metallurgica, Vol. 5, 1971, pp. 213-216.

[50] J.M. Krafft, “An Interpretation of Lower Yield Point Plastic Flow in the Dynamic Testing of Mild Steel,” Acta Metallurgica, Vol. 10, 1962, pp. 85-93.

[51] G.T. Van Rooyen, “The Stress and Strain Distribution in a Propagating Lüders Front Accompanying the Yield-Point Phenomenon in Iron,” Material Science and Engineering, Vol. 3, 1968, pg. 105, as reported by D.W. Moon, “Consideration on the Present State of Lüders Band Studies,” Materials Science and Engineering, Vol. 8, 1971, pp. 235-243.

[52] F.T. Humble, "Yielding Behavior in Low Carbon Sheet Steel: An Assessment of Surface Topography Changes associated with Lüders Band Formation," M.S. Thesis: MT-SRC-004-001, Colorado School of Mines, Golden, CO, January, 2004.

[53] R.D. Butler and D.V. Wilson, "The Mechanial Behaviour of Temper Rolled Steel Sheets," Journal of the Steel Institute, Vol. 201, 1963, pp. 16-33.

[54] E.O. Hall, "An Optical Method for Studying the Deformation of Mild Steel," *Proceedings*, Physical Society Section B, Vol. 63, 1950, pp. 724-726.

[55] R. Iricibar, J. Mazza, and A. Cabo, "The Microscopic Strain Profile of a Propagating Lüders Band Front in Mild Steel," Scripta Metallurgica, Vol. 9, 1975, pp. 1051-1058.

[56] G.H. Schaffer, "The Many Faces of Surface Texture", American Machinist & Automated Manufacturing, June 1988 as reported by S. Lippold and J. Podlesny, WYKO Surface Profilers Technical Reference Manual, Veeco Process Metrology, 1998, pg. A-2.

[57] A.F. Bastawros and J.G. Speer, "A Procedure to Determine Surface Waviness." Proceedings of the 34th Mechanical Working and Steel Processing Conference, Montreal, Canada, 1992, pp. 491-498.

[58] S. Lippold and J. Podlesny, WYKO Surface Profilers Technical Reference Manual, Veeco Process Metrology, 1998, pp. 1-10.

[59] R.L. Norton, Machine Design: and Integrated Approach, 2 Ed., Prentice Hall, Upper Saddle River, NJ, 2000, pp. 447-448.

[60] T.R. Thomas, Rough Surfaces, 2 Ed., Imperial College Press, London, 1999, pp. 122-123.

[61] W.D. Dong, N.L. Luo, P.J. Sullivan, and K.J. Stout, "Visualisation Techniques and a Primary Parameter Set for Characterizing Three Dimensional Surface Topography" in Three Dimensional Surface Topography; Measurement, Interpretation, and Applications, edited by K.J. Stout, Penton Press, London, 1994, pp. 90-121.

[62] N.H. Polakowski, Journal of the Iron and Steel Institute, Vol. 172, 1952, pp.369-376 as reported by B.B. Hundy, "Elimination of 'Stretcher Strains' in Mild Steel Pressings," Journal of the Iron and Steel Institute, Vol. 178, 1954, pp. 127-138.

[63] B.B. Hundy, "Elimination of 'Stetcher Strains' in Mild Steel Pressings," Journal of the Iron and Steel Institute, Vol. 178, 1954, pp. 127-138.

[64] B. Amiot and J. Despujols, "Strains in Extra-Low-Carbon Steel Sheets after Weak (Skin-Pass) Rolling," Metals Technology, Vol. 10, 1983, pp. 161-166.

[65] B.B. Hundy, "Inhomogeneous Deformation During the Temper-Rolling of Annealed Mild Steel," Journal of the Iron and Steel Institute, Vol. 181, 1955, pp. 313-315.

[66] D.A. Chatfield and C.A. Beiser, "A Study of the Surface Irregularities Caused by the Nonhomogeneous Nature of Temper Rolling," Blast Furnace and Steel Plant, Vol. 56, no. 8, pp. 696-703, 727, 742, 1968.

[67] ASTM E-8, "Standard Test Methods for Tension Testing of Metallic Materials," ASTM International, West Conshohocken, PA, 2004, pp. 62-84.

[68] D.V. Wilson and B. Russell, "The Contribution of Atmosphere Locking to the Strain-Aging of Low Carbon Steels," Acta Metallugica Vol. 8, pp.36-45, 1960.

[69] D.A. Buford, "Frictional and Geometric Effects in Punch-Stretch Sheet Metal Formability Testing", Ph.D. Thesis MT-SRC-087-042, Colorado School of Mines, Golden, CO, November 1987, p. 248.

[70] "Statistics`Data Smoothing`," Mathematica 5.0 documentation, Wolfram Research Inc. Champaign, IL, 2003.

[71] A. Parmar, P.B. Mellor and J. Chakrabar, Int. J. Mech. Sci., Vol. 19, pp. 389, 1977 as reported by M. Jain, D.J. Lloyd and S.R. Macewen, "Hardening Laws, Surface Roughness and Biaxial Tensile Limit Strains of Sheet Aluminum Alloys," Int. J. Mech. Sci., Vol. 38, No. 2, pp. 219-232, 1996.

[72] Y.M Choi, "Topography Assessment of Coated Steel Surface Imperfections in Relation to Appearance After Painting," Ph.D. Thesis T-5634, Colorado School of Mines, Golden, CO, July 2002.

[73] B.D. Lakamp, "Yielding Behavior of Low Carbon Sheet Steel: Assessment of Lüders Band Surface Topography and Formation in Zinc Coated Steel Sheet," M.S. Thesis, Colorado School of Mines, Golden, CO, April 2007.

APPENDIX A IN-SITU MECHANICAL DESIGN

The capabilities of the in-situ mechanical test frame included a crosshead displacement of 24.5 mm, and 6.6 kN maximum load. Displacements were monitored by a 50.8 mm (2 in) 50% extensometer connected between the connection block and the crosshead of the apparatus. Crosshead displacement was provided by a linear travel 8.9 kN (1 ton) jack screw with rotary input. It was driven by a server motor connected via a flexible shaft. The motor travel signals were provided by the digital output of the data acquisition system. A block diagram of these interactions is shown in Figure A.1. Shop drawings of the parts machined for this device are shown in Figures A.2 through A.7. The various components purchased for this device are listed in Table A.1and Table A.2.

For future study, the machine could be fitted with a load transducer and connected to the data acquisition system (DAQ). This load transducer could be accomplished by the addition of a sensitive strain gage attached to the load transfer bar and could be calibrated between load and voltage change across strain gages in a half Wheatstone bridge configuration. Higher travel velocities could be created with the DAQ controlling an electrical pulse generator.

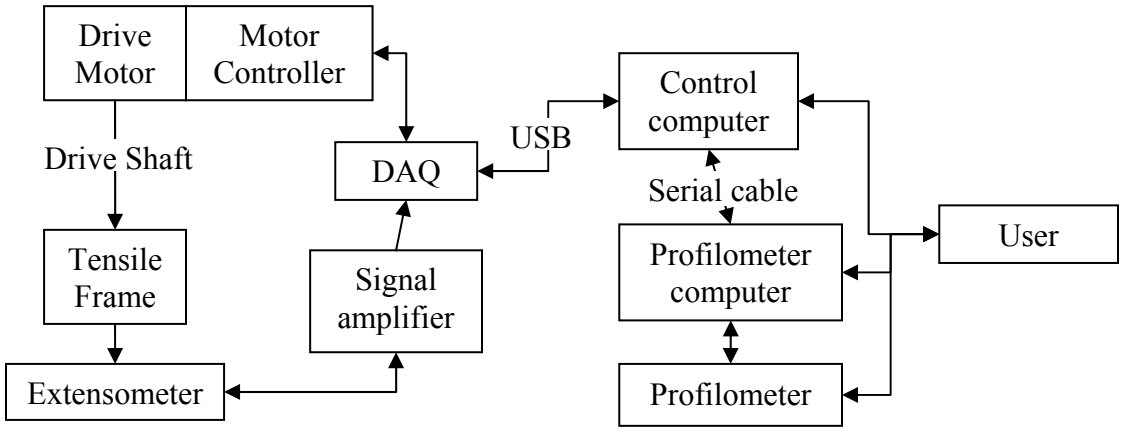

Figure A.1 Block diagram of electrical and mechanical connection between components for in-situ straining device.

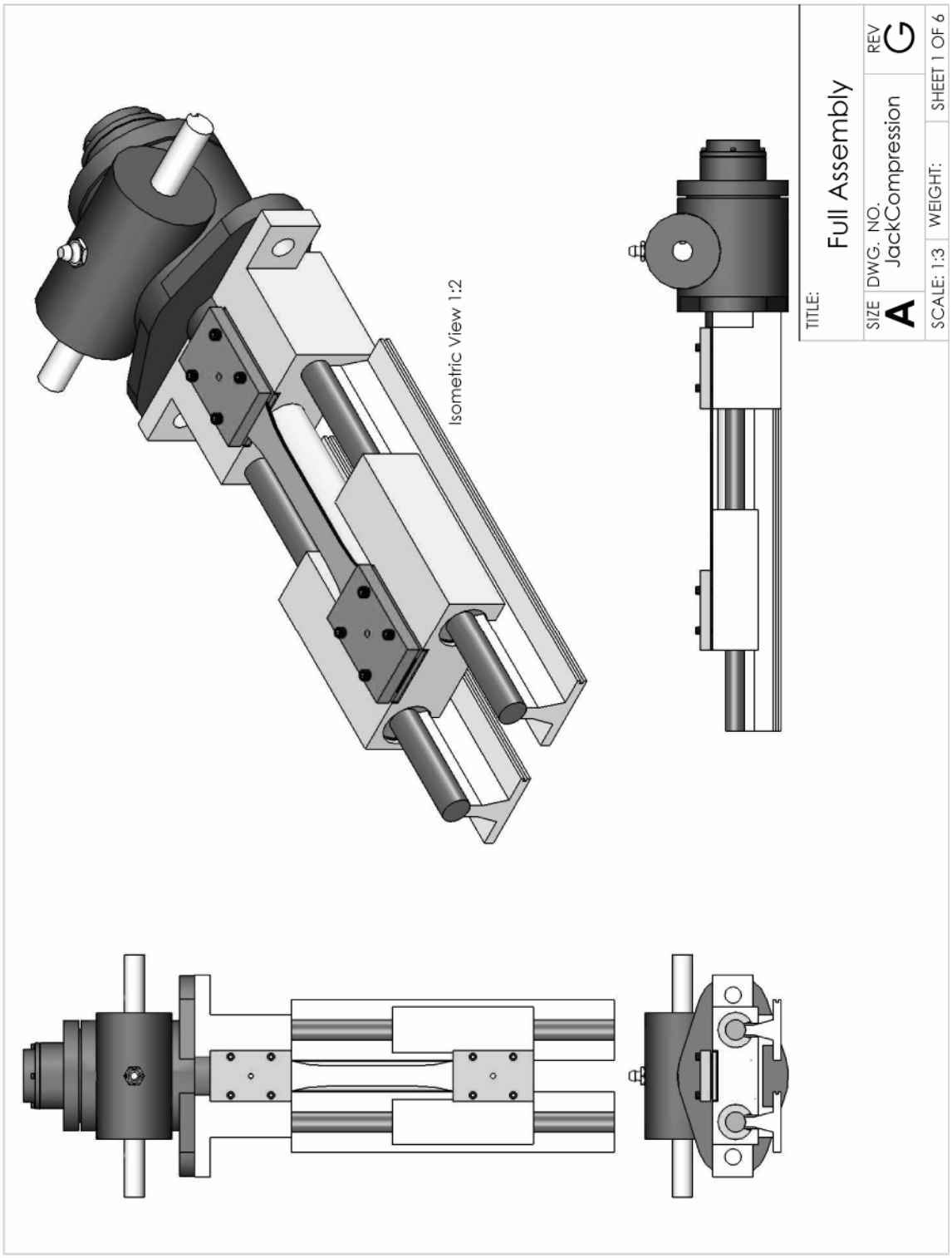

Figure A.2 Fully assembled view of in-situ test frame.

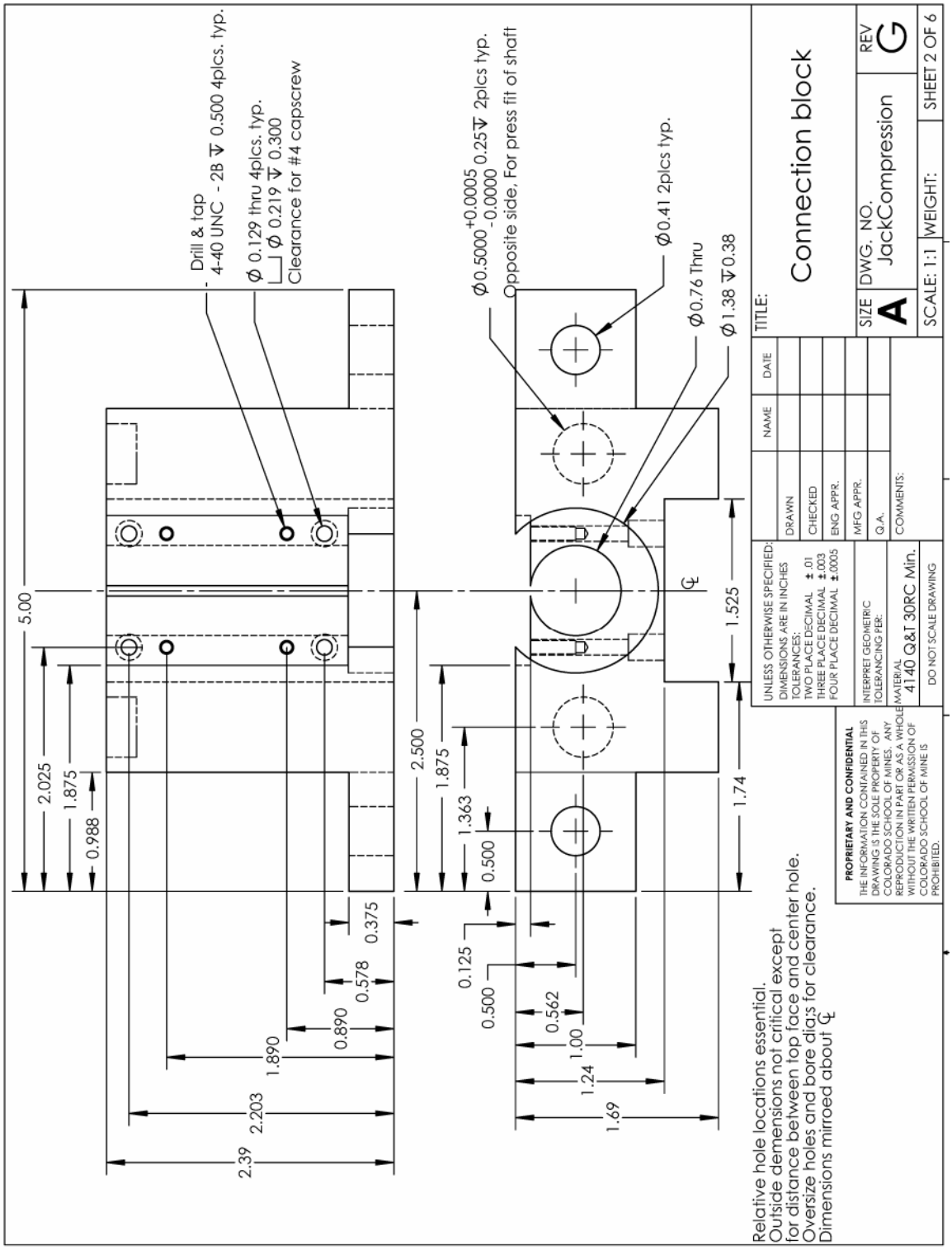

Figure A.3 Shop drawing of connection block, connecting jackscrew to linear guide rails and containing one of the grips.

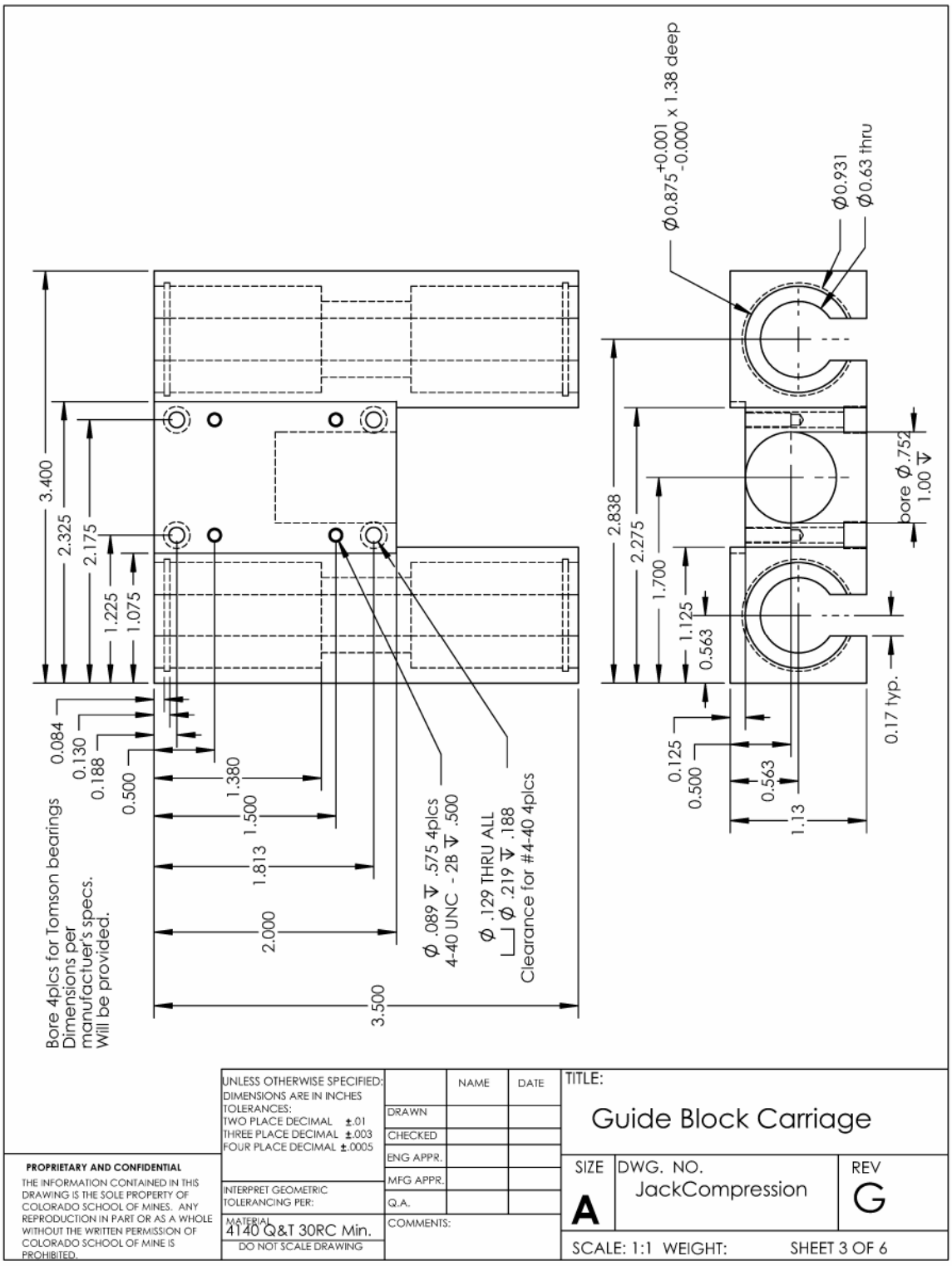

Figure A.4 Shop drawing of guide block carriage, also know as the crosshead. Contains linear bearings and travels across the guide rails linear shafts. It also contains the second grips.

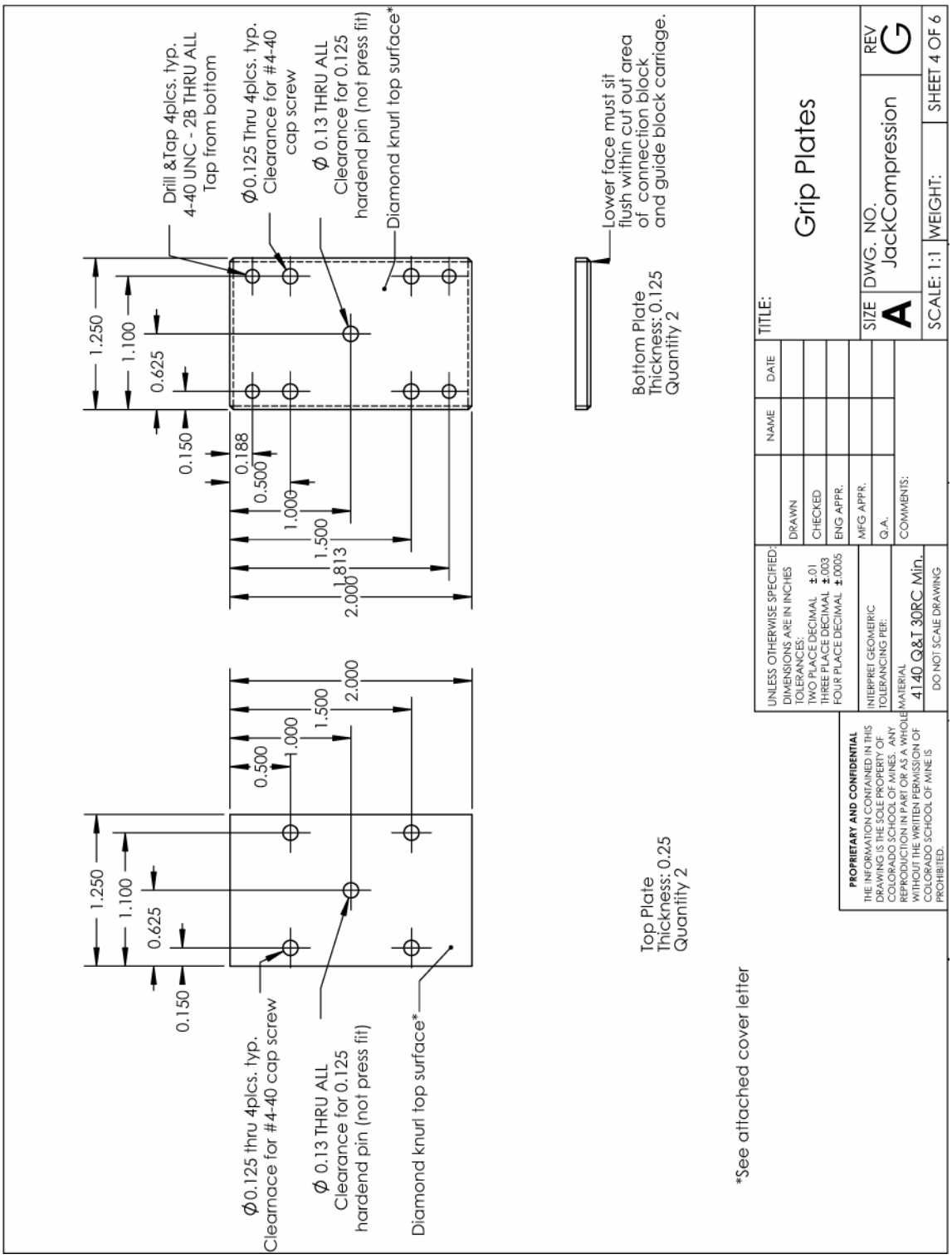

Figure A.5 Shop drawing of grip plates. Plates were textured with a diamond cut pattern to reduce sample slip. Samples were clamped in between grip plates.

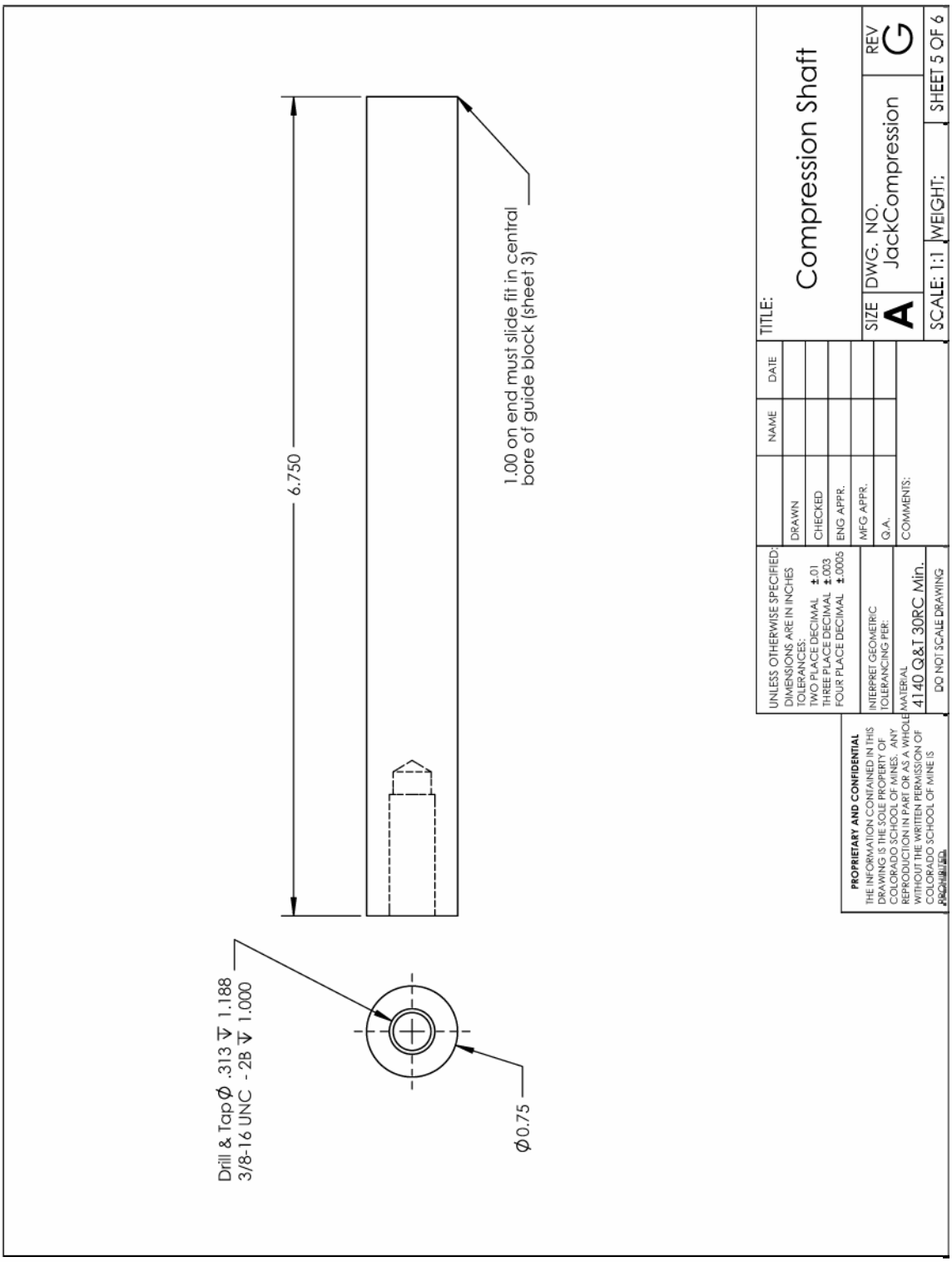

Figure A.6 Shop drawing of compression shaft. The shaft attached directly onto the screw jack and press against the guide block carriage.

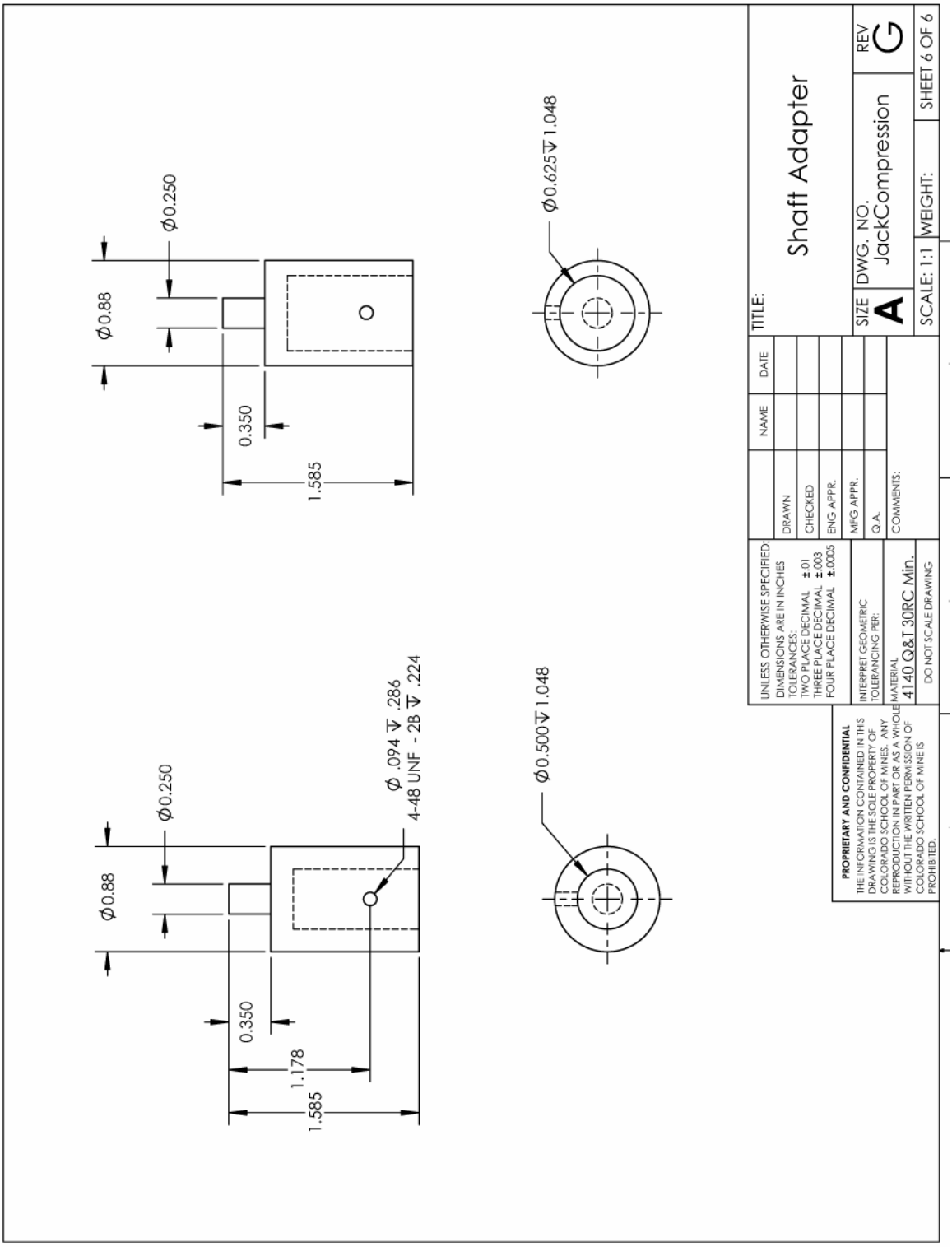

Figure A.7 Shop drawing of shaft adapters. The adapters allowed the flexible shaft to connect to the screw jack and the drive motor.

TableA.1 Mechanical parts bill of materials

Part Name	Part Number (retailer)	Quantity
Machined parts (Figure A.2 through A.6)		1
Nook Industries Jack Screw	1AB-MSJ-IK-20:1/SSE-2/FT/1/S(Nook Industries)	1
24 in long 0.5 in diameter linear guide rail	59585K83 (McMaster Carr)	1
0.5 in ID open linear bearing	6489K7 (McMaster Carr)	4
External retaining rings	9968K24 (McMaster Carr)	4
36 in long, 0.25 in diameter flexible drive shaft	3787K26 (McMaster Carr)	1

TableA.2 Electronic parts bill of materials

Part Name	Part Number (retailer)	Quantity
5-phase stepper motor	Vexta PK5913AW (Oriental Motor)	1
Stepper motor controller	Vexta RKD514H-A (Oriental Motor)	1
12-bit USB DAQ	USB-1208LS(Measurement Computing)	1
Strain gage/extensometer amplifier		1
2 in 50% extensometer		1

APPENDIX B IN-SITU OPERATIONAL PROGRAM DESIGN

The controller component of the in-situ profilometer was written in National Instruments LabView 7.1 graphical programming language. Controlling was conducted with three different programs. Each program was specialized to a specific purpose.

The first program was a diagnostic program of the crosshead displacement. It was used while setting up a test and calibrating the crosshead. The user interface is shown in Figure B.1 and the program schematic flow chart is shown in Figure B.2. It read voltage of analog input (crosshead extensometer) and displayed the input in two forms, a graphical strip chart or as a numerical average of multiple samples. The data was displayed as either the raw voltage signal or was processed by a conversion function into actual distance.

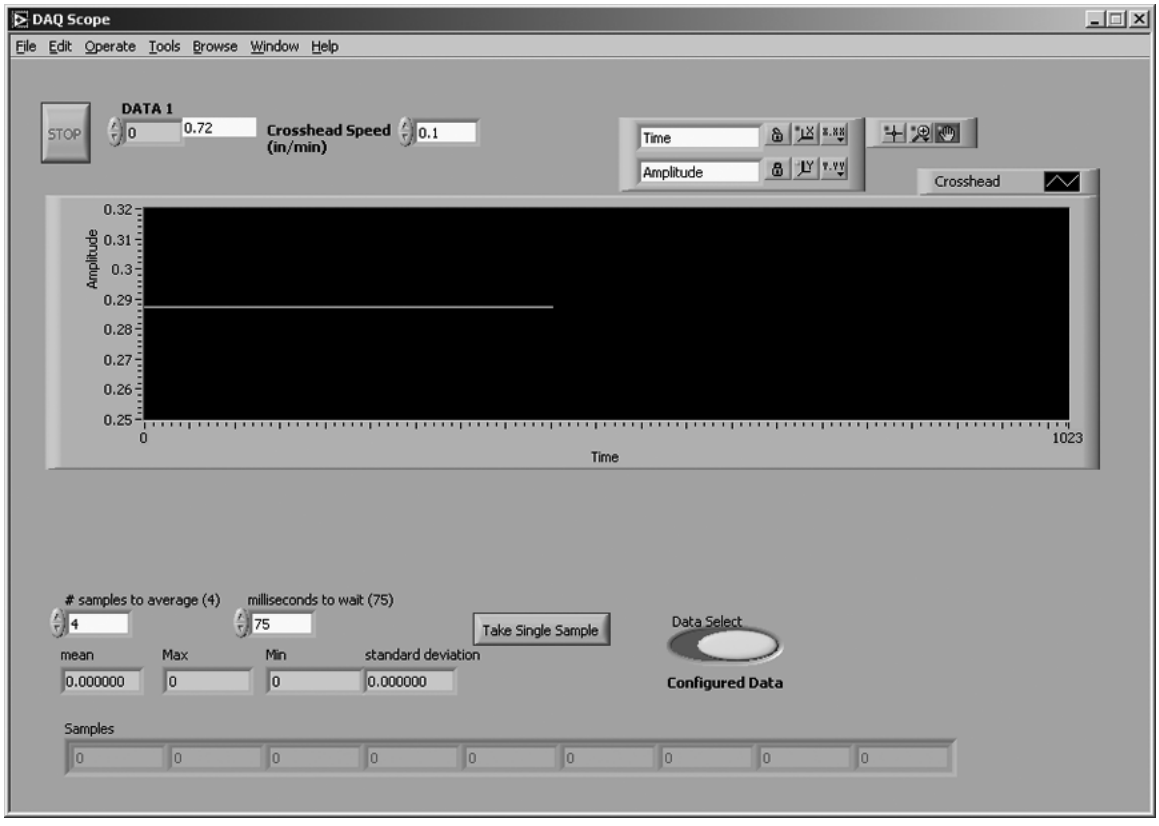

Figure B.1 DAQ Scope user interface.

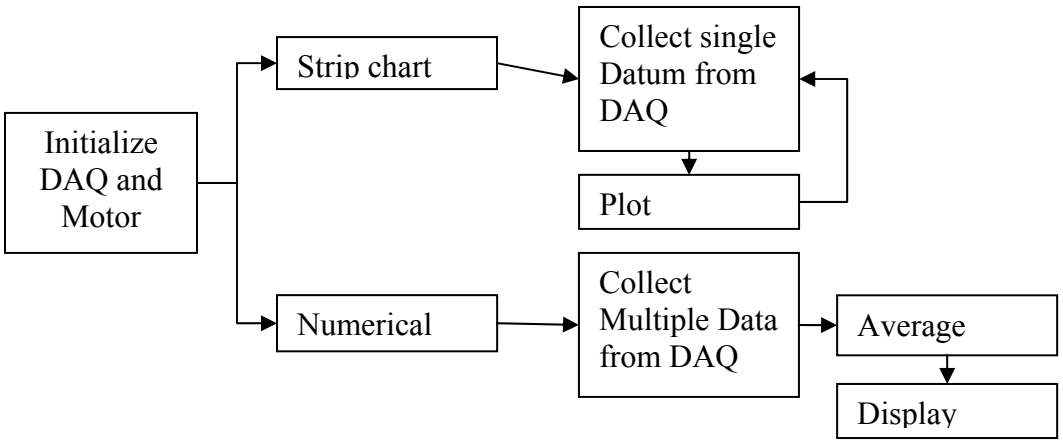

Figure B.2 DAQ Scope: schematic data flow chart, plotting to the strip chart is set as the default, and is interrupted to process the numerical command.

The second program controlled a fully automated test. The user interface (Figure B.3) was split into several regions. The "Extensometer Setup" region controlled crosshead distance traveled between topographic measurements. The "Motor Setup" region defined parameters directly affecting the speed of the drive motor. The "COM Port communication" contained several items which deal with how the control program communicated with the profilometer across a serial connection. Specific user inputs included the location to save files, setup and configuration file, length of time to wait between scans on the profilometer and serial port communication speed. The control program used delay times because the profilometer did not return a signal to the control program indicating when a topography measurement was finished. The "Real Time readouts" region on the user interface displayed information from various components of the system. After the user indicated that the file locations were appropriate, the three other buttons in the center section became available to press. The pre-strain buttons allowed the user to directly control the extension of the crosshead without defining a distance to travel. The "Begin Pulling Sample in Tension" button started the automated test. At the end of the test, the user was prompted to save displacement data. The end of the test occurred by all indicated measurements being taken, or by the user manually canceling the test. A simplified flow chart of the program is given in Figure B.4.

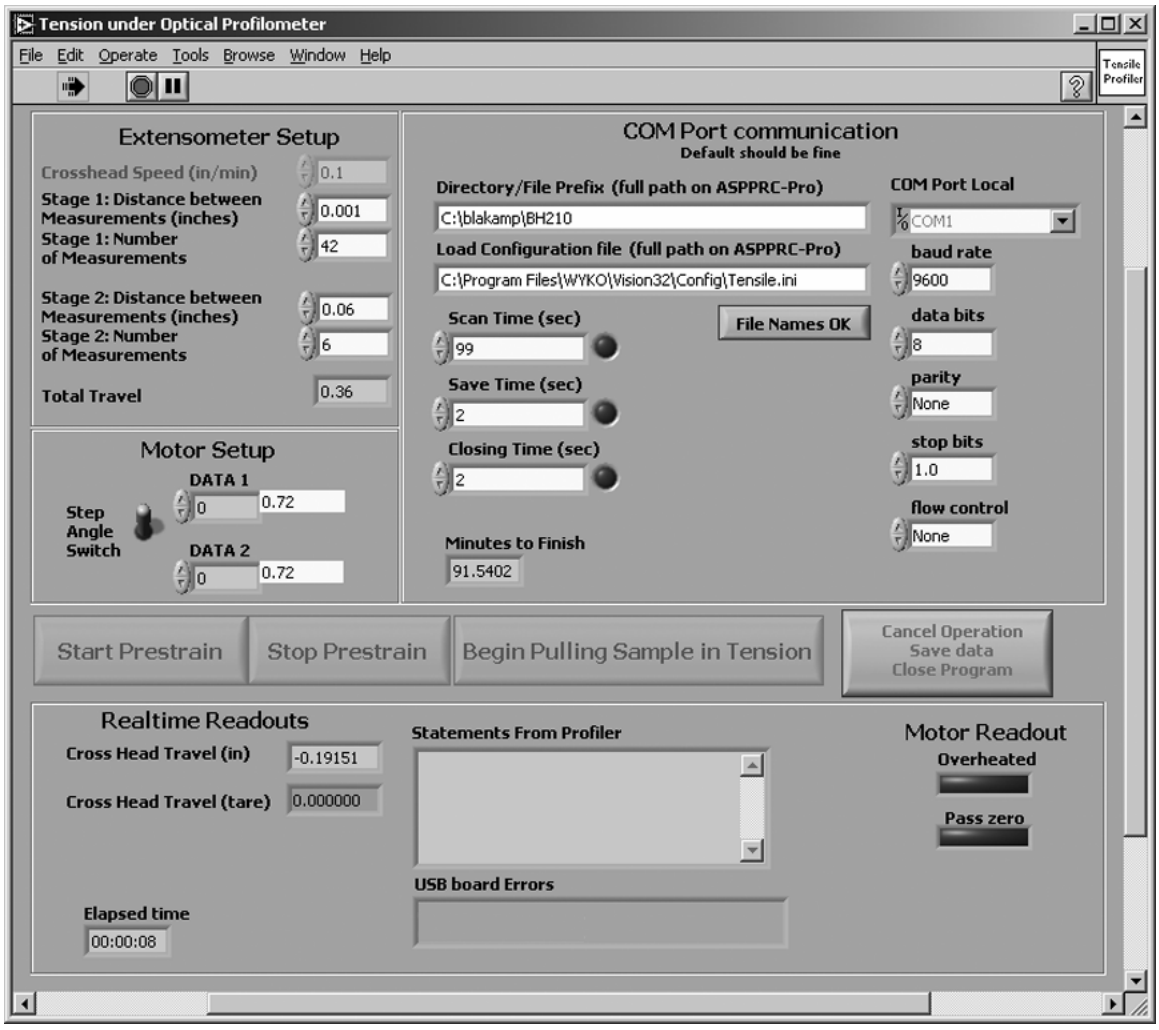

Figure B.3 Automated Tension under Optical Profilometer user interface.

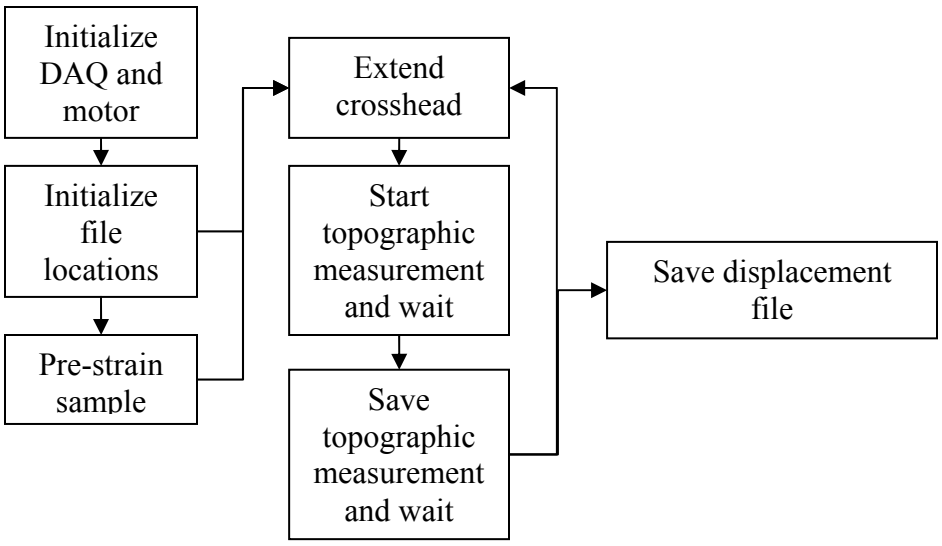

Figure B.4 Automated Tension under Optical Profilometer schematic data flow chart, plotting to the strip chart is set as the default and is interrupted to process the numerical command.

The third program allowed for full user control of the extension of the crosshead, and measurement of topographic data. The user interface is shown in B.5 with flow chart in B.6. When the program starts the user is prompted for a file to save displacement location information. The "Go To" button extended the crosshead forward by a certain increment. The "Pre-strain" button continuously extended the crosshead until the user pressed the button a second time. When extension was paused, the user could manually start a new topographic measurement. The user then could enter information about a topographic measurement and save crosshead location and information to file. This program gives the most flexibility because the user can adjust tilt and focus during the test, therefore constant supervision is also necessary.

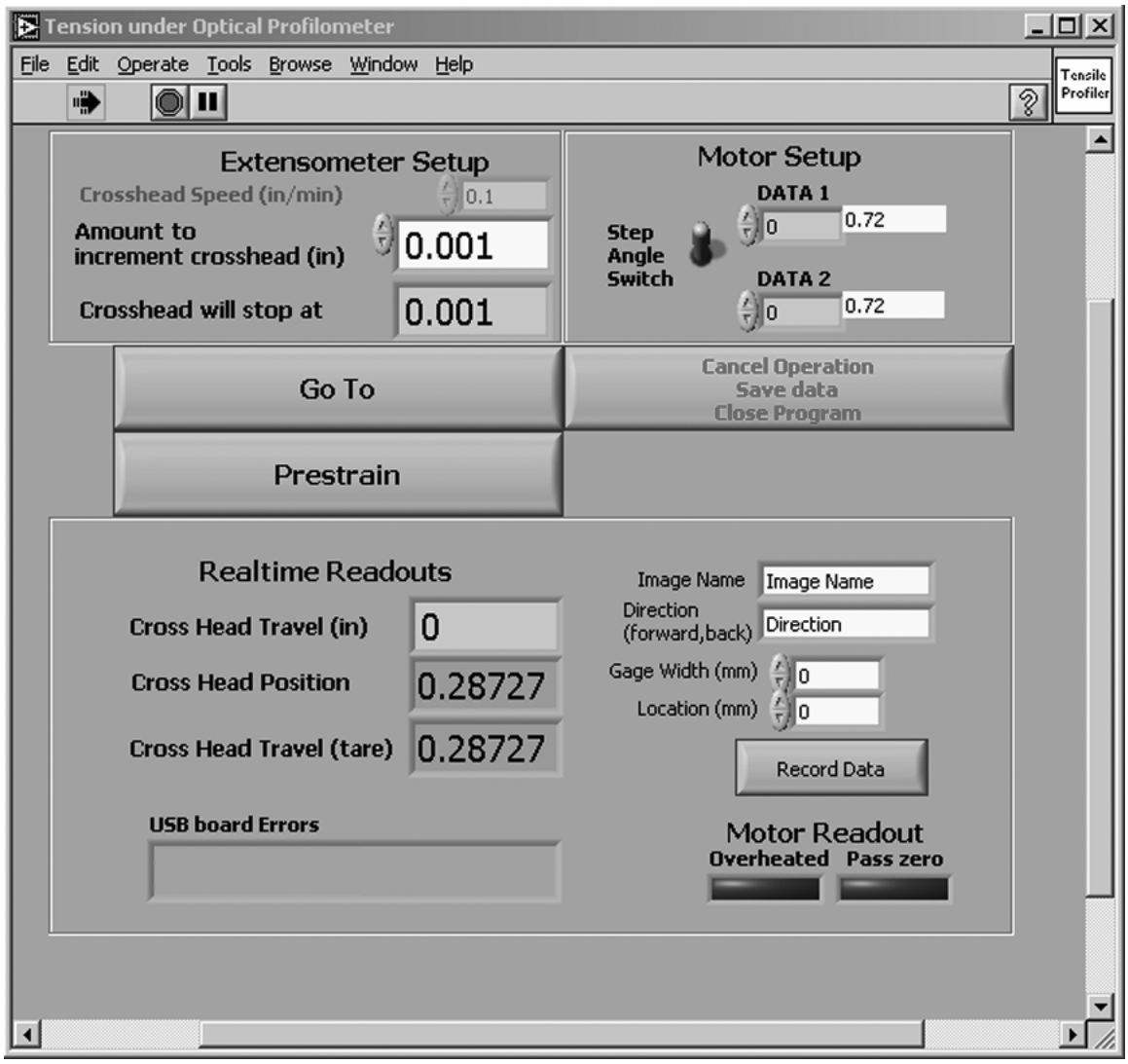

Figure B.5 Tension under Optical Profilometer user interface, nicknamed “GoTo”.

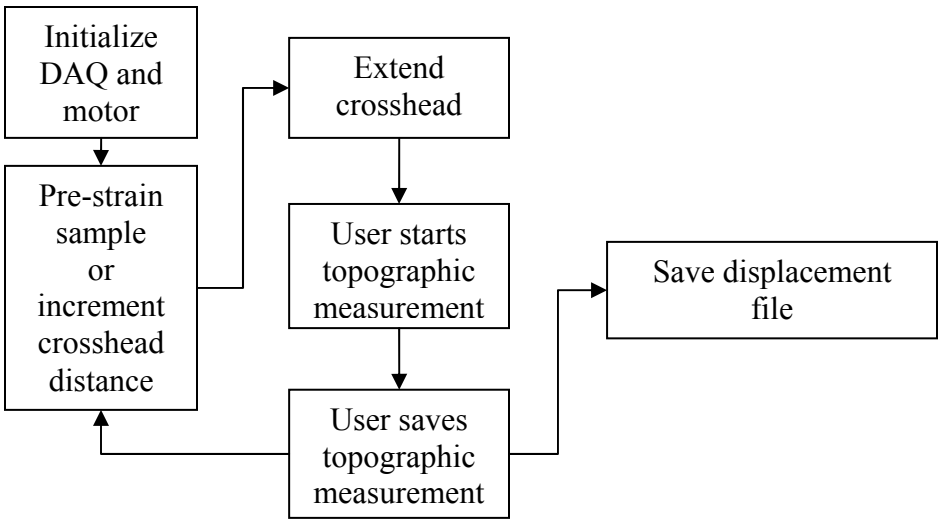

Figure B.6 Tension under Optical Profilometer schematic data flow chart.

APPENDIX C VISION32 OPTIONS – (OPTICAL PROFILING PROCEDURES)

Figures C.1 through C.4 show various settings and techniques used to capture and analyze topography data.

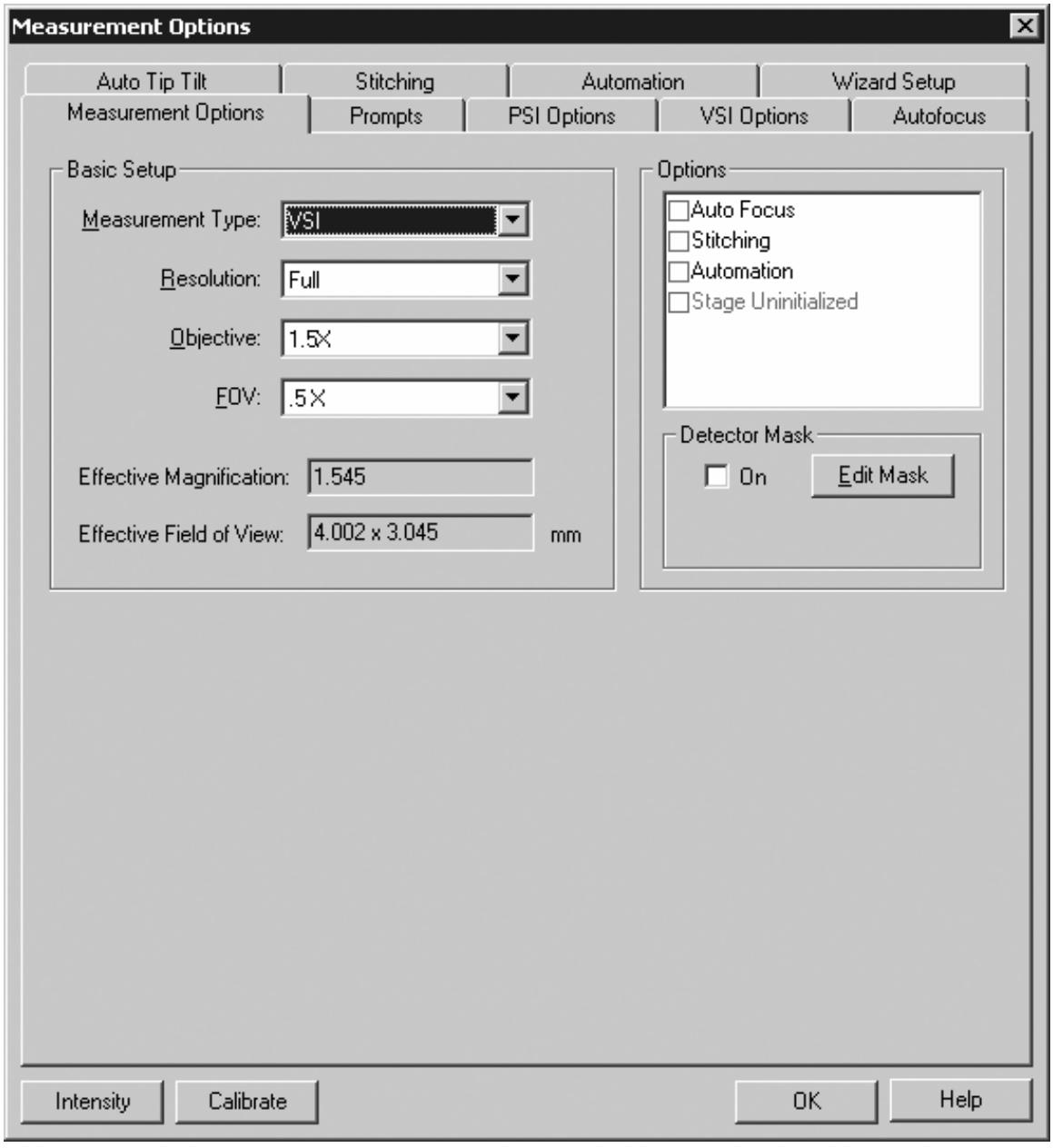

Figure C.1 Vision32 measurement options.

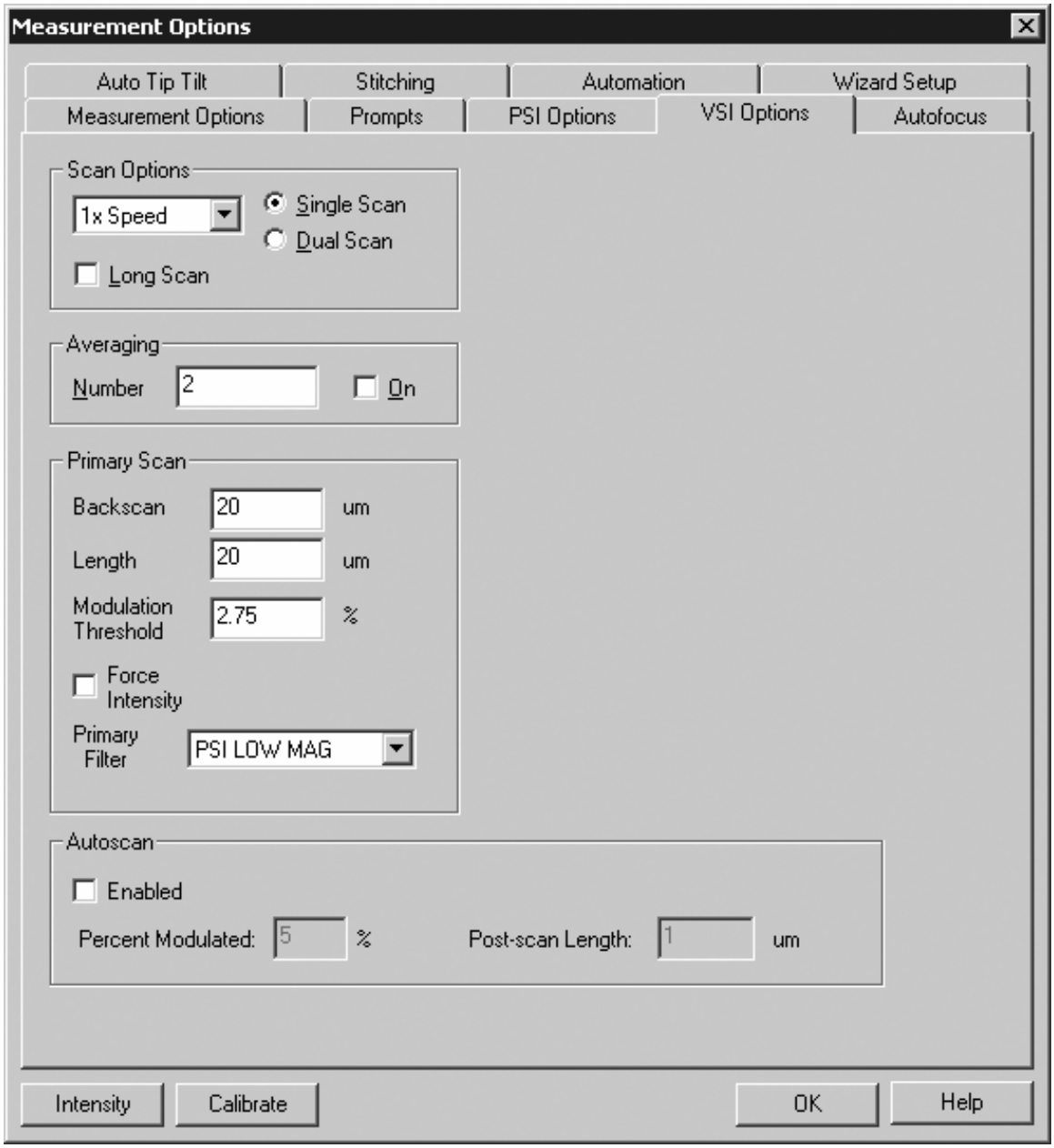

Figure C.2 Vision32 VSI options. Modulation threshold is set low to obtain more data on more difficult surfaces. Also, the red filter of PSI Low Magnification was used to capture more data.

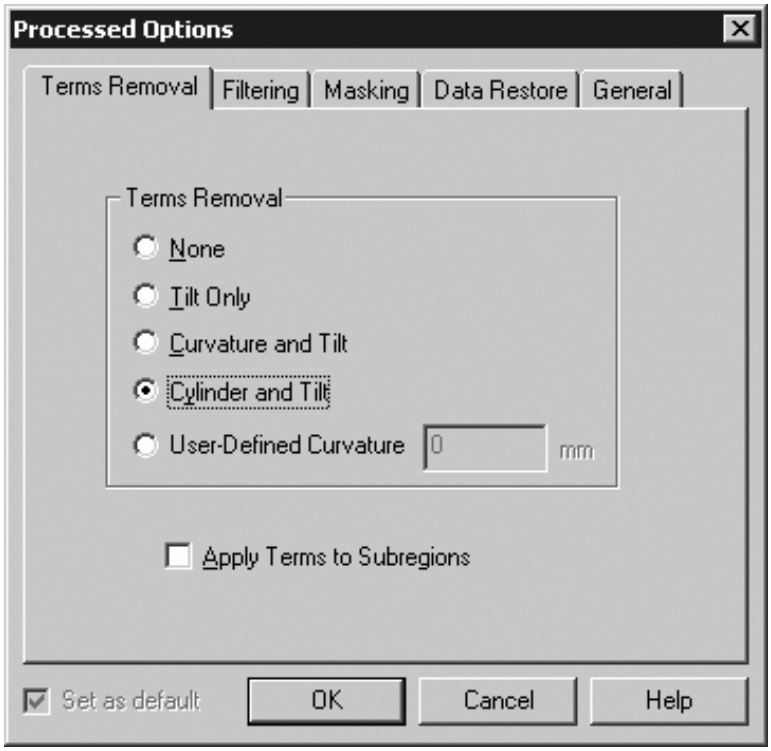

Figure C.3 Processed options removed cylinder and tilt from the recorded images. Images were always saved with "None" selected, and were processed each time the image was analyzed.

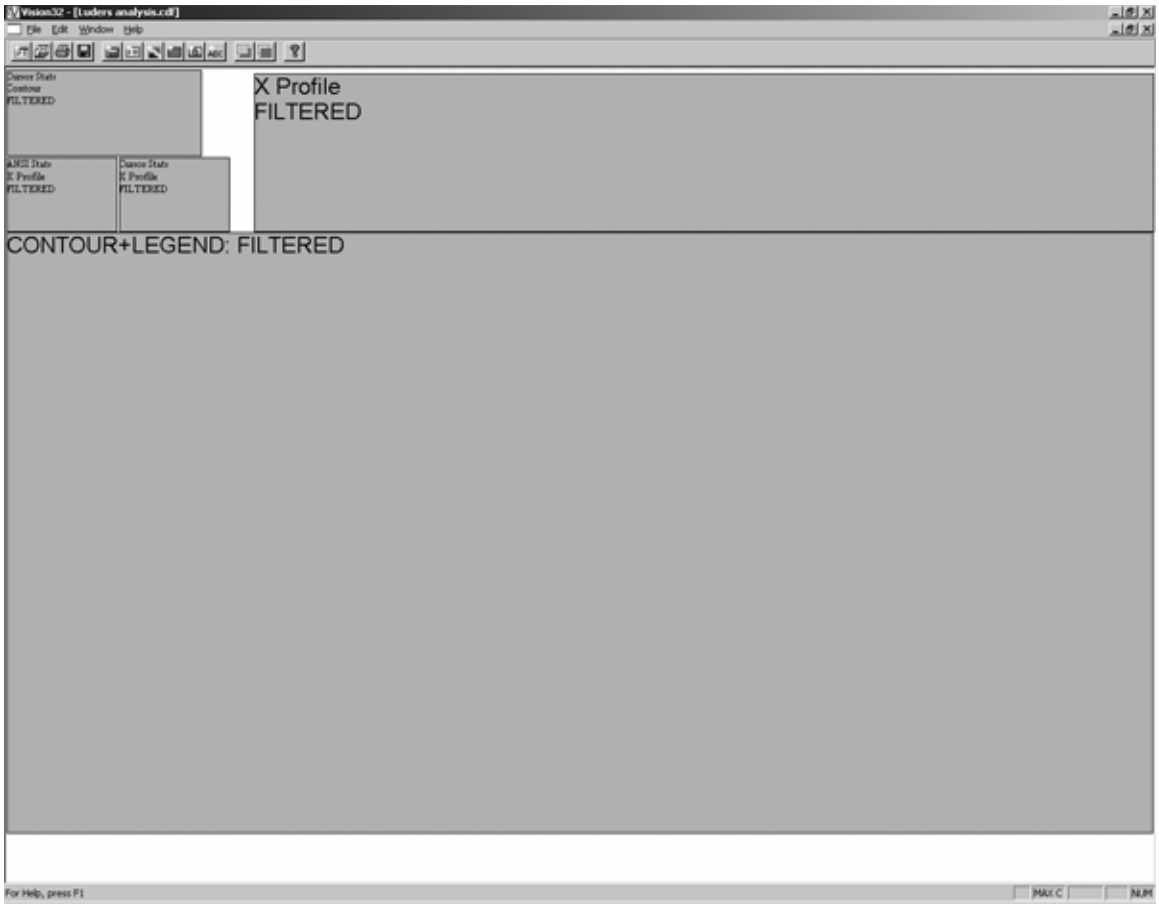

Figure C.4 A custom display was created to give a very large display of the contour plot and present a two-point trace on the contour plot.